

ABSTRACT

GUZMÁN SANTIAGO, ALEXIS JAVIER. Identification and Study of Key Functionalization Species for the Cp*Ir(III)-Catalyzed Halogenation of Benzamides. (Under the direction of Elon A. Ison).

The focus of this document is the development and study of the Cp*Ir(III)-catalyzed halogenation of *N,N*-diisopropylbenzamides. The optimized conditions for the iodination reaction consists of 0.5 mol% [Cp*IrCl₂]₂ in 1,2-dichloroethane at 60 °C for 1 h to form a variety of iodinated benzamides in high yields. Silver triflate and acetic acid were required for the reaction to take place. Increasing the catalyst loading to 5 mol% and the time to 4 h enabled the bromination reaction of the same substrates. Isolation and study of an isolated acetylhypohalite species revealed that this is the active halogen in the reaction. This enabled optimization of the bromination of benzamides and enabled the analogous chlorination reaction. A variety of functional groups on the *para*-position of the benzamide were well tolerated. Kinetic studies showed the first order dependence in catalyst, the positive dependence in benzamide, and no dependence in halosuccinimide. Through independent H/D kinetic isotope effect studies we observed an H/D KIE of 2.5. These results suggest that C–H bond activation is involved prior to or during the rate determining step of the reaction. Two mechanisms were explored, differing in the functionalization step of the reaction. Computational studies (DFT-BP3PW91-D3) indicate that a CMD mechanism is more likely than an oxidative addition pathway for C–H bond activation. The calculated functionalization step involving an Ir(V) resulting from oxidative addition of haloacetate seems like the most favorable pathway. Attempts at making a Ir(V) –X (X = I, Br) complex have not been successful to this point. Computational data suggests that oxidative addition is the RDS of the reaction.

© Copyright 2020 by Alexis Javier Guzmán Santiago

All Rights Reserved

Identification and Study of Key Functionalization Species of the Cp*Ir(III)-Catalyzed
Functionalization of Benzamides

by
Alexis Javier Guzmán Santiago

A thesis submitted to the Graduate Faculty of
North Carolina State University
in partial fulfillment of the
requirements for the degree of
Doctor of Philosophy

Chemistry

Raleigh, North Carolina
2020

APPROVED BY:

Dr. Elon A. Ison
Committee Chair

Dr. Reza Ghiladi

Dr. Elena Jakubikova

Dr. David Shultz

DEDICATION

This dissertation is dedicated to...

My Parents, Mayra and Juan, for their unwavering support

My grandfather, José, who never got to see my achievement

The wonderful friends that have made this journey endurable

BIOGRAPHY

Alexis Javier Guzman Santiago was born on April 2nd, 1992 in San Juan, Puerto Rico to parents Mayra Santiago Amador and Juan C. Guzmán Ramos. He was raised with the help of his grandparents Julia Ramos and José Juan Guzmán. He has a younger sister, Jessica, who is pursuing a career in psychology. Alexis attended the same school as his father, Colegio Nuestra Señora de Lourdes, where he graduated in 2010 with honors and discovered his curiosity for science. He obtained his bachelor's degree in chemistry from the university of Puerto Rico, Rio Piedras campus in 2015, where he was exposed to chemical research in coordination chemistry under the direction of Dr. Raphael Raptis and Dr. Dalice Piñero. In 2015, Alexis began his chemistry PhD thesis work in organometallic chemistry at North Carolina State University under the direction of Dr. Elon A. Ison. Upon graduation in 2020, Alexis plans to pursue a professional career in chemical industry.

TABLE OF CONTENTS

LIST OF TABLES	v
LIST OF FIGURES	vi
LIST OF SCHEMES	vii
Chapter 1: Introduction	1
Chapter 2: Cp*Ir(III)-Catalyzed Ortho Halogenation of Benzamide via C-H Bond Activation	10
Introduction	11
Results and Discussion	16
Iodination Reaction Optimization	16
Solvent Screening	17
Additive and Oxidant Screening	18
Iodination Substrate Scope	22
Bromination Reaction Optimization	23
Reaction Kinetics	24
Mechanistic Proposal	31
Stoichiometric Reactivity	34
Computational Mechanistic Analysis	39
Attempted Synthesis of Ir(V)-X	51
Conclusion	52
Experimental	53
References	80
Chapter 3: Improvement of the Generation of Hypervalent Halonium Species for the Halogenation of Benzamides	84
Introduction	85
Results and Discussion	86
Chlorination and Bromination	86
Lewis Base Effect on Chlorination	91
Fluorinations	95
Conclusion	97
Experimental	98
References	101

LIST OF TABLES

Table 2.1	Catalyst loading	17
Table 2.2	Solvent screening	18
Table 2.3	Oxidant screening.....	19
Table 2.4	Acid loading	20
Table 2.5	Stoichiometric reactivity of acetyl hypiodite adduct with 6(DMSO)	39

LIST OF FIGURES

Figure 1.1 General examples of directed C-H activation and examples of directing groups.....	3
Figure 1.2 BDE and pka values for representative unactivated hydrocarbons.....	3
Figure 2.1 Relevant compounds with important C-X bonds	12
Figure 2.2 GC calibration curve for <i>N,N</i> -diisopropylbenzamide	24
Figure 2.3 GC calibration curve for iodinated product.....	25
Figure 2.4 Time profile for the iodination of <i>N,N</i> -diisopropylbenzamide.....	26
Figure 2.5 Time profiles for the iodination of <i>N,N</i> -diisopropylbenzamide at various catalyst loadings	27
Figure 2.6 Plot for the dependence of the reaction on (Cp*IrCl ₂) ₂	27
Figure 2.7 Time profiles for the iodination of <i>N,N</i> -diisopropylbenzamide at various concentrations of benzamide	28
Figure 2.8 Plot for the dependence of the reaction on <i>N,N</i> -diisopropylbenzamide	28
Figure 2.9 Time profiles for the iodination of <i>N,N</i> -diisopropylbenzamide at various concentrations of <i>N</i> -iodosuccinimide	29
Figure 2.10 Plot for the dependence of the reaction on <i>N</i> -iodosuccinimide	29
Figure 2.11 Plot for the KIE by parallel reactions of <i>N,N</i> -diisopropylbenzamide (red) and <i>N,N</i> -diisopropylbenzamide- <i>d</i> ₅ (blue)	30
Figure 2.12 ¹ H-NMR spectrum of Cp*Ir(DMSO)(Benz)(6(DMSO)) in CDCl ₃	34
Figure 2.13 X-ray crystal structure of 6(DMSO)	35
Figure 2.14 Examples of stable Iodine(I) compounds	36
Figure 2.15 ¹ H-NMR spectrum of Cp*Ir(DMSO)(Benz) (6(DMSO)) in CDCl ₃	36
Figure 2.16 ¹ H-NMR spectrum of the halosuccinimide in the presence of tetrabutylammonium acetate at room temperature in CDCl ₃	38
Figure 2.17 X-ray crystal structure of SuccIOAc adduct.....	38

Figure 3.1 Species compatible for the chlorination of *N,N*-diisopropylbenzamide 87

LIST OF SCHEMES

Scheme 1.1 Previous work on C–H activation in the Ison group	5
Scheme 2.1 Representative cross-coupling name reactions using organic halides as substrates	11
Scheme 2.2 Traditional methods for the synthesis of halogenated arenes	12
Scheme 2.3 Examples of Pd-catalyzed directed arene halogenations.....	13
Scheme 2.4 Examples of Rh-catalyzed directed halogenation of arenes and heteroarenes.....	13
Scheme 2.5 Proposed mechanisms for the Rh-catalyzed directed halogenation of benzamides	14
Scheme 2.6 Catalyst screening.....	16
Scheme 2.7 Proposed mechanism for the formation of iodotrifluoroacetate	21
Scheme 2.8 Optimized reaction conditions for the iodination of benzamides with a representative ¹ H-NMR spectrum of the model substrate.....	21
Scheme 2.9 Scope of iodinated <i>para</i> -substituted <i>N,N</i> -diisopropylbenzamides	22
Scheme 2.10 Scope of brominated <i>para</i> -substituted <i>N,N</i> -diisopropylbenzamides.....	23
Scheme 2.11 Proposed mechanism for the halogenation of benzamides from halosuccinimide	32
Scheme 2.12 Proposed mechanism for the halogenation of benzamides from haloacetate	33
Scheme 2.13 DFT (B3PW91-D3) calculated energetics for the association of acetate anion (OAc) with <i>N</i> -halosuccinimide in 1,2-dichloroethane solvent	41
Scheme 2.14 Pathways for C-H bond activation	42
Scheme 2.15 DFT (B3PW91-D3) calculated energetics for the C-H activation step in 1,2-dichloroethane	43
Scheme 2.16 Scope of brominated <i>para</i> -substituted <i>N,N</i> -diisopropylbenzamides.....	44
Scheme 2.17 DFT (B3PW91-D3) calculated energetics for the Ir(III)-catalyzed iodination with <i>N</i> -iodosuccinimide in 1,2-dichloroethane.....	45

Scheme 2.18 Proposed Mechanism for the Coordination of Acetyl Hypoiodite and the Functionalization of Benzamide	46
Scheme 2.19 DFT (B3PW91-D3) calculated energetics for the Ir(III)-catalyzed iodination with I(OAc) in 1,2-dichloroethane	47
Scheme 2.20 DFT (B3PW91-D3) calculated energetics for the oxidative addition of X(OAc) (X = halide) in 1,2-dichloroethane	49
Scheme 2.21 DFT (B3PW91-D3) calculated energetics for the oxidative addition of I(OAc) to iridacycles bearing varying substituents in the <i>para</i> -position in 1,2-dichloroethane	50
Scheme 2.22 Attempts at isolating an Ir(V) iodide complex	51
Scheme 3.1 Reactivity of hypervalent iodine (I)	85
Scheme 3.2 DFT (B3PW91-D3) calculated energetics for the oxidative addition of Cl(carboxylate) to INT-4 in 1,2-dichloroethane solvent	87
Scheme 3.3 BDE table for a series of electrophilic chlorinating agents	88
Scheme 3.4 Scope of Chlorinated <i>Para</i> -Substituted <i>N,N</i> -diisopropylbenzamides	89
Scheme 3.5 BDE table for a series of electrophilic brominating agents	90
Scheme 3.6 Scope of Brominated <i>para</i> -Substituted <i>N,N</i> -diisopropylbenzamides under adjusted reaction conditions	90
Scheme 3.7 DFT (B3PW91-D3) comparison of the calculated energetics of the comparison between the association of halosuccinimide with acetate and thioacetate	92
Scheme 3.8 DFT (B3PW91-D3) calculated energetics for the oxidative addition of Cl(thiobenzoate) to INT-4 in 1,2-dichloroethane solvent	92
Scheme 3.9 DFT (B3PW91-D3) calculated energetics for the oxidative addition of Cl(benzoate) to INT-4 in 1,2-dichloroethane solvent.....	93
Scheme 3.10 DFT (B3PW91-D3) calculated energetics for the oxidative addition of Cl(<i>N</i> -methylbenzamide) to INT-4 in 1,2-dichloroethane solvent.....	94
Scheme 3.11 BDE table for a series of electrophilic fluorinating agents	96

CHAPTER 1 - General Introduction

Organometallic Chemistry

Organometallic chemistry is a subfield of coordination chemistry. In this field the interaction between a metal center and organic molecules is studied to answer fundamental questions in the areas of inorganic and synthetic chemistry.^{1,2} Organometallic catalysts have been commonly used in industrial processes, but are now routinely utilized in research for problems in methods development and elucidating reaction mechanisms. Homogeneous catalysis, where both substrate and catalyst are in the same phase, has its advantages when dealing with a chemical transformation. A homogeneous catalyst is easier to tune in terms of sterics and electronics allowing access to a range of reactivities that might not be accessible in heterogeneous systems. In addition, catalytic systems are considered easier to probe and study because spectroscopic techniques, like ¹H-NMR spectroscopy can be utilized to determine structures of species in solution and monitor reaction kinetics.

The catalysis of organic reactions is one of the major fields of study in organometallic chemistry. Among those reactions, direct C–H bond activation and functionalization reactions have attracted the attention of not only inorganic chemists, but also organic and computational chemists. Most C–H bonds are not viewed as an exploitable functionality in organic synthesis. However, because the C–H unit is ubiquitous in organic compounds, direct C–H bond functionalization shows great promise as a viable tool for atom and step economical C–C and C–heteroatom bond forming reactions.

There are two notable limitations in direct C–H bond functionalization that make this synthetic transformation challenging. The first is achieving site selectivity in molecules that contain multiple C–H bonds. It has been shown that common Lewis basic functionalities can be used as useful directing groups (DG) to assure site selectivity in intramolecular C–H bond activation and functionalization reactions (**Figure 1.1**).³

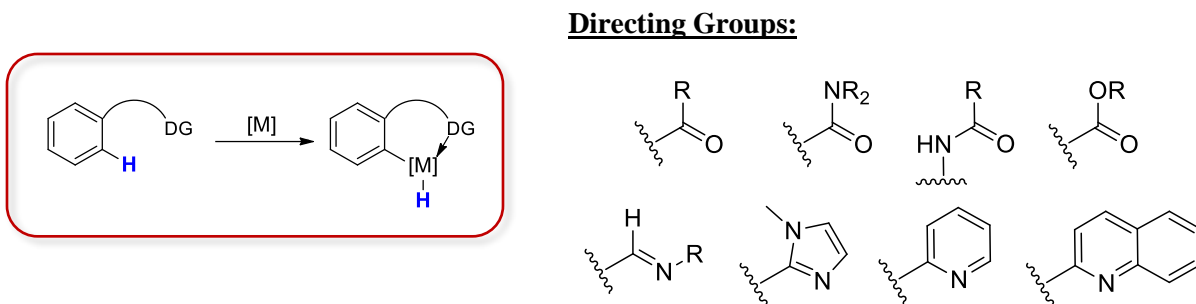


Figure 1.1 General example of directed C-H activation and examples of directing groups

A DG will coordinate to the metal center and will facilitate the interaction between the metal center and the C–H bond. This strategy has commonly been applied using nitrogen, sulfur, and phosphorous containing DG, which will strongly coordinate to the metal center. This type of DG is synthetically restrictive, often they are installed then later removed from the substrate or they are a permanent part of it.⁴ Conversely, weakly coordinating DG, like amides, ethers, carboxylic acids and ketones, are commonly found functionalities in organic molecules that can serve the same purpose. In addition, these do not stabilize metal intermediates as well as strongly coordinating DG, which leads to better reactivity.

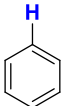
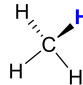
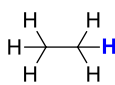
			
	<i>Benzene</i>	<i>Methane</i>	<i>Ethane</i>
pKa	~43	~48	~50
BDE			
(kcal/mol)	~113	~105	~111

Figure 1.2. BDE and pKa values for representative unactivated hydrocarbons

Secondly, the inert nature of the C–H bond has also been an issue in developing efficient direct functionalization strategies. Unactivated C–H bonds have a high bond dissociation energy (BDE), and their pKa values range from 43 to 50 (**Figure 1.2**).⁵⁻⁷ Bergman and Jones were the first to show the potential of $[\text{Cp}^*\text{MPR}_3\text{X}_2]$ ($\text{M} = \text{Ir}, \text{Rh}$)

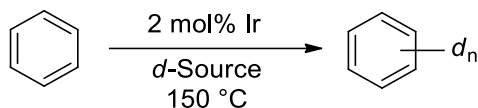
complexes to activate C–H bonds.^{8,9} Subsequent work showed that such late transition metals are capable of C–H bond activation in the presence of an acetate source.¹⁰ In this area, the pioneering work of Periana, and the seminal work from Satoh and Miura was focused on catalytic C–H bond activation.¹¹⁻¹⁵ Specifically, the work by Satoh and Miura focused on dehydrogenative cross-coupling reactions using $[\text{Cp}^*\text{RhCl}_2]_2$ as a catalyst.

The reactivity of $[\text{Cp}^*\text{Rh(III)}]$ complexes has been well established. It serves as a catalyst for many direct C–H bond functionalization methodologies which have enabled not only C–C bond forming reactions,¹⁶⁻³⁷ but C–heteroatom bond forming reactions as well.³⁸⁻⁴⁷ On the other hand, iridium complexes have also been shown to be highly active in stoichiometric C–H bond activation reactions.⁴⁸⁻⁵⁰ Despite this, their use in catalytic reactions is still scarce, only a few $\text{Cp}^*\text{Ir(III)}$ -based catalytic methods have been developed, when compared to Rh.⁵¹⁻⁵³ Differences in reactivity and mechanistic pathways between Ir(III) and other transition metal complexes are not completely understood.⁵⁴ This lack of mechanistic understanding has kept the area of direct C–H bond functionalization with the $[\text{Cp}^*\text{Ir(III)}]$ fragment underdeveloped.

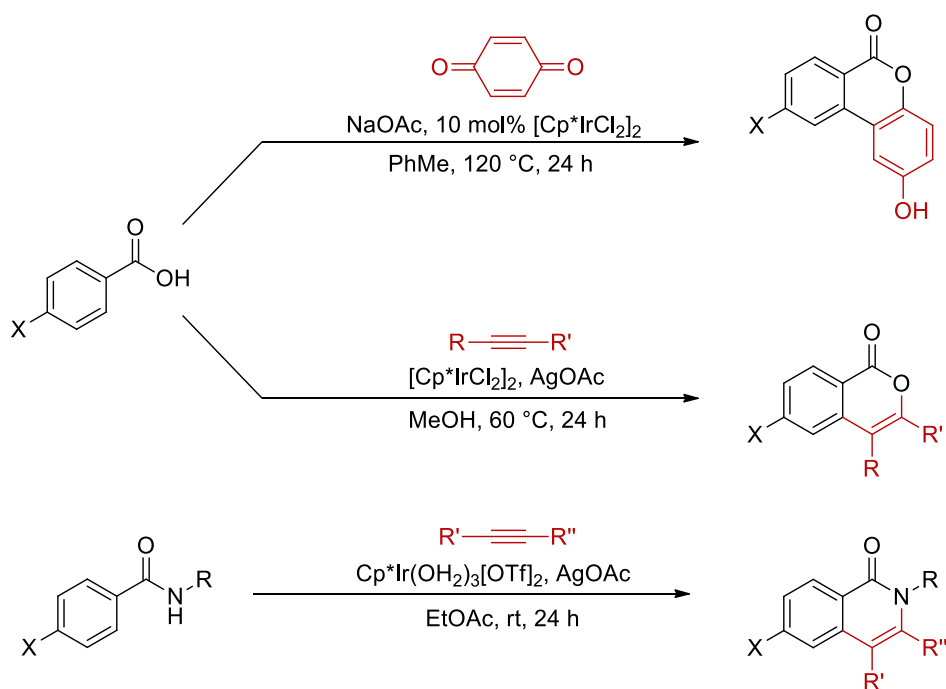
Previously our group demonstrated that benzene C–H bond activation by H/D exchange experiments could be achieved with a variety of $\text{Cp}^*\text{Ir(III)}$ complexes (**Scheme 1.1 A**).⁵⁵ This work led to the catalytic C–H bond activation and functionalization of benzoic acids with benzoquinones and alkynes to form the respective benzochromenones⁵⁶ and isocoumarins.⁵⁷ In more recent work from our group, it was demonstrated that this chemistry can be extended to the synthesis of isoquinolones, the nitrogen containing analogue, through C–H bond activation and functionalization of benzamides with alkynes (**Scheme 1.1 B**).⁵⁸

Scheme 1.1. Previous Work on C–H Activation in the Ison Group

A. C–H bond activation of Benzene via H/D Exchange with Cp*Ir(III) Complexes



B. Synthesis of Benzochromenones, Isocoumarins and Isoquinolones via directed C–H bond Activation with Cp*Ir(III)



Scope of this dissertation

The work found in this thesis mainly shows an experimental and computational investigation into the C–H bond activation and functionalization for the halogenation of benzamides. In Chapter 2 the optimization and scope for the iodination and bromination of *N,N*-disubstituted benzamides is shown, as well as an extensive study of the reaction mechanism experimentally, through kinetic and stoichiometric studies, as well as computationally (DFT). An acetyl hypohalite species generated *in situ* under our reaction

conditions was identified as the halogen source. This study leads to the development of modified reaction conditions, in Chapter 3, by changing the Lewis base that generates the halogen source. This improves the yields for the bromination reaction and enables the chlorination of the same benzamides which were not observed previously. A computational study was then pursued to identify the species that would further improve the system towards the halogenation of benzamides.

References

1. Cornils, B.; Herrmann, W. A. *Applied Homogeneous Catalysis*; Wiley VCH, Weinheim, 2002.
2. Crabtree, R. H. *The Organometallic Chemistry of the Transition Metals*; Wiley, New Jersey, 2005.
3. Roque, G.; Chatani, N. *Angew. Chemie - Int. Ed.* **2013**, 11726.
4. Engle, K. M.; Mei, T. S.; Wasa, M.; Yu, J. Q. *Acc. Chem. Res.* **2012**, 780.
5. Bordwell, F. G. *Acc. Chem. Res.* **1988**, 456.
6. Blanksby, S. J.; Ellison, G. B.; *Acc. Chem. Res.* **2003**, 255.
7. Smith, M. B. *March's Advanced Organic Chemistry*; Wiley, New York, 2013, pp 314-318.
8. Janowicz, A. H.; Bergman, R. G. *J. Am. Chem. Soc.* **1983**, 3929.
9. Jones, W. D.; Feher, F. J. *J. Am. Chem. Soc.* **1985**, 620.
10. Han, Y. F.; Jin, G. X. *Chem. Soc. Rev.* **2014**, 2799.
11. Matsumoto, T.; Periana, R.A.; Taube, D.J.; Yoshida, H. *J. Catal.* **2002**, 272.
12. Ueura, K.; Satoh T.; Miura, M. *Org. Lett.* **2007**, 1407.
13. Ueura, K.; Satoh T.; Miura, M. *Org. Lett.* **2007**, 5362.
14. Umeda, N.; Tsurugi, H.; Satoh, T.; Miura, M. *Angew. Chemie - Int. Ed.* **2008**, 4019.
15. Umeda, N.; Hirano, K.; Satoh, T.; Miura, M. *J. Org. Chem.* **2009**, 7094.
16. Satoh, T.; Miura, M. *Chem. Eur. J.* **2010**, 16, 11212.
17. Patureau, F. W.; Wencel-Delord, J.; Glorius, F. *Aldrichimica Acta* **2012**, 45, 31.
18. Song, G.; Wang, F.; Li, X. *Chem. Soc. Rev.* **2012**, 41, 3651.
19. Stuart, D. R.; Bertrand-Laperle, M.; Burgess, K. M. N.; Fagnou, K. *J. Am. Chem. Soc.* **2008**, 130, 16474.
20. Rakshit, S.; Patureau, F. W.; Glorius, F. *J. Am. Chem. Soc.* **2010**, 132, 9585.
21. Zhang, J.; Qian, H.; Liu, Z.; Xiong, C.; Zhang, Y. *Eur. J. Org. Chem.* **2014**, 8110.
22. Morimoto, K.; Hirano, K.; Satoh, T.; Miura, M. *Chem. Lett.* **2011**, 40, 600.
23. Hyster, T. K.; Rovis, T. *J. Am. Chem. Soc.* **2010**, 132, 10565.
24. Mochida, S.; Umeda, N.; Hirano, K.; Satoh, T.; Miura, M. *Chem. Lett.* **2010**, 39,

- 744.
25. Guimond, N.; Gouliaras, C.; Fagnou, K. *J. Am. Chem. Soc.* **2010**, *132*, 6908.
 26. Luo, C. Z.; Jayakumar, J.; Gandeepan, P.; Wu, Y. C.; Cheng, C. H. *Org. Lett.* **2015**, *17*, 924.
 27. Satoh, T.; Ueura, K.; Miura, M. *Pure. Appl. Chem.* **2008**, *80*, 1127.
 28. Jia, J.; Shi, J.; Zhou, J.; Liu, X.; Song, Y.; Xu, H. E.; Yi, W. *Chem. Commun.* **2015**, *51*, 2925.
 29. Morimoto, K.; Hirano, K.; Satoh, T.; Miura, M. *Org. Lett.* **2010**, *12*, 2068.
 30. Morimoto, K.; Hirano, K.; Satoh, T.; Miura, M. *J. Org. Chem.* **2011**, *76*, 9548.
 31. Su, Y.; Zhao, M.; Han, K.; Song, G.; Li, X. *Org. Lett.* **2010**, *12*, 5462.
 32. Hyster, T.K.; Rovis, T. *Chem. Sci.* **2011**, *2*, 1606.
 33. Mochida, S.; Hirano, K.; Satoh, T.; Miura, M. *J. Org. Chem.* **2009**, *74*, 6295.
 34. Unoh, Y.; Hashimoto, Y.; Takeda, D.; Hirano, K.; Satoh, T.; Miura, M. *Org. Lett.* **2013**, *15*, 3258.
 35. Qi, Z.; Wang, M.; Li, X. *Org. Lett.* **2013**, *15*, 5440.
 36. Umeda, N.; Hirano, K.; Satoh, T.; Shibata, N.; Sato, H.; Miura, M. *J. Org. Chem.* **2011**, *76*, 13.
 37. Song, G.; Gong, X.; Li, X. *J. Org. Chem.* **2011**, *76*, 7583.
 38. Colby, D. A.; Tsai, A. S.; Bergman, R. G.; Ellman, J. A. *Acc. Chem. Res.* **2012**, *45*, 814.
 39. Song, G.; Wang, F.; Li, X. *Chem. Soc. Rev.* **2012**, *41*, 3651.
 40. Chiba, S. *Chem. Lett.* **2012**, *41*, 1554.
 41. Takahama, Y.; Shibata, Y.; Tanaka, K. *Chem. Eur. J.* **2015**, *21*, 9053.
 42. Shi, Z.; Boultadakis-Arapinis, M.; Glorius, F. *Chem. Commun.* **2013**, *49*, 6489.
 43. Shi, Z.; Boultadakis-Arapinis, M.; Koester, D. C.; Glorius, F. *Chem. Commun.* **2014**, *50*, 2650.
 44. Webb, N. J.; Marsden, S. P.; Raw, S. A. *Org. Lett.* **2014**, *16*, 4718.
 45. Otley, K. D.; Ellman, J. A. *Org. Lett.* **2015**, *17*, 1332.
 46. Zhang, M.; Zhang, H. J.; Han, T.; Ruan, W.; Wen, T. B. *J. Org. Chem.* **2015**, *80*, 620.
 47. Yu, S.; Li, X. *Org. Lett.* **2014**, *16*, 1200.

48. Li, L.; Brennessel, W. W.; Jones, W. D. *J. Am. Chem. Soc.* **2008**, 130, 12414.
49. Kohl, G.; Pritzkow, H.; Enders, M. *Eur. J. Inorg. Chem.* **2008**, 27, 230.
50. Liu, J.; Wu, X.; Iggo, J. A.; Xiao, J. *Coord. Chem. Rev.* **2008**, 252, 782.
51. Atzrodt, J.; Derdau, V.; Fey, T.; Zimmermann, J. *Angew. Chemie - Int. Ed.* **2007**, 46, 7744.
52. Choi, J.; Goldman, A. S. *Top. Organomet. Chem.* **2011**, 34, 139.
53. Erbing, E.; Sanz-Marco, A.; Vazquez-Romero, A.; Malmberg, J.; Johanson, M. J.; Gomez-Bengoa, E.; Martin-Matute, B. *ACS Catal.* **2018**, 8, 920.
54. Figg, T. M.; Park, S.; Park, J.; Chang, S.; Musaev, D. G. *Organometallics* **2014**, 33, 4076.
55. Lehman, M. C.; Gary, J. B.; Boyle, P. D.; Sanford, M. S.; Ison, E. A. *ACS Catal.* **2013**, 3, 2304.
56. Engelman, K. L.; Feng, Y.; Ison, E. A. *Organometallics* **2011**, 30, 4572.
57. Frasco, D. A.; Lilly, C. P.; Boyle, P. D.; Ison, E. A. *ACS Catal.* **2013**, 3, 2421.
58. Unpublished results.

CHAPTER 2 – Cp*Ir(III)-Catalyzed Ortho Halogenation of Benzamides via C-H bond Activation and Functionalization

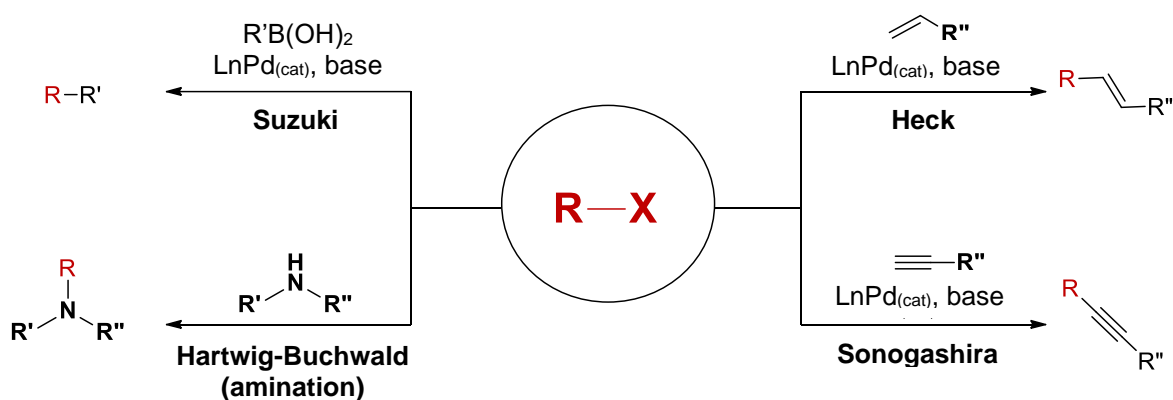
Portions of this chapter were published in:

Guzmán Santiago, A.J.; Brown, C.A.; Sommer, R.D.; Ison, E.A. Dalton Trans.,
2020, Advance Article

Introduction

Catalytic C–H bond activation has become one of the most valuable methods for the step- and atom- economic synthesis of functionalized molecules. This strategy has been exploited for the development of numerous C–C bond forming reactions.¹⁻¹⁵ There has been significant improvement in recent years on the development of C–heteroatom bond forming reactions,¹⁶⁻³⁷ but the development of C–X (X = halogen) bond forming reactions is still surprisingly under developed.³⁸⁻⁴⁴ Organic halides have been commonly used as electrophiles in various substitution reactions⁴⁵ as core building blocks for the synthesis of nucleophilic organometallic reagents, like Grignard reagents,⁴⁶ and as suitable substrates for numerous cross-coupling reactions (**Scheme 2.1**).⁴⁷

Scheme 2.1. Representative cross-coupling name reactions using organic halides as substrates



In addition, the $C(sp^2)-X$ motif plays a key role in the properties of many agrochemicals, pharmaceuticals, and natural products (**Figure 2.1**). Hence, there is great promise in combining direct C–H bond halogenation and established cross-coupling methodologies for the development of new and more efficient synthetic routes in pursuit of known or inaccessible natural products,⁴⁸ agrochemicals,⁴⁹ biologically active compounds and pharmaceuticals.⁵

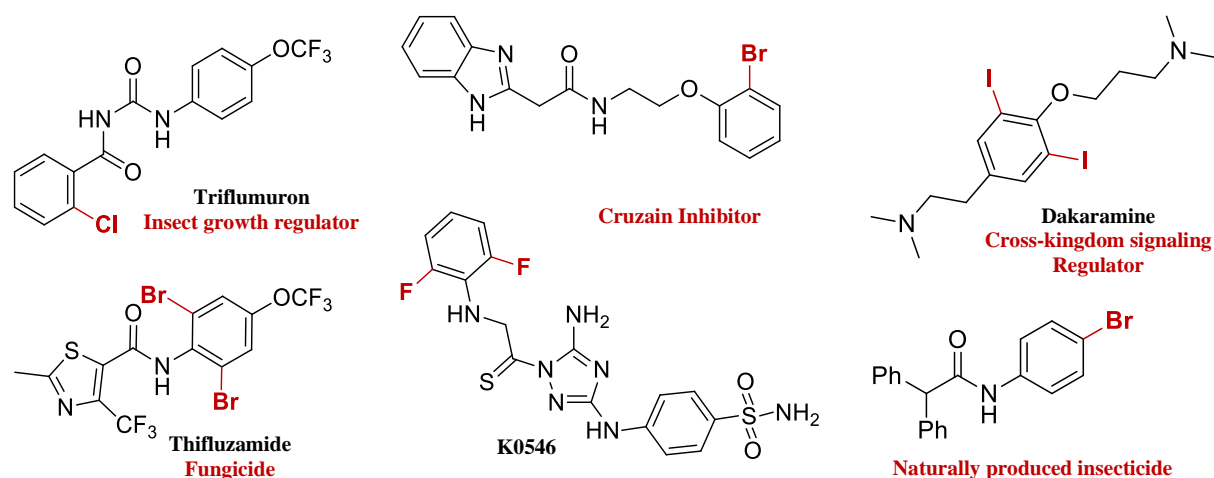
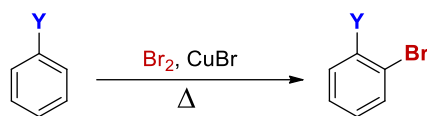


Figure 2.1. Relevant compounds with important C–X bonds

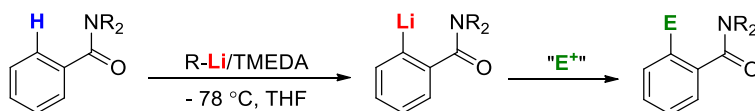
Traditional organic methodologies for the synthesis of halogenated arenes rely mostly on Freidel-Crafts- and Sandmeyer-type reactions,⁵¹ and directed *ortho* lithiation (DoL) strategies followed by quenching with an electrophilic halogen source (**Scheme 2.2**).⁵² Despite their wide application in organic synthesis, these approaches are limited by a few factors: a) these methodologies usually rely on pre-activated substrates, b) in addition, harsh reaction conditions limit the tolerance towards functional groups, and give rise to issues in terms of regioselectivity and polyhalogenation. To circumvent these drawbacks, efforts have focused on directed metal-catalyzed strategies.

Scheme 2.2. Traditional methods for the synthesis of halogenated arenes

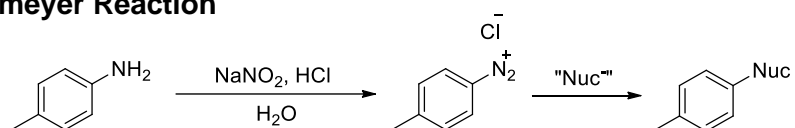
Electrophilic Aromatic Substitution (EAS)



Directed *ortho* Lithiation (DoL)

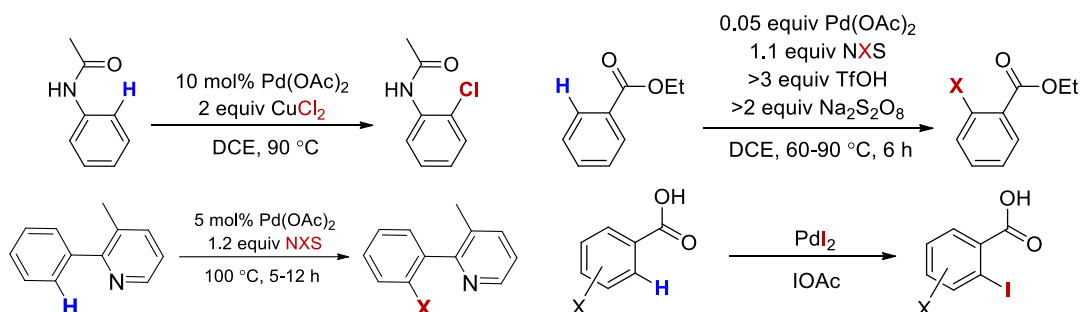


Sandmeyer Reaction



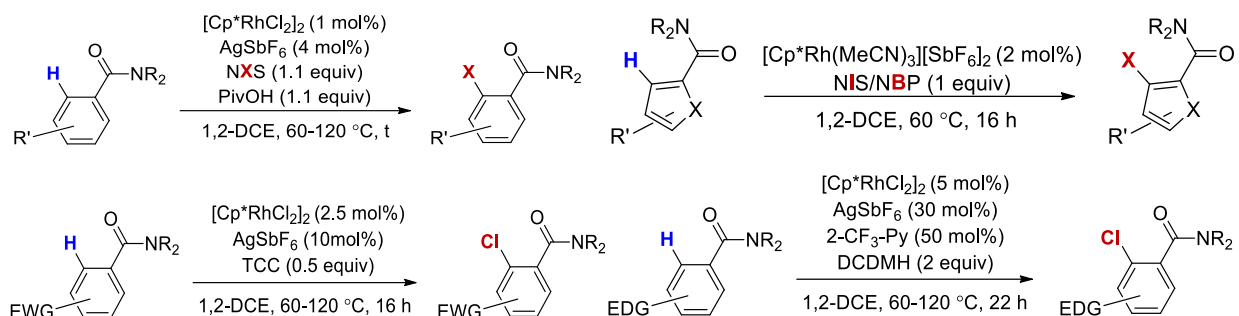
Most of the early examples of catalytic C–X bond formation reactions use a palladium catalyst (**Scheme 2.3**).⁵³⁻⁶⁰ These approaches were generally limited by their substrate scope, their efficiency and adaptability (harsh conditions and moderate yields), or their suitability for only one type of C–X bond formation. Therefore, there is a need for a general method that enables the selective formation of C–X bonds, that is compatible with a diverse substrate scope.

Scheme 2.3. Examples of Pd-catalyzed directed arene halogenations



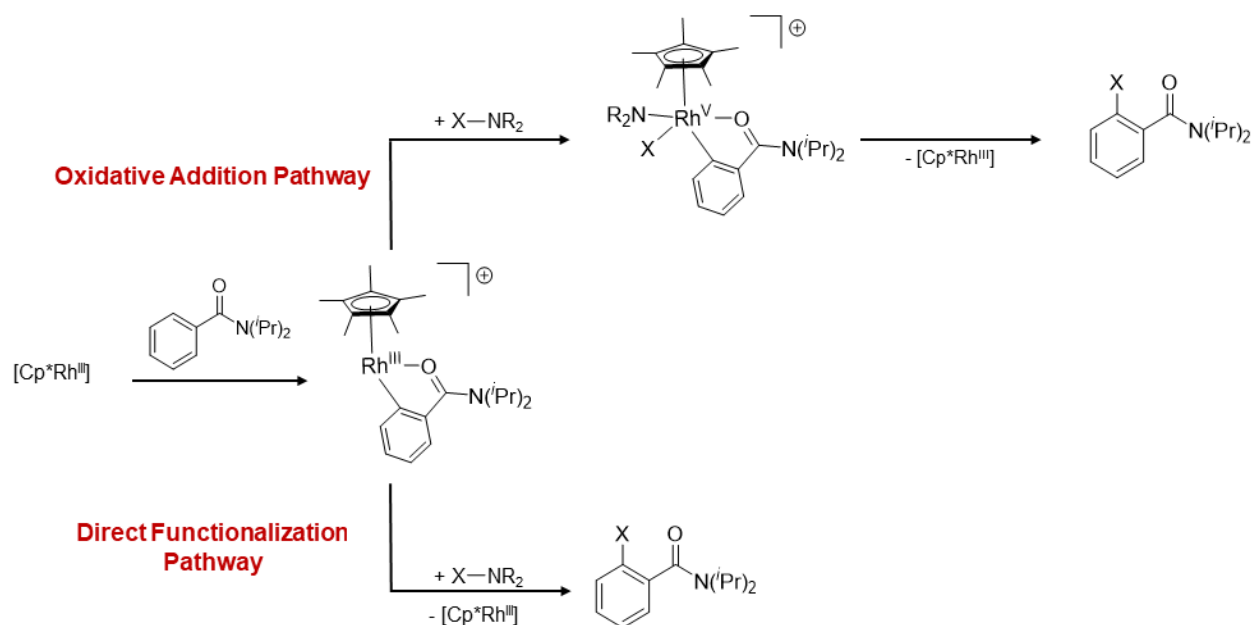
[Cp*Rh(III)] has emerged as an effective catalyst for C–H bond halogenation (**Scheme 2.4**).^{38, 40, 61} The Glorius group has developed a Rh(III) system for the directed catalytic halogenation of arenes and heterocycles.

Scheme 2.4. Examples of Rh-catalyzed directed halogenation of arenes/heteroarenes



The reaction was proposed to follow one of two mechanistic scenarios (**Scheme 2.5**). After cyclometallation of the $[\text{Cp}^*\text{Rh}(\text{III})]$ catalyst with the substrate, the functionalization may occur via one of two pathways: (1) The rhodacycle may react with the halosuccinimide through oxidative addition to generate a Rh(V) complex, which can then reductively eliminate the functionalized product (**Pathway A**). (2) Alternatively, the cyclometalated complex can undergo a nucleophilic addition type reaction to the halosuccinimide to directly form the product (**Pathway B**).

Scheme 2.5. Proposed mechanisms for the Rh-catalyzed directed halogenation of benzamides



Despite the efficiency of this system there are still some key drawbacks: 1) This methodology still relies on harsh conditions (depending on the substrate), 2) this system is not a general strategy for halogenation. Reaction conditions for the directed Rh(III)-catalyzed chlorination of arenes have also been developed by the same group. However, these conditions differ from the iodine and bromine counterparts in catalyst loading, halogen source, additives, and time. It was also observed that different conditions were needed depending on the electronic nature of the substrate and 3) lastly, there is still some uncertainty with respect to the mechanism. The authors of this work propose that C–H bond activation is the (rate determining step) RDS for the mechanism (KIE of 3.9). Subsequent work, done computationally on the mechanism for the bromination reaction, concluded that the reaction mechanism was controlled by the electronic nature of the substrate. Another key observation from this work was that the Rh oxidation state varied depending on the favored pathway.⁶² Because of the discrepancies in the proposed mechanism, and lack of experimental mechanistic evidence, we sought to develop a catalytic system based on the [Cp*Ir(III)] motif to further probe and understand the reaction mechanism.

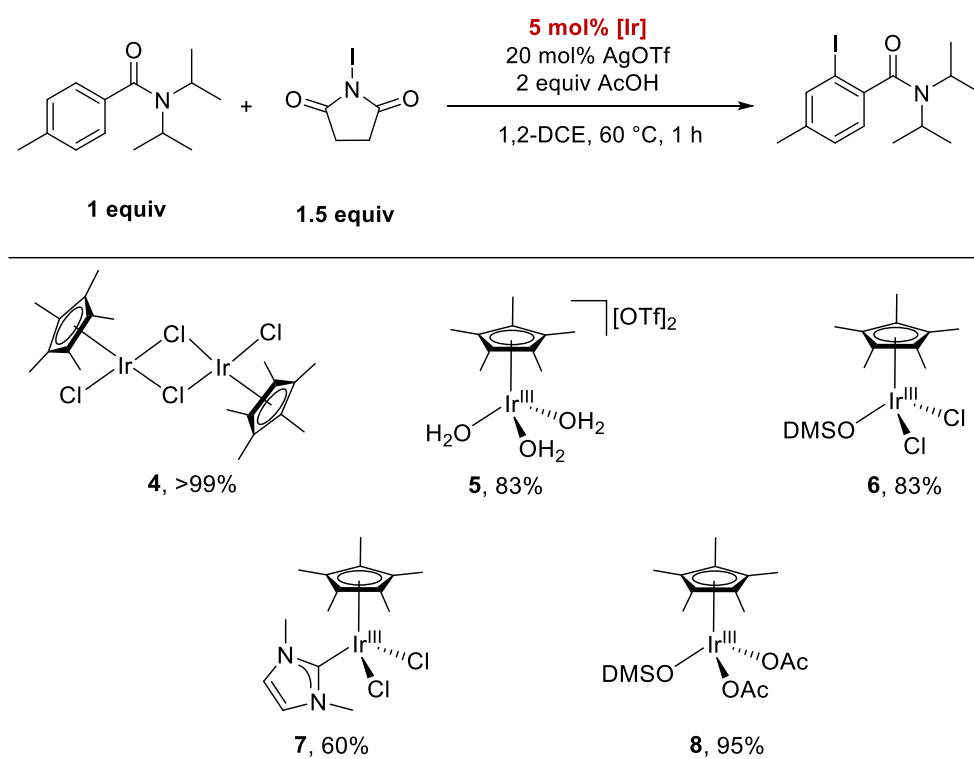
As shown in Chapter 1, arene C–H bonds can be activated and functionalized with a variety of [Cp*Ir(III)] catalysts using DG strategies. To address these mechanistic questions, an iridium system for the directed catalytic halogenation of benzamides was developed. Through detailed mechanistic experiments, isolation of intermediates and computational studies we aim to elucidate the reaction mechanism. Understanding the reaction mechanism will help to extend this chemistry not only towards the synthesis of other aromatic halides, but also to the functionalization of different types of C–H bonds.

Results and Discussion

Iodination Reaction Optimization

We began our studies on the directed halogenation of benzamides by Cp*Ir(III) complexes with a screening of several synthetically accessible Cp*Ir(III) complexes as catalysts for the reaction between 4-methyl-*N,N*-diisopropylbenzamide and *N*-iodosuccinimide according to **Scheme 2.6**. This benzamide was chosen as the model substrate due to the valuable spectroscopic handle (the CH₃ group) in the *para*-position for ¹H-NMR spectroscopy.

Scheme 2.6. Catalyst screening



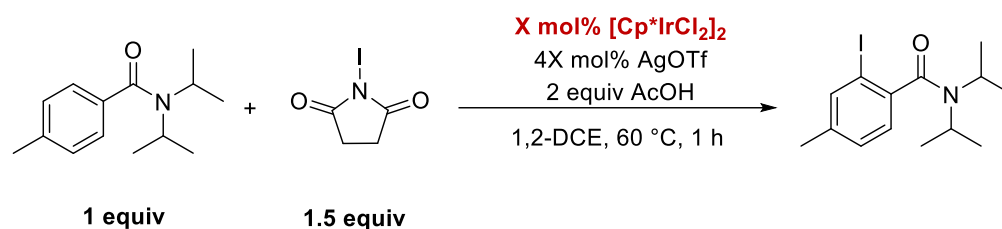
Reaction conditions: benzamide (0.25 mmol), succinimide (0.38 mmol), catalyst (0.013 mmol), AgOTf (0.05 mmol), AcOH (0.5 mmol), 1,2-dichloroethane (1 mL) in a 3 mL sealed reaction vessel at 60 °C for 1 h. %Conversion determined by integrating *p*-methyl protons of the starting material with respect to the corresponding protons of the product.

Of the complexes tested, full conversion was observed after 1 h for [Cp*IrCl₂]₂ (**4**), followed by the DMSO bis-acetate complex **8** with 95% conversion. Although complexes

4 and **8** seem like suitable catalysts for this reaction, catalyst **4** was utilized in future studies due to its simpler synthesis.

Attempts were then made to reduce the catalyst loading of complex **4** in the reaction. These results are summarized in **Table 2.1**. A difference in %conversion was not observed until the amount of iridium catalyst was reduced to 0.25 mol% (entry 5), this shows that the optimum amount of catalyst **4** is 0.5 mol% for product formation under these conditions (entry 4).

Table 2.1. Catalyst loading

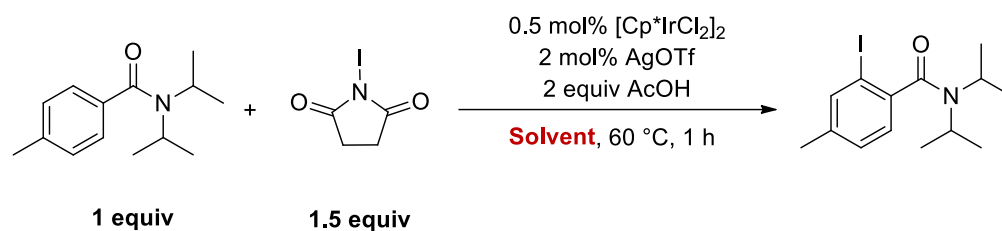


Entry	mol% (4)	%Conversion
1	5.0	> 99
2	2.5	> 99
3	1.0	> 99
4	0.5	> 99
5	0.25	75

%Conversion determined by integrating *p*-methyl protons of the starting material with respect to the corresponding protons of the product. Reaction conditions: benzamide (0.25 mmol), succinimide (0.38 mmol), AgOTf (four times the mmol of catalyst), AcOH (0.5 mmol), 1,2-dichloroethane (1 mL) in a 3 mL reaction vessel at 60 °C for 1 h.

Solvent Screening

With the optimal catalyst and catalyst loading for the reaction established in the previous section, the effect of solvent was then tested. A variety of common organic solvents with dielectric constants ranging from 2.02 to 37.5 were screened for their compatibility with the reaction. These results are summarized in **Table 2.2** and arranged in order of increasing solvent polarity.

Table 2.2. Solvent screening

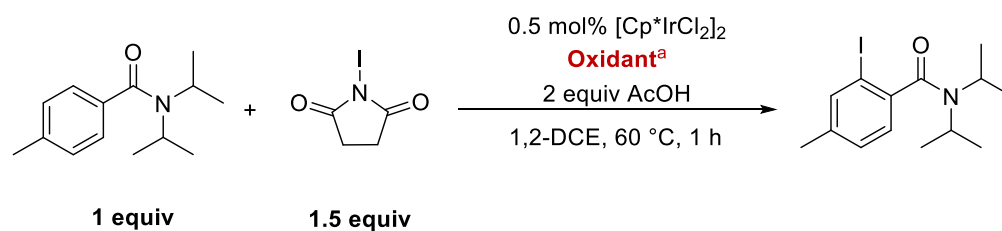
Entry	Solvent	Dielectric Constant	% conversion
1	Cyclohexane	2.02	54
2	Toluene	2.38	13
3	Chloroform	4.81	64
4	Ethyl Acetate	6.02	80
5	1,2-Dichloroethane	10.4	> 99
6	Methanol	32.7	9
7	Acetonitrile	37.5	2

%Conversion determined by integrating *p*-methyl protons of the starting material with respect to the corresponding protons of the product. Reaction conditions: benzamide (0.25 mmol), succinimide (0.38 mmol), catalyst (1.3×10^{-2} mmol), AgOTf (0.01 mmol), AcOH (0.5 mmol), Solvent (1 mL) in a 3 mL reaction vessel at 60 °C for 1 h.

There is no apparent trend in terms of the product yield as a function of the dielectric constant. Full conversion of the starting material to product was achieved in 1,2-dichloroethane. Solvents displayed in red indicate that the starting materials and catalyst were not soluble while those in black indicate that the starting materials and/or catalyst were soluble.

Additive and Oxidant Screening

With the optimal solvent and catalyst in hand, a screening of oxidants was pursued to determine if an oxidant is needed, and if so, which one works best for the catalyzed halogenation of benzamides.

Table 2.3. Oxidant screening

Entry	Oxidant (2 mol%)	% Conversion
1	AgOAc	15
2	AgOTf	> 99
3	AgCO ₃	ND
4	AgTFA	30
5	AgSO ₄	ND
6	Selectfluor	ND
7	Cu(OAc) ₂	ND
8	^t BuOOH	ND
9	H ₂ O ₂	ND
10 ^a	NaOTf	72

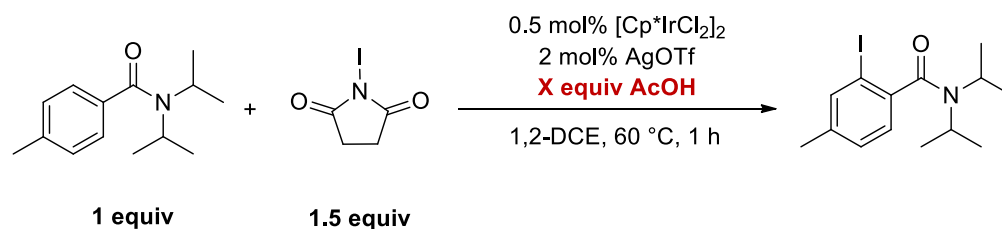
%Conversion determined by integrating *p*-methyl protons of the starting material with respect to the corresponding protons of the product. Reaction conditions: benzamide (0.25 mmol), succinimide (0.38 mmol), catalyst (1.3×10^{-2} mmol), oxidant (0.01 mmol), AcOH (0.5 mmol), 1,2-dichloroethane (1 mL) in a 3 mL reaction vessel at 60 °C for 1 h.^a Reaction conditions: benzamide (0.25 mmol), succinimide (0.38 mmol), $\text{Cp}^*\text{Ir}(\text{OH}_2)_3[\text{OTf}]_2$ (0.003 mmol), NaOTf (0.01 mmol), AcOH (0.5 mmol), 1,2-dichloroethane (1 mL) in a 3 mL reaction vessel at 60 °C for 1 h

A variety of silver (AgOAc, AgCO₃, AgOTf, AgTFA, AgSO₄) and copper (Cu(OAc)₂) metal oxidants as well as peroxides (^tBuOOH, H₂O₂) were screened. Silver sulfate and carboxylate type oxidants like silver acetate, silver trifluoroacetate and silver carbonate had low to no improvement on the yield of the product (entries 1, 3-5). On the other hand, the use of silver triflate gave full conversion of the halogenated product in 1 h (entry 2). The silver salt likely abstracts the chloride ligands from the iridium precatalyst to promote the formation of an iridium acetate species which may be the active catalyst.⁸¹ To test this hypothesis, other non-silver oxidants were examined. This was confirmed when formation of product was observed by changing the iridium chloride dimer precatalyst for the

Cp*Ir(OH₂)₃[OTf]₂ precatalyst, and replacing silver by sodium in entry 10. None of the other oxidants aided in product formation of the halogenated product (entries 6-9).

The effect of acetic acid in the reaction was also examined. These results are summarized in **Table 2.4**. It was found that acetic acid is needed for the reaction (entry 1). To verify this, we ran the reaction with silver acetate in the absence of acetic acid (entry 2). This demonstrates that not only is an acetate source needed, but an acidic proton is also required. One interesting result was the observation that two equivalents were needed for full conversion to the product (entry 4).

Table 2.4. Acid loading

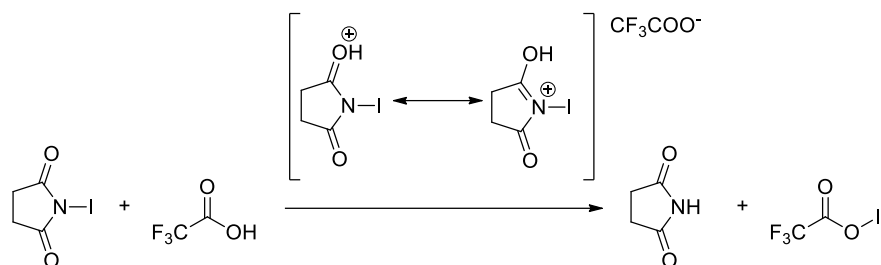


Entry	Equiv AcOH	% Conversion
1	0	ND
2 ^a	0	ND
3	1	30
4	2	> 99

%Conversion determined by integrating *p*-methyl protons of the starting material with respect to the corresponding protons of the product. Reaction conditions: benzamide (0.25 mmol), succinimide (0.38 mmol), catalyst (1.3x10⁻² mmol), AgOTf (0.01 mmol), 1,2-dichloroethane (1 mL) in a 3 mL reaction vessel at 60 °C for 1 h. ^aReaction conditions: benzamide (0.25 mmol), succinimide (0.38 mmol), AgOTf (0.01 mmol), 1,2-dichloroethane (1 mL) in a 3 mL reaction vessel at 60 °C for 1 h

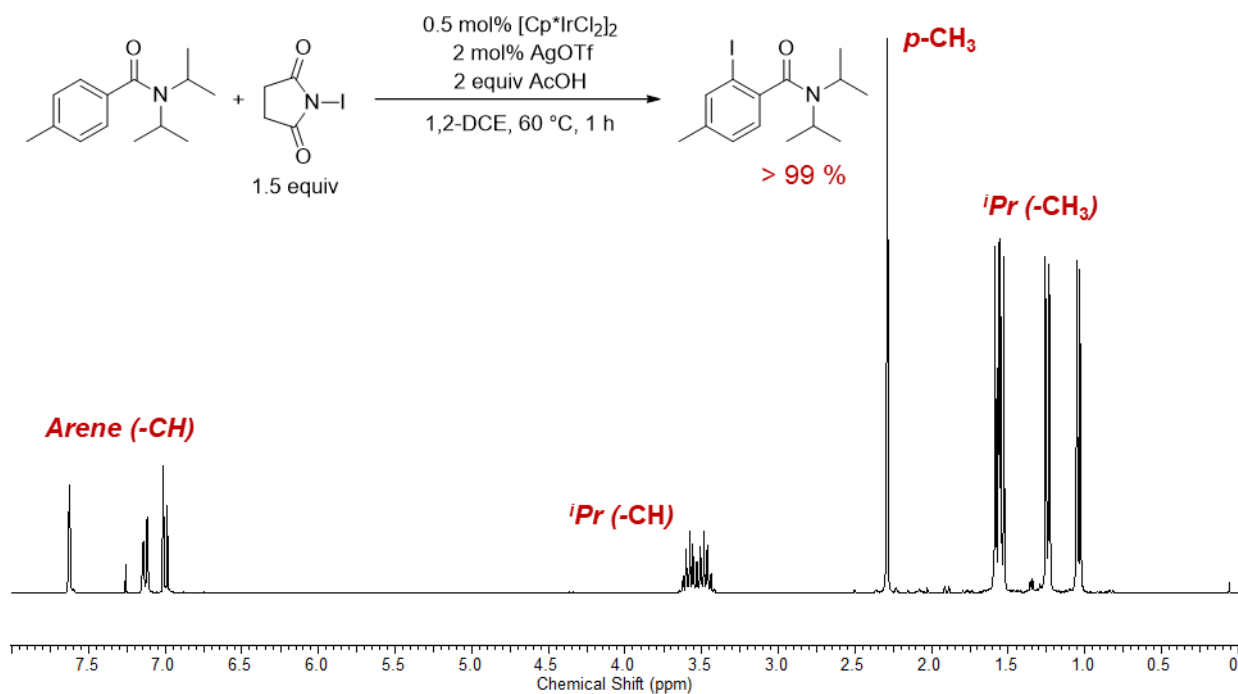
In 2002, Colobert and coworkers developed a system for the iodination of electron rich substrates based on *N*-iodosuccinimide and trifluoroacetic acid.⁶³ It was proposed that the active species for the iodination reaction was iodotrifluoroacetate which was generated *in situ* (**Scheme 2.7**), and can act as a reactive electrophilic iodine source. This would help rationalize the equivalents of acetic acid needed for the reaction and will be discussed in more detail in the upcoming section dealing with the reaction mechanism.

Scheme 2.7. Proposed mechanism for the formation of iodotrifluoroacetate



The optimized conditions (**Scheme 2.8**), in comparison to those developed by the Glorius group for the $[\text{Cp}^*\text{Rh(III)}]$ system, are milder and more efficient. Halogenation of the substrate is achieved at a lower catalyst loading (0.5 mol%). In addition, full conversion of the substrate is attained at a standard temperature of 60 °C after 1 h, as shown in the next section.

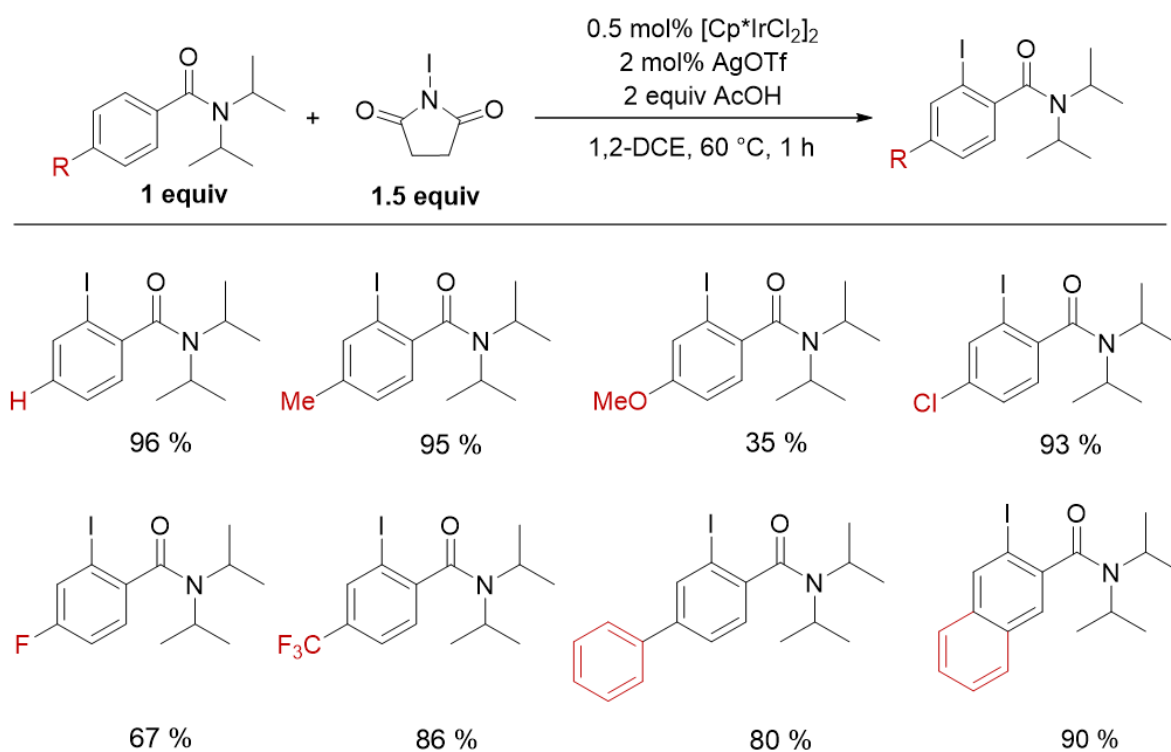
Scheme 2.8. Optimized reaction conditions for the iodination of benzamides with a representative $^1\text{H-NMR}$ spectrum for the model substrate.



Substrate Scope with Optimized Conditions

As shown in in **Scheme 2.8**, with the optimized conditions in hand, the scope of the reaction under study was examined. A variety of *para*-substituted *N,N*-diisopropylbenzamides were well tolerated under the optimized reaction conditions. The isolated yields for a series of iodinated products are shown in **Scheme 2.9**.

Scheme 2.9. Scope of iodinated *para*-substituted *N,N*-diisopropylbenzamides



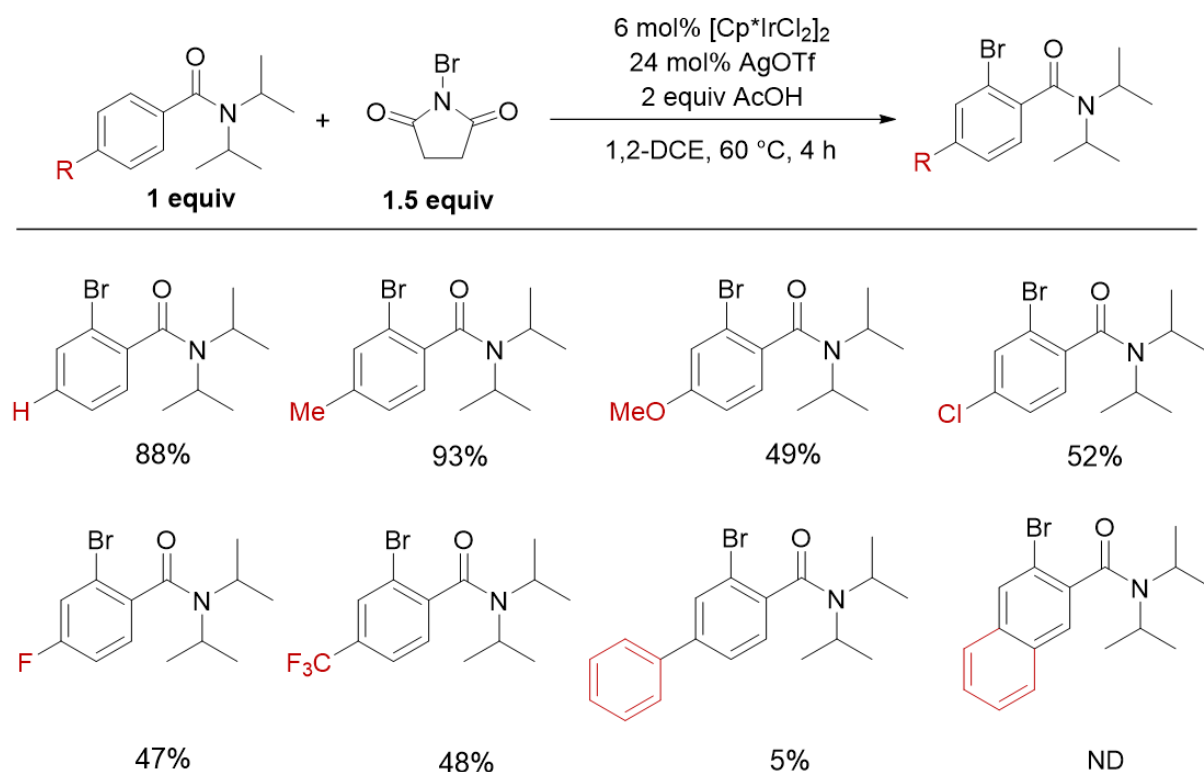
Overall, both electron donating and electron withdrawing groups were well tolerated under the optimized reaction conditions. In general, electron rich substrates gave better yields than electron poor substrates. It is worth noting that the 4-methoxy-*N,N*-diisopropylbenzamide was low yielding. Although we are still trying to rationalize this, the same result was observed in our previous work focused on the Cp*Ir(III)-catalyzed synthesis of isocoumarins.¹⁵ Based on the success of the iodination reaction, we sought to extend this chemistry to the analogous bromination reaction using *N*-bromosuccinimide (NBS) as the halogen source.

Bromination Reaction Optimization

Substrate Scope with Optimized Conditions

In our efforts to extend this chemistry to the analogous bromination reaction, we screened various reaction conditions with the use of *N*-bromosuccinimide (NBS) as a bromine source. The reaction proceeded smoothly with NBS as a suitable halogen source. Higher catalyst loadings (6 mol%), and reaction times (4 h) were required for full conversion of the model substrate. With the optimized conditions in hand, the substrate scope for this reaction was examined. A variety of *para*-substituted *N,N*-diisopropylbenzamides were tolerated under the optimized reaction conditions. The yields for a series of brominated products are shown in **Scheme 2.10**.

Scheme 2.10. Scope of brominated *para*-substituted *N,N*-diisopropylbenzamides



It is worth mentioning that lower yields were observed overall for all substrates for the bromination reaction. This is particularly true for the naphthyl substituted substrate, as no yield was observed by ¹H-NMR spectroscopy or GC.

Reaction Kinetics

Kinetic data were obtained to gain further insight into the mechanism for the halogenation of these substrates. For these studies, *N,N*-diisopropylbenzamide was used as the model substrate as it was observed to be higher yielding in both cases and is commercially available. Gas chromatography (GC) was chosen as a convenient method for sampling and monitoring the consumption of the starting material *N,N*-diisopropylbenzamide and the production of the halogenated product. To begin, a GC method under 15 min was developed and calibration curves using hexafluorobenzene as an internal standard were generated to quantify the amount of starting material and product in solution (**Figures 2.2. and 2.3.**).

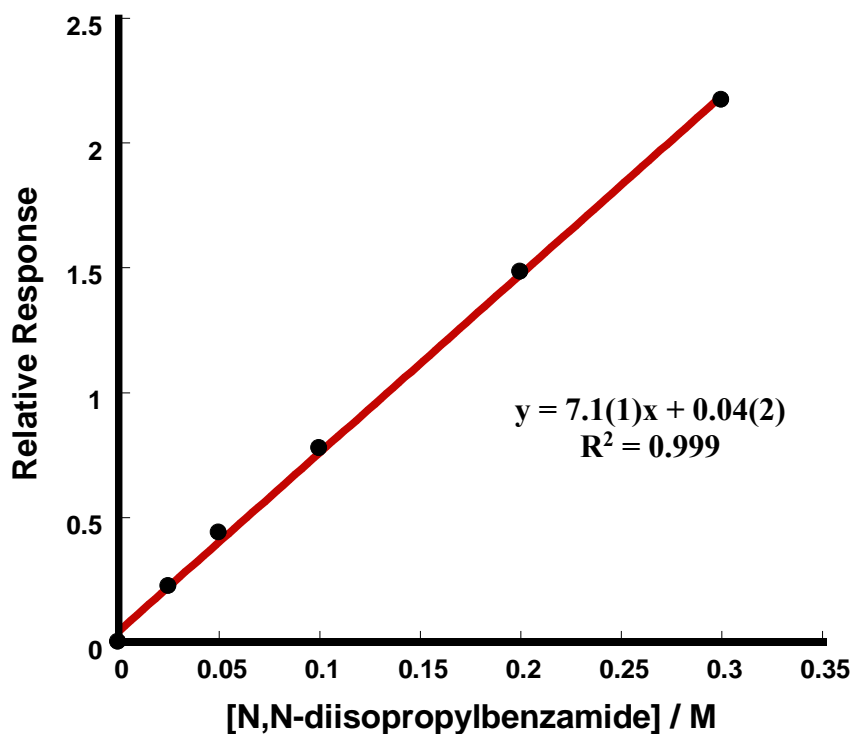


Figure 2.2. GC calibration curve for *N,N*-diisopropylbenzamide

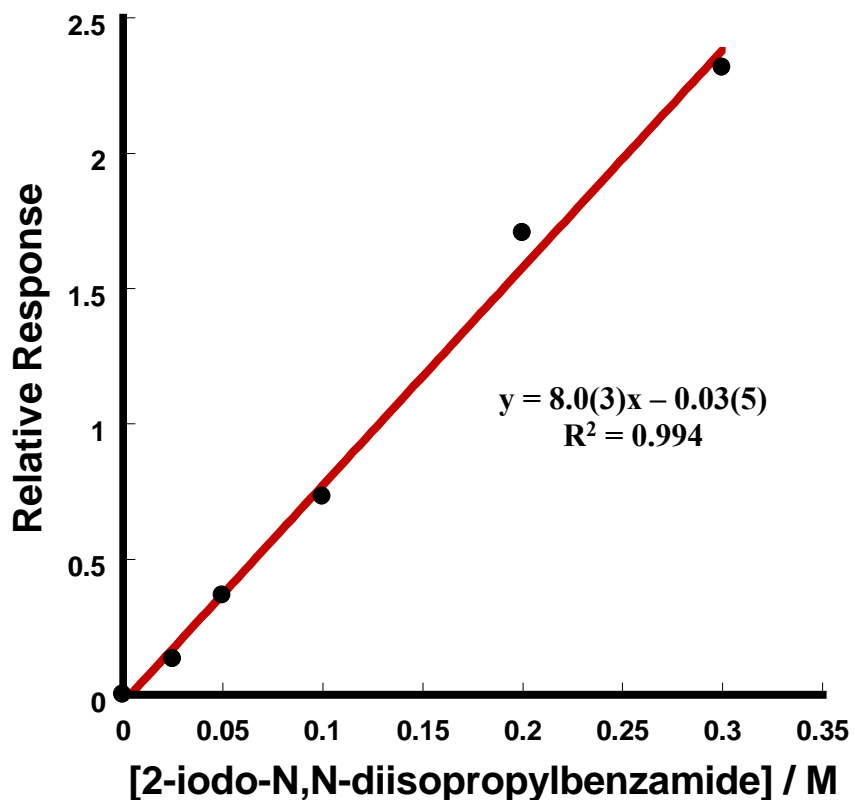


Figure 2.3. GC calibration curve for iodinated product

Having developed a method to quantify the reaction, the time course was monitored under the optimized conditions. The reaction time course under the optimized reaction conditions is shown in **Figure 2.4**. Both the consumption of starting material and appearance of product occur at approximately the same rate (within error) indicating that the reaction proceeds directly to product with no side reactions.

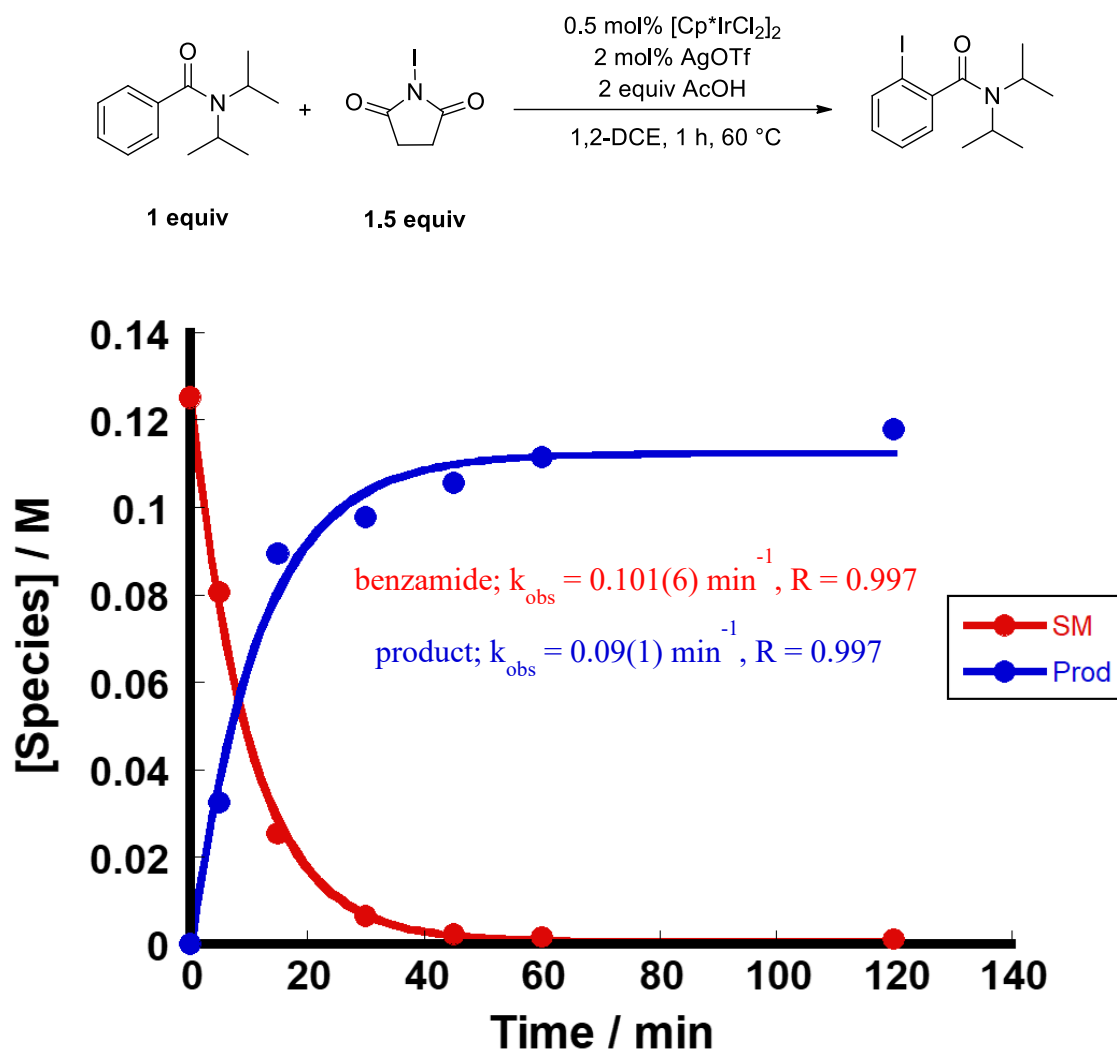


Figure 2.4. Time profile for the iodination of *N,N*-diisopropylbenzamide

Reaction conditions: benzamide (0.25 mmol), succinimide (0.38 mmol), AgOTf (0.1 mmol), AcOH (0.5 mmol), 1,2-DCE (2 mL). Concentration of the reactant was determined by dividing the reactant area by the area of the internal standard peak and calculated based on the fit equation from the calibration curve for each respective reactant.

Next, the dependence of the reaction was probed with respect to iridium, benzamide and *N*-iodosuccinimide by measuring the full-time profile of the reaction at various catalyst loadings and ratios respectively. The k_{obs} for each profile can be extracted and plotted against the varying concentration of the species to obtain the dependence of the reaction on that species. Increasing the catalyst loading and benzamide concentration resulted in an increase of the reaction rate. On the other hand, increasing the

concentration of *N*-iodosuccinimide resulted in no change of the reaction rate. The results for these experiments are summarized in **Figures 2.5.-2.11**.

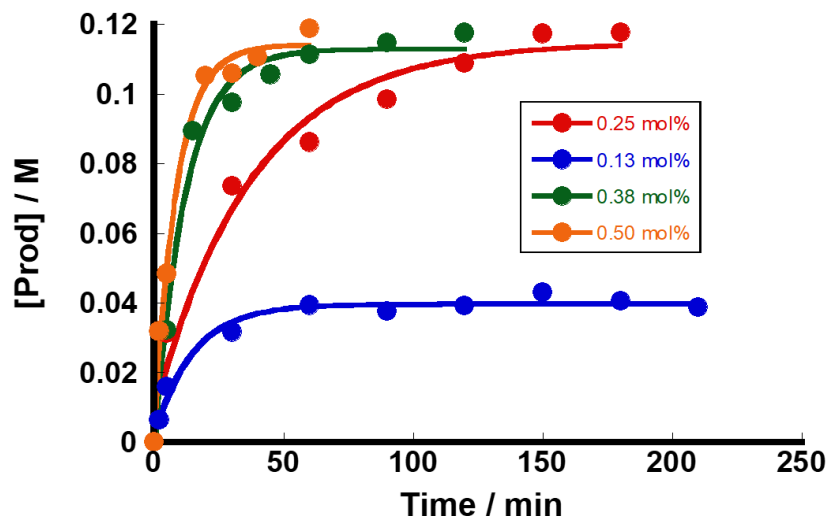


Figure 2.5. Time profiles for the iodination of *N,N*-diisopropylbenzamide at various catalyst loadings

Time profiles for the iodination of *N,N*-diisopropylbenzamide at various catalyst loadings. Reaction conditions: benzamide (0.25 mmol), succinimide (0.38 mmol), AcOH (0.5 mmol), 1,2- dichloroethane (2 mL). Concentration of the reactant was determined by dividing the reactant area by the area of the internal standard peak and calculated based on the fit equation from the calibration curve for each respective reactant.

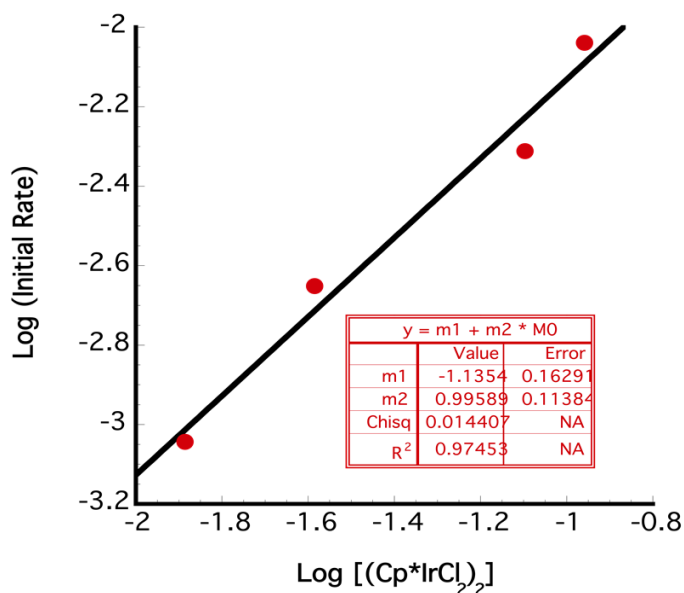


Figure 2.6. Plot for the dependence of the reaction on iridium $(Cp^*Ir_2Cl_2)_2$

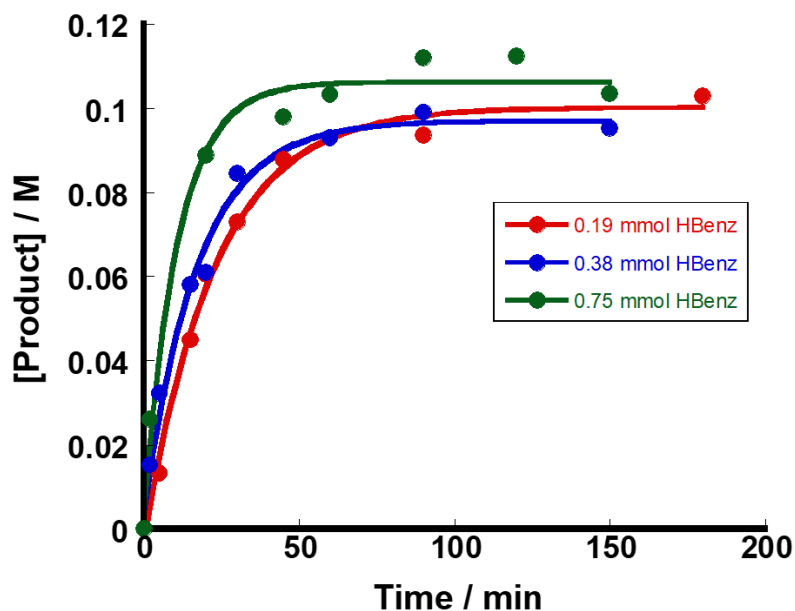


Figure 2.7. Time profiles for the iodination of *N,N*-diisopropylbenzamide at various concentrations of benzamide

Time profiles for the iodination of *N,N*-diisopropylbenzamide at various concentrations of Benzamide. Reaction conditions: $(\text{Cp}^*\text{IrCl}_2)_2$, (0.714, μmol), succinimide (0.188 mmol), AcOH (0.5 mmol), 1,2-dichloroethane (2 mL). Concentration of the reactant was determined by dividing the reactant area by the area of the internal standard peak and calculated based on the fit equation from the calibration curve for each respective reactant.

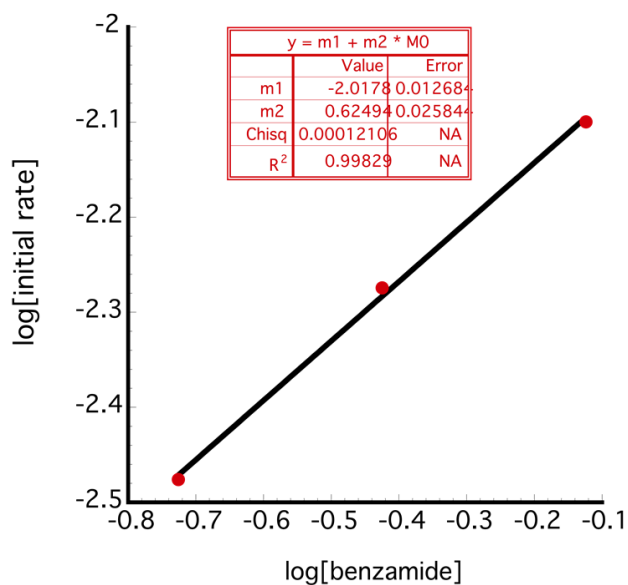


Figure 2.8. Plot for the dependence of the reaction on *N,N*-diisopropylbenzamide

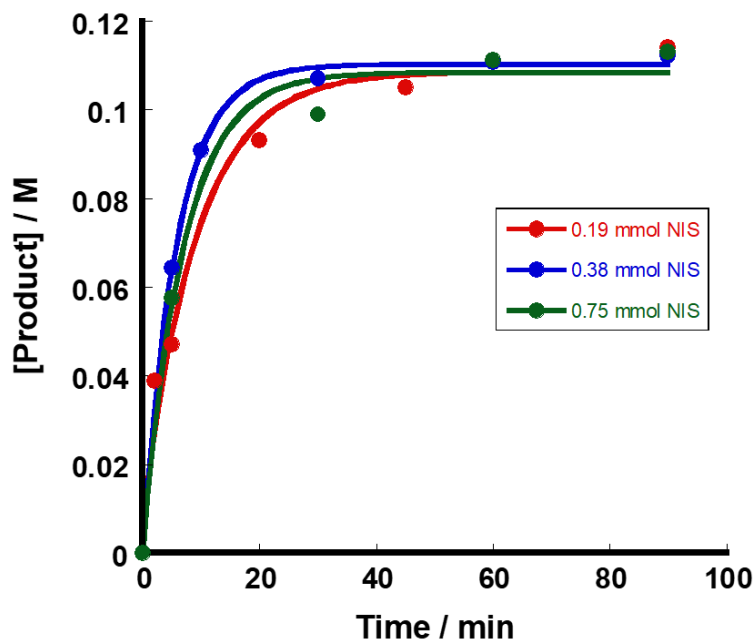


Figure 2.9. Time profiles for the iodination of *N,N*-diisopropylbenzamide at various concentrations of *N*-iodosuccinimide

Time profiles for the iodination of *N,N*-diisopropylbenzamide at various concentrations of *N*-iodosuccinimide. Reaction conditions: $(\text{Cp}^*\text{IrCl}_2)_2$, (0.714 μmol), benzamide (0.188 mmol), AcOH (0.5 mmol), 1,2-dichloroethane (2 mL). Concentration of the reactant was determined by dividing the reactant area by the area of the internal standard peak and calculated based on the calibration curve for each respective reactant.

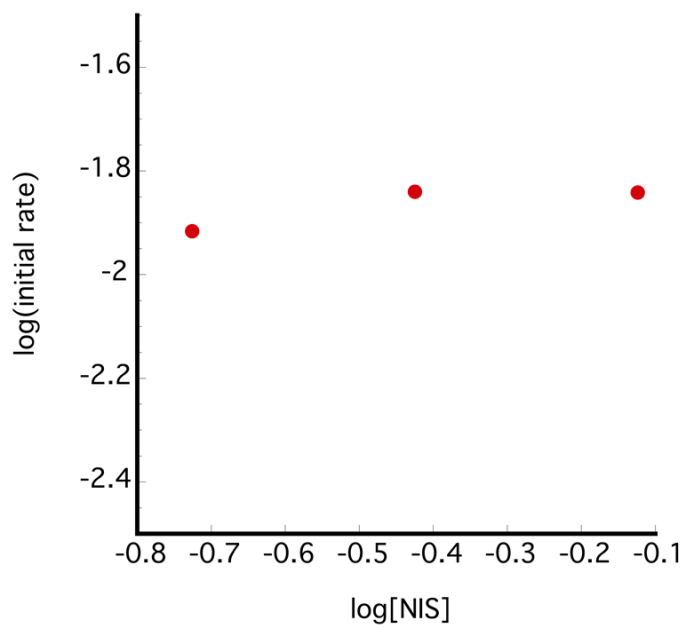


Figure 2.10. Plot for the dependence of the reaction on *N*-iodosuccinimide

The reaction was observed to have a positive order dependence with respect to benzamide, and iridium, and approximately a zeroth order dependence on *N*-iodosuccinimide. Traditionally, proposed mechanisms for directed C–H activation begin with coordination of the substrate to the metal center, followed by C–H activation. An H/D kinetic isotope effect experiment was undertaken to determine if C–H activation occurs prior to or during the turnover limiting step of the reaction. The rate of the reaction was measured independently using **1a** and *d*₅-*N,N*-diisopropylbenzamide. The reaction with *d*₅-benzamide was found to be approximately half as fast as the reaction with the fully protiated substrate, resulting in a KIE (k_H/k_D) of 2.5. The observed value for the KIE is significant and suggests that C–H activation occurs prior to or during the turnover limiting step for the mechanism (Figure 2.10).⁸³

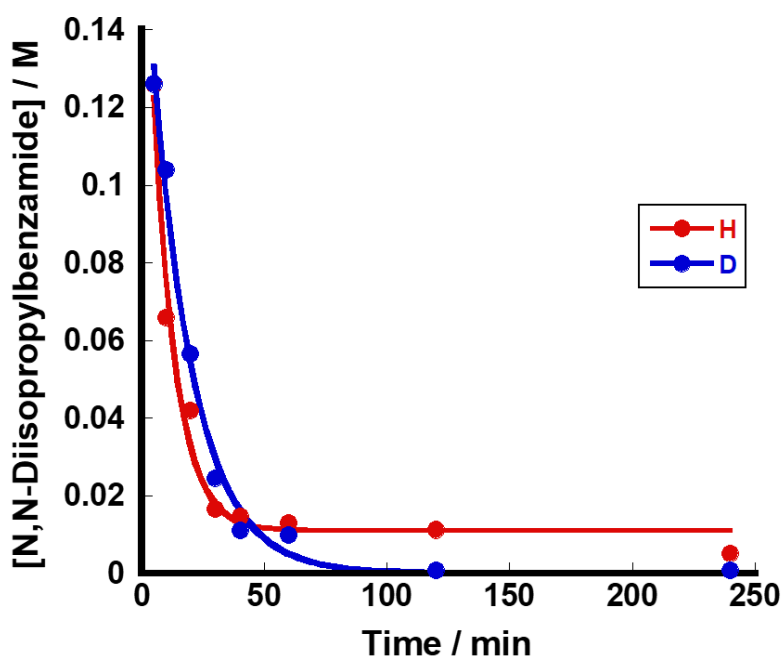


Figure 2.11 Plot for the KIE by Parallel reactions of *N,N*-diisopropylbenzamide (red) and *N,N*-diisopropylbenzamide-*d*₅ (blue)

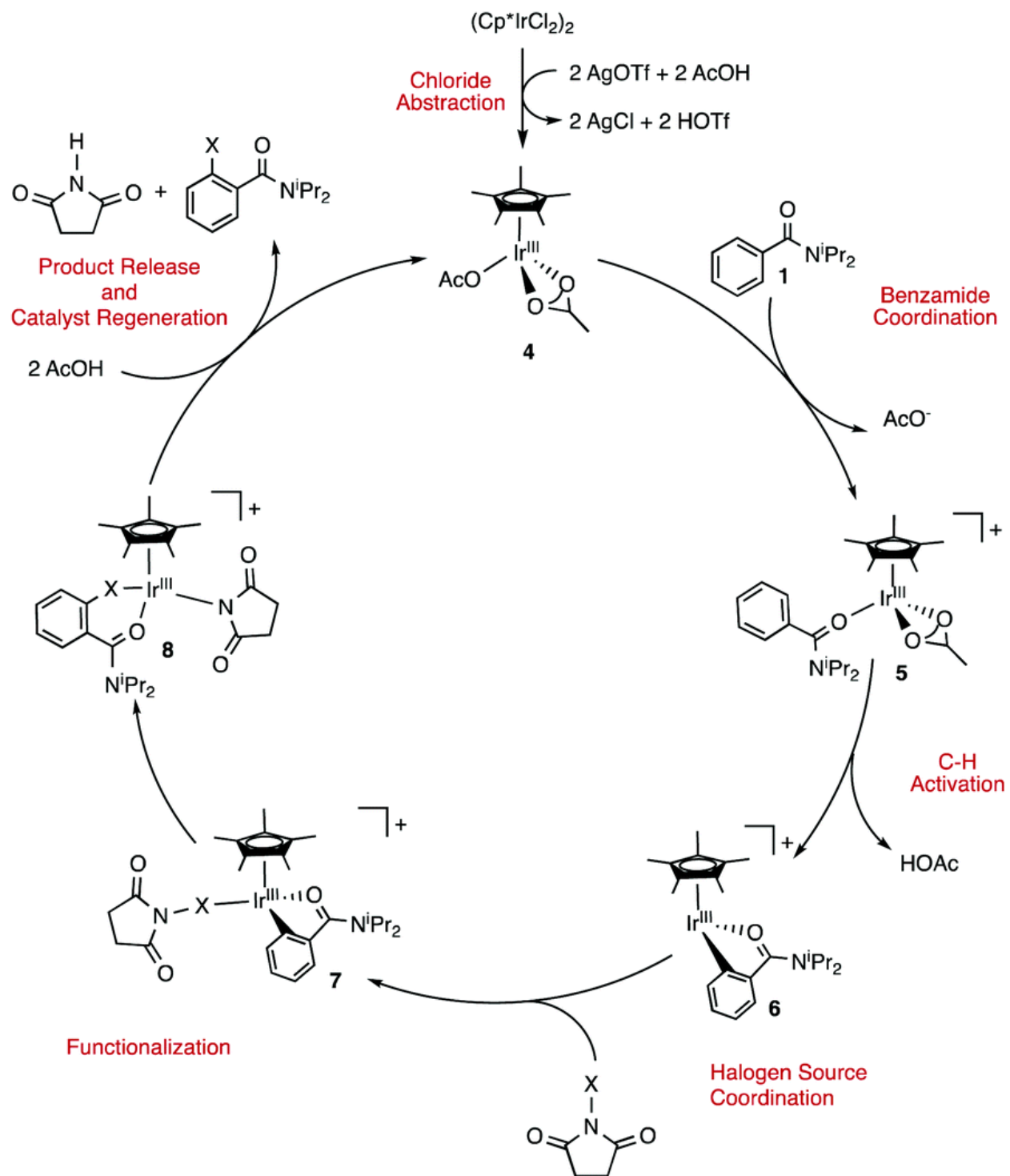
Plot for the KIE by parallel reactions of *N,N*-diisopropylbenzamide (red) and *N,N*-diisopropylbenzamide-*d*₅ (blue). Reaction conditions: (Cp^*IrCl_2)₂, (0.158 μmol), benzamide (0.25 mmol), benzamide-*d*₅ succinimide (0.38 mmol), AgOTf (0.1 mmol), AcOH (0.5 mmol), 1,2-dichloroethane (1 mL). Concentration of the reactant was determined by dividing the reactant area by the area of the internal standard peak and is calculated based on the calibration curve for each respective reactant. The initial rates were obtained from a fifth-order polynomial fit of the concentration-time profile, as in $[\text{benzamide}]_t = [\text{benzamide}]_0 - m_1t - m_2t^2 - \dots - m_5t^5$, from which $V_i = m_1$. This analysis gives a KIE ($k_H/k_D = 2.5$).

Mechanistic Proposal

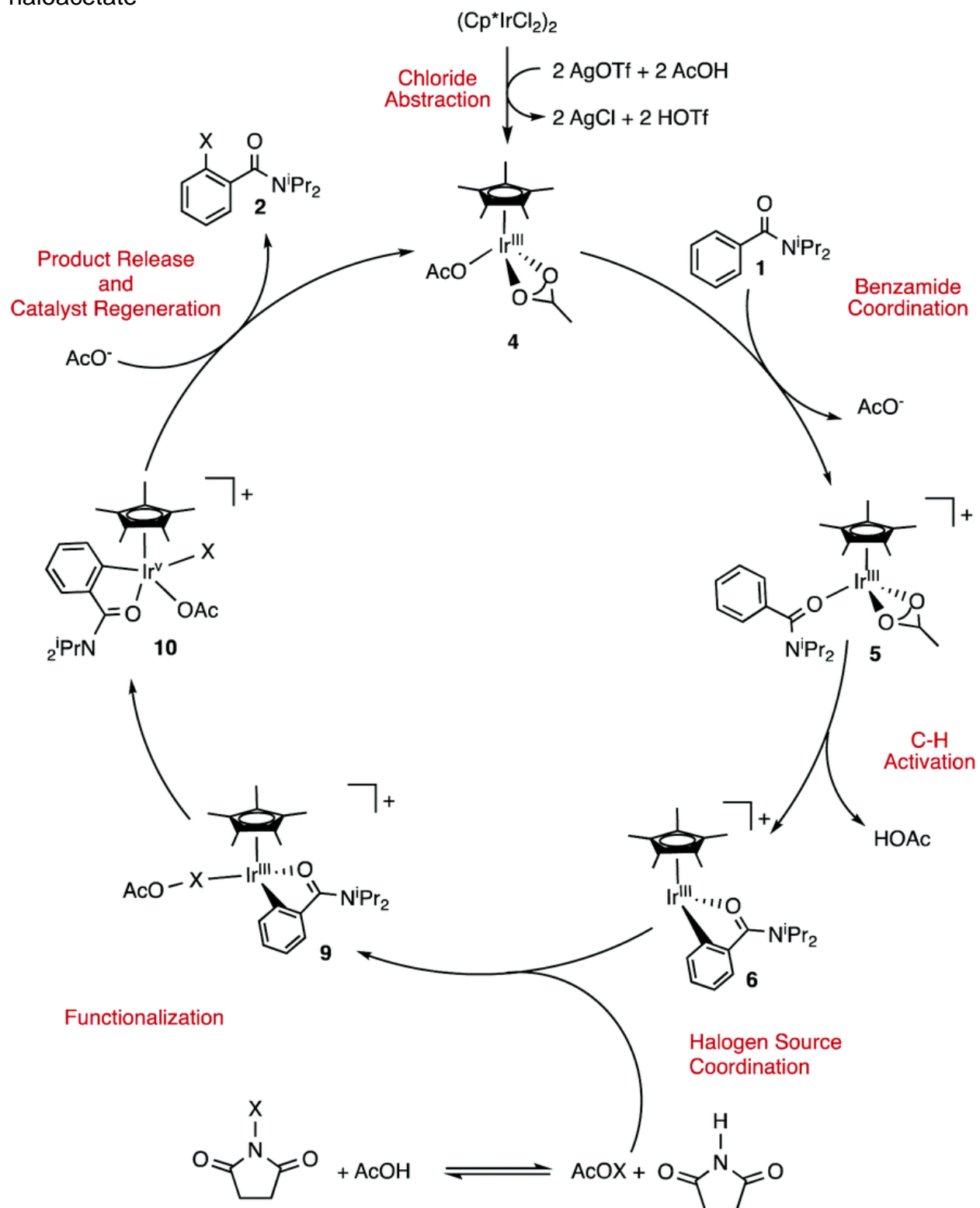
Based on the data, two preliminary mechanisms are proposed where the functionalization step differs in the halogen source. The first mechanism begins with chloride abstraction from $[\text{Cp}^*\text{IrCl}_2]_2$ by AgOTf to generate the active $\text{Cp}^*\text{Ir}(\text{OAc})_2$ complex **9**. Benzamide coordination then occurs displacing the κ_1 acetate ligand to form the $\text{Cp}^*\text{Ir}(\text{III})$ -benzamide complex **10**. C–H activation can then occur to form the cyclometallated iridacycle **11** with formation and loss of acetic acid. Incoming halosuccinimide then coordinates to the iridium center to form complex **12**. Halogenation can then occur to form complex **13**, and two equivalents of acetic acid to regenerate the active $\text{Cp}^*\text{Ir}(\text{III})$ complex (**Scheme 2.11**).

The lack of an observed dependence in halosuccinimide suggests that this species may not be the active halogen source. An alternative mechanism is proposed, where a haloacetate species is produced *in situ*, from an off-cycle equilibrium between acetic acid and the halosuccinimide, and this species acts as the active halogen source. This haloacetate can coordinate to the iridium center to form complex **14**. Upon coordination, halogenation of the substrate can occur forming complex **15**, and one equivalent of acetic acid regenerates the $\text{Cp}^*\text{Ir}(\text{III})$ catalyst (**Scheme 2.12**).

Scheme 2.11. Proposed mechanism for the halogenation of benzamides from halosuccinimide



Scheme 2.12. Proposed mechanism for the halogenation of benzamides from haloacetate



Stoichiometric Reactivity

Cp*Ir(DMSO)(Benz)(6(DMSO))

An analogous cyclometalated complex, stabilized by DMSO, to the proposed complex **6**, has been successfully synthesized and characterized (**Figure 2.12**). A 1 : 1 : 1 ratio of Cp*Ir(DMSO)Cl₂, *N,N*-diisopropylbenzamide and acetic acid was treated with two equivalents of silver triflate, to abstract the chlorides from the iridium complex and generate the cyclometalated complex, **6(DMSO)** as a yellow solid in 90% yield. This complex has been characterized by ¹H, ¹³C-NMR spectroscopy, and elemental analysis. The X-ray crystal structure for **6(DMSO)** is shown in **Figure 2.13**. Bond lengths and angles are similar to the analogous complex with a benzoate ligand that has been previously reported by our group.¹⁵

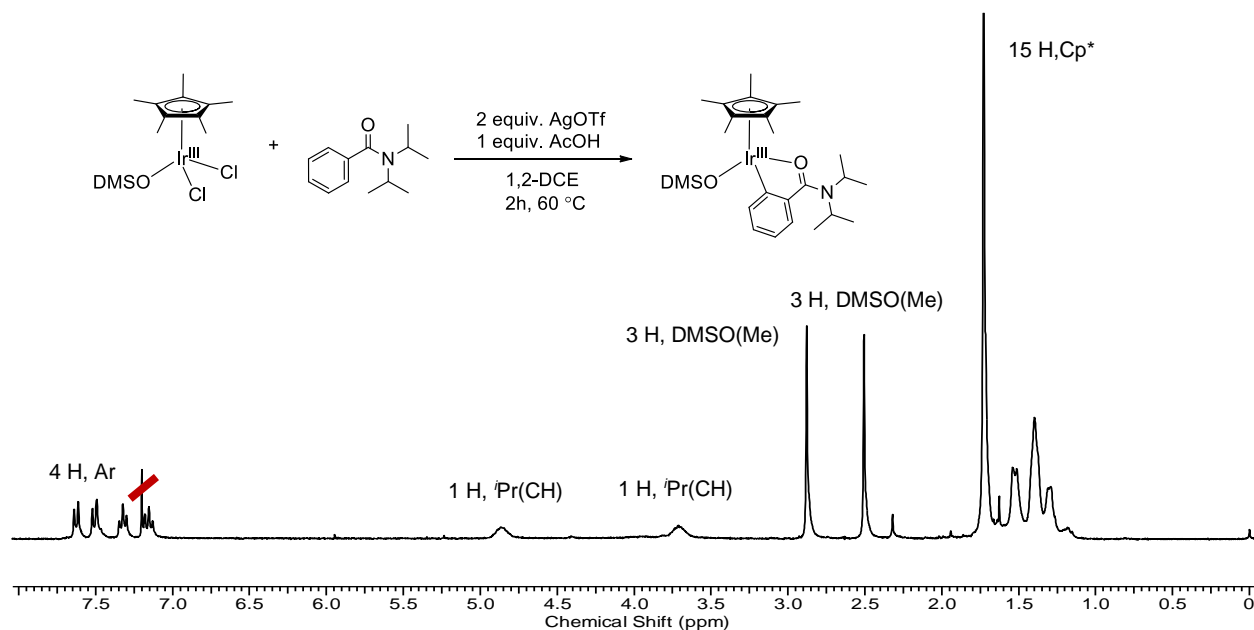


Figure 2.12. ¹H-NMR spectrum of Cp*Ir (DMSO) (Benz) (**6(DMSO)**) in CDCl₃

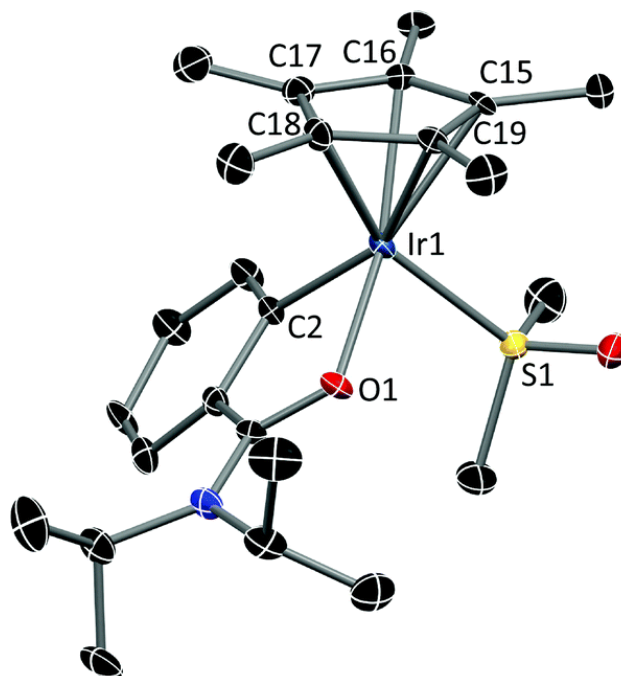


Figure 2.13. X-ray crystal structure of **6(DMSO)**. Thermal ellipsoid plot (50% ellipsoids) of cationic fragment of 6(DMSO). The triflate anion is omitted for clarity. Selected bond lengths (Å): Ir1-S1, 2.267; Ir1-O1, 2.115; Ir1-C2, 2.036; Ir1-Cp*(average), 2.209.

Formation and Reactivity of IOAc

Recently, hypervalent iodine reagents have gained interest in the synthetic community for the oxidative functionalization of hydrocarbons as an alternative source of electrophilic iodine.^{63, 65, 66} This has been accomplished through the stabilization of iodine by either neutral or anionic ligands.⁶⁷⁻⁷¹ Although these dioxiodanes have only been used for the oxyiodination of alkenes and alkynes, it was proposed that the active halogen source is the haloacetate monomer generated *in situ* from the acid promoted decomplexation.

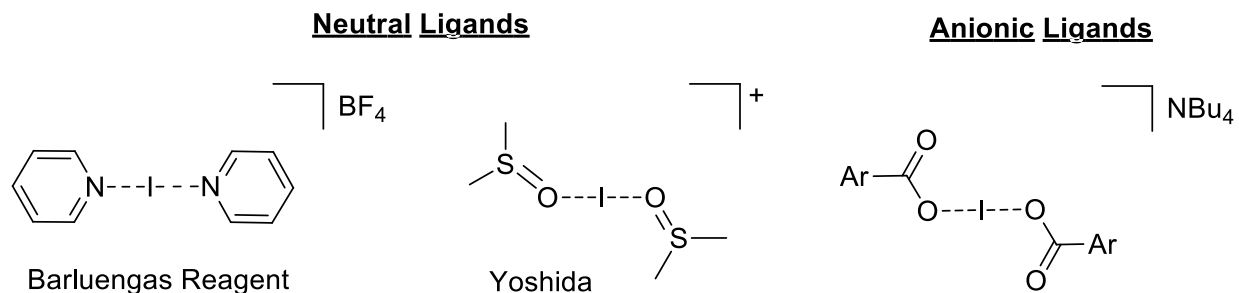


Figure 2.14. Examples of stable iodine(I) compounds

Based on this work we were interested in studying the reactivity of the isolated cyclometalated intermediate towards both the iodoacetate and *N*-iodosuccinimide. We began by generating iodoacetate *in situ* from molecular iodine and silver acetate. The presence of the haloacetate was confirmed by ¹H-NMR spectroscopy. This mixture, with a known concentration of iodoacetate, was then filtered and added to a solution of the iridium complex **6(DMSO)**. A ¹H-NMR spectrum of the crude reaction mixture shows clear product formation after the reaction time.

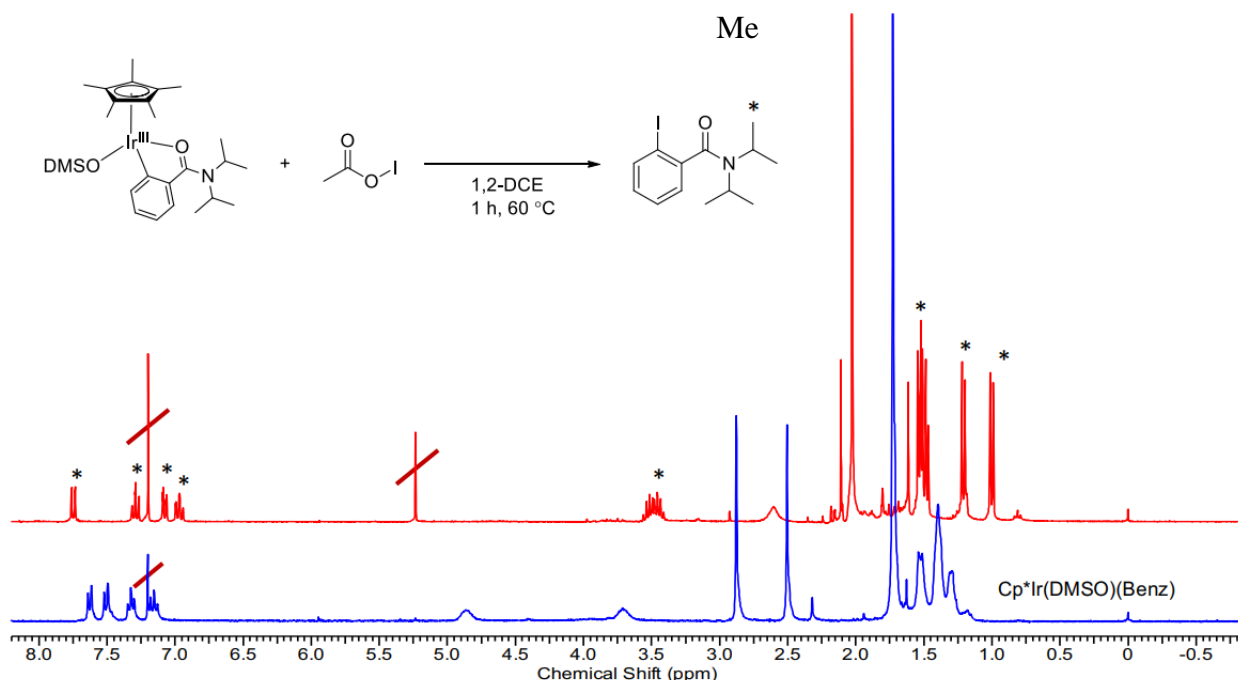


Figure 2.15. $^1\text{H-NMR}$ spectrum of $\text{Cp}^*\text{Ir}(\text{DMSO})(\text{Benz})$ (**6(DMSO)**) in CDCl_3

Acetyl Hypoiodite Reactivity

Based on the results from the stoichiometric studies of **6(DMSO)** and the acetyl hypoiodite generated by combining silver acetate (AgOAc) and iodine (I_2), as shown in **Figure 2.15**, we decided to explore the formation of this species under our reaction conditions. From the $^1\text{H-NMR}$ spectrum (**Figure 2.16**) of a solution containing *N*-halosuccinimide with tetrabutylammonium acetate (TBAOAc), a shift can be observed for the signal corresponding to the methyl of the acetate group from 1.95 ppm (TBAOAc) to 2.70 ppm (NIS) and to 2.85 ppm for NCS. The corresponding complex from NIS and TBAOAc, was further characterized by X-ray crystallography as shown in **Figure 2.17**. As expected, the structure features an approximately linear geometry (174°) around the central iodine atom. The iodine–oxygen bond length is significantly longer (2.29 \AA) than an analogous benzoate complexes reported by Muniz and co-workers ($2.16\text{--}2.20 \text{ \AA}$).⁸⁴

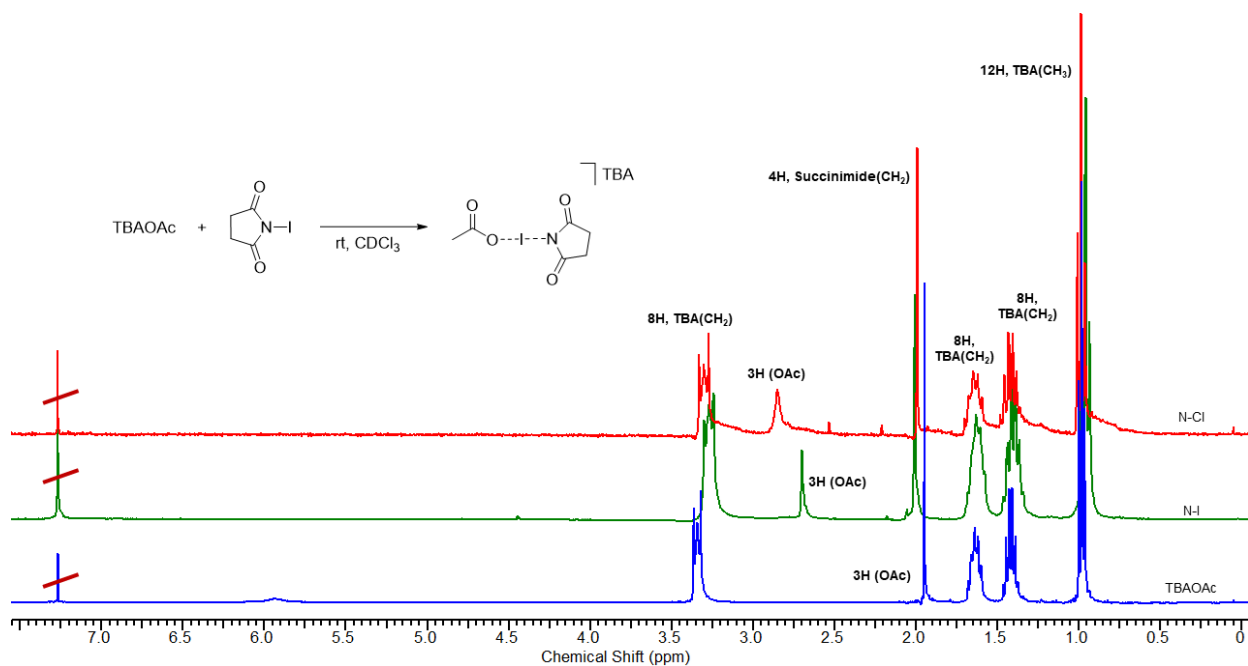


Figure 2.16. $^1\text{H-NMR}$ spectrum of the halosuccinimide in the presence of tetrabutylammonium acetate at room temperature in CDCl_3

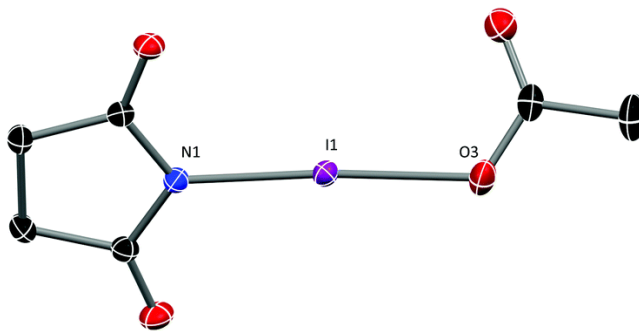
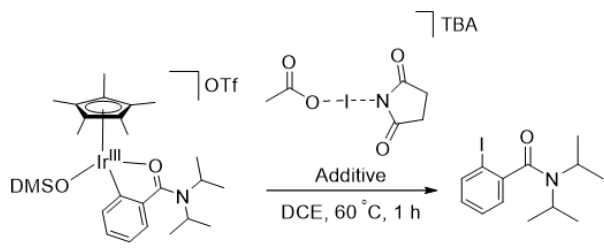


Figure 2.17. X-ray crystal structure of SuccIOAc adduct. Thermal ellipsoid plot (50% ellipsoids) for the anion in $[(\text{C}_4\text{H}_4\text{O}_2\text{N})\text{I}(\text{OCOCH}_3)][\text{Bu}_4\text{N}]$. The cation has been omitted for clarity. Selected bond lengths (\AA) and angles: N1-I1-O3 , 174° ; I1-O3 , 2.293 ; I1-N1 , 2.166 . Tetrabutylammonium counterion is not shown for clarity.

This acetyl hypoiodite adduct was then examined as a halogen source (**Table 2.5**). In the absence of a proton source very little reactivity was observed, **Table 2.5** (entry 1). When a polar protic solvent was utilized, or two equivalents of H_2O , were included as an additive, significant yields of the iodinated benzamide from complex **6(DMSO)** were observed (entries 3–10). These results suggest that an acidic proton is needed to generate the active $\text{I}(\text{OAc})$ species *in situ*. It should also be noted that protic sources with

coordinating counterions like acetate could result in the formation of other stabilized complexes which are less reactive. This was demonstrated when $[\text{I}(\text{OAc})_2](\text{TBA})$ (Table 2.5, entry 2) was utilized. Moreover, a bis-succinimide stabilized complex was identified by X-ray crystallography in the reaction of NIS with TBAOAc.

Table 2.5. Stoichiometric reactivity for acetyl hypoiodite adduct with **6(DMSO)**



Entry	Solvent	Additive	% conversion
1	DCE	-	10
2*	DCE	-	Traces
3	DCE	2 equiv H ₂ O	63
4	MeCN	-	20
5	MeCN	2 equiv H ₂ O	37
6	MeOH	-	27
7	MeOH	2 equiv H ₂ O	34
8	^t AmylOH	-	52
9	^t AmylOH	2 equiv H ₂ O	75

General reaction conditions: 15 mg (0.02 mmol) of **6(DMSO)**, (0.02 mmol) of the halogen source, and (0.04 mmol) of an additive in 1 mL of 1,2-dichloroethane under air. Percent conversion was determined by GC with the use of hexafluorobenzene as an internal standard. ^aThe halogen source was changed to $[\text{I}(\text{OAc})_2](\text{TBA})$.

Computational Mechanistic Analysis

Previously, when our group investigated the Cp*Ir(III)-catalyzed synthesis of isocoumarins from benzoic acids and alkynes, a computational mechanistic analysis was carried out to further understand the mechanism for the reaction under study.^{15,72} This approach was applied to our system to gain further mechanistic insight. Specifically,

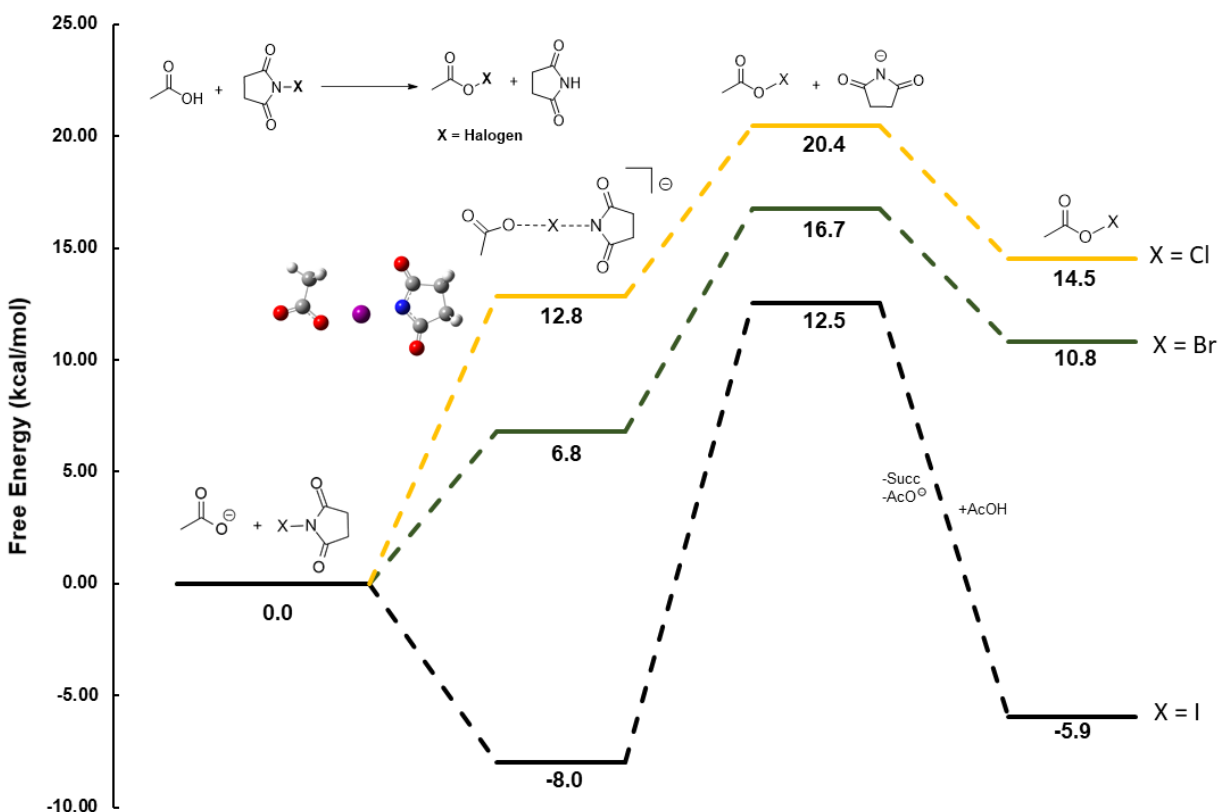
efforts were focused on the mechanism for acetyl hypoiodite formation, C–H bond activation, and the nature of the functionalization step.

This study was carried out using density functional theory (DFT) with the Gaussian09,⁷³ implementation of the B3PW91 functional.⁷⁴ All geometry optimizations were carried out using tight convergence criteria (“opt=tight”) on an ultrafine grid (“int=ultrafine”). The Stuttgart-Dresden (SDD) relativistic effective core potential (RECP) basis set was used for iridium with an additional f polarization function.^{75, 76} The def2-TZVP effective core potential (ECP)^{77, 78} and basis set was used for the halogens. The 6-31G** basis set was used for all other atoms. Solvation energies were computed with geometries optimized in the gas phase using the SMD method,⁷⁹ with dichloroethane as the solvent, as implemented in Gaussian 09. In this method an IEFPCM calculation is performed with radii and electrostatic terms from Truhlar and co-workers’ SMD solvation model.⁸⁰ Energetics were calculated using the 6-311++G** basis set for all atoms and the SDD basis set with an added f polarization function on iridium. The def2-TZVP ECP and basis set was used for the halogens. All energies are reported in kcal/mol. This investigation was divided into two steps to probe each of the steps in the catalytic cycle: C-H activation and functionalization.

Acetyl Hypoiodite Formation

We began our computational study by modeling the formation of the proposed acetyl hypohalite by the association of acetate anion with NXS (X = Cl, Br, I) computationally (**Scheme. 2.13**). The association to form **12** is exergonic ($\Delta G^\circ = -5.9$ kcal mol⁻¹) for X = I, but endergonic for X = Br ($\Delta G^\circ = 10.8$ kcal mol⁻¹) and X = Cl, ($\Delta G^\circ = 14.5$ kcal mol⁻¹). The results are consistent with the observed catalytic reactions as iodination was most facile, followed by bromination (which required higher temperature and catalysts loadings). However, chlorination was not observed under any catalytic conditions.

Scheme 2.13. DFT (B3PW91-D3) calculated energetics for the association of acetate anion (OAc) with *N*-halosuccinimide in 1,2-dichloroethane solvent.

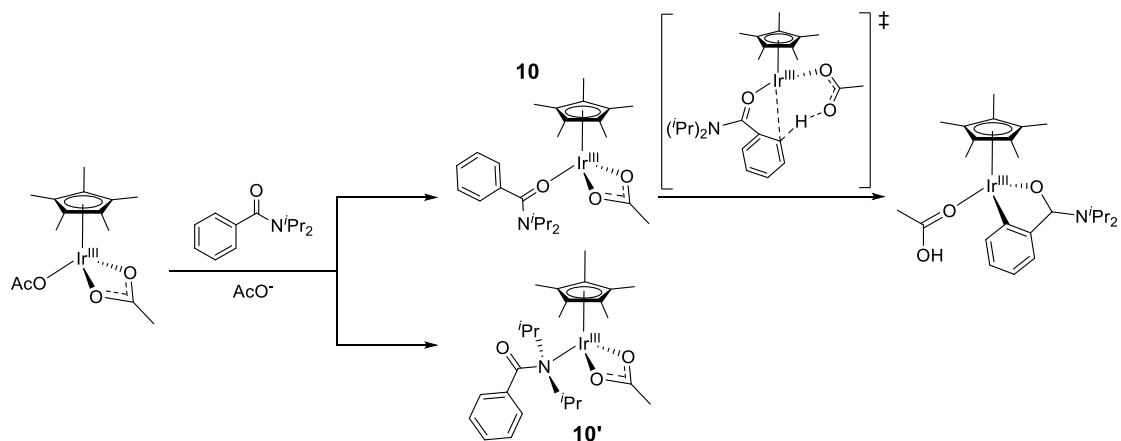


C–H Activation Step

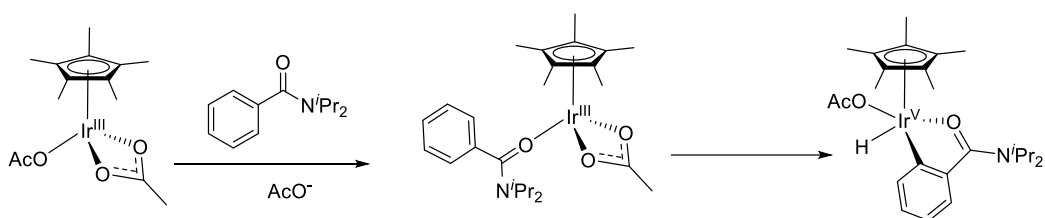
For simplicity, the halogenation of *N,N*-diisopropylbenzamide was modelled. For the C–H activation step of the mechanism, both a (concerted-metalation–deprotonation) CMD⁸⁵ (**Scheme 2.14 A**) and a direct oxidative addition pathway were considered (**Scheme 2.14 B**).

Scheme 2.14.

A) CMD Pathway for C–H Bond Activation

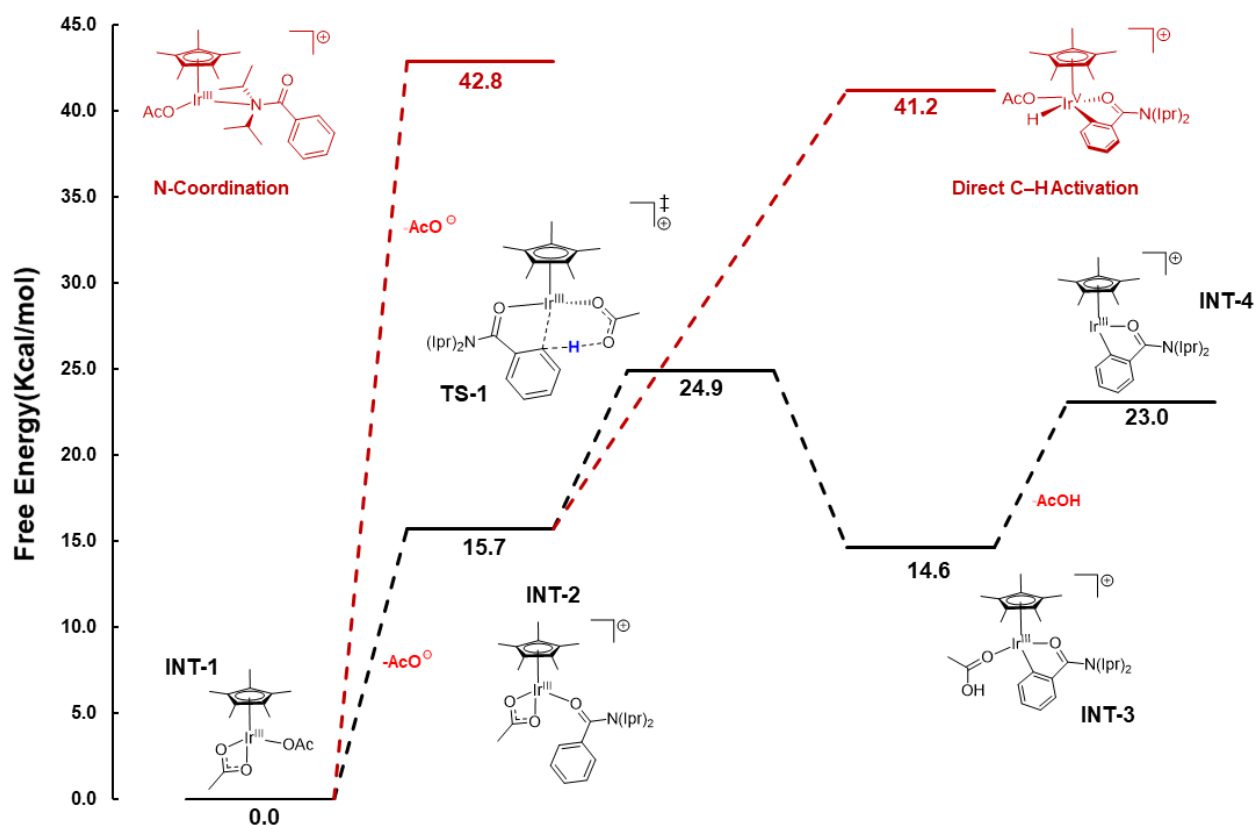


B) Oxidative Addition Pathway for C–H Bond Activation



Starting from a proposed iridium bisacetate, **INT-1**, addition of benzamide was considered via one of two coordination modes to yield **INT-2** and **INT-3**. Benzamide coordination through the oxygen resulted in **INT-2** ($\Delta G^\circ = 15.7 \text{ kcal mol}^{-1}$). Alternatively, coordination of benzamide through the nitrogen yields **INT-3** ($\Delta G^\circ = 42.8 \text{ kcal mol}^{-1}$). **INT-3** is too high in energy compared to **INT-2**, which suggests that oxygen coordination is more likely. The CMD pathway for C–H bond activation can occur through **TS-1** ($\Delta G^\ddagger = 24.9 \text{ kcal mol}^{-1}$). On the other hand, the oxidative addition pathway resulted in a ground state energy for **INT-4** at $41.2 \text{ kcal mol}^{-1}$. The high energy of this intermediate (**INT-4**) indicates that this pathway is unlikely for C–H bond activation. Thus, the acetate assisted CMD pathway is lower in energy than that the oxidative addition pathway and is more likely to occur for C–H bond activation, as shown in **scheme 2.15**.

Scheme 2.15. DFT (B3PW91-D3) calculated energetics for the C–H activation step in 1,2-dichloroethane.



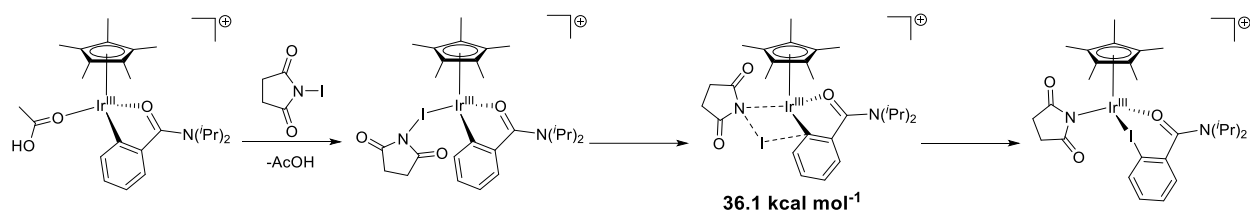
Functionalization Step

Functionalization with *N*-iodosuccinimide

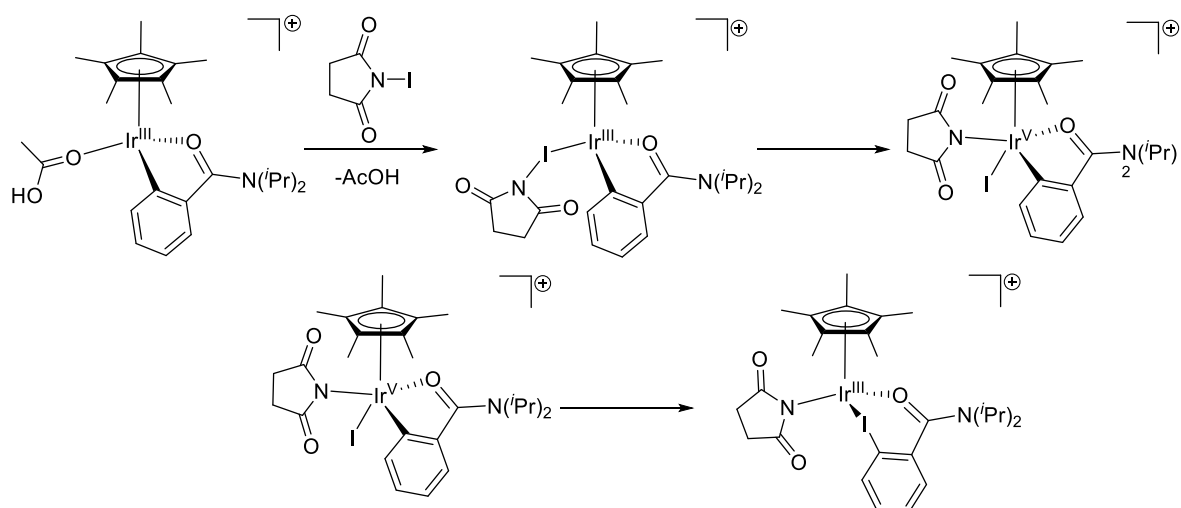
For the functionalization step of the mechanism, both an oxidative addition and a direct functionalization pathway were considered for the functionalization step as depicted in **Scheme 2.16**. The direct functionalization pathway was quickly discarded, as the TS energy was inaccessible at 36.1 kcal/mol. Alternatively, an oxidative addition pathway was explored for the functionalization with *N*-iodosuccinimide.

Scheme 2.16.

A) Direct Functionalization Pathway for the Iodination of *N,N*-diisopropylbenzamide

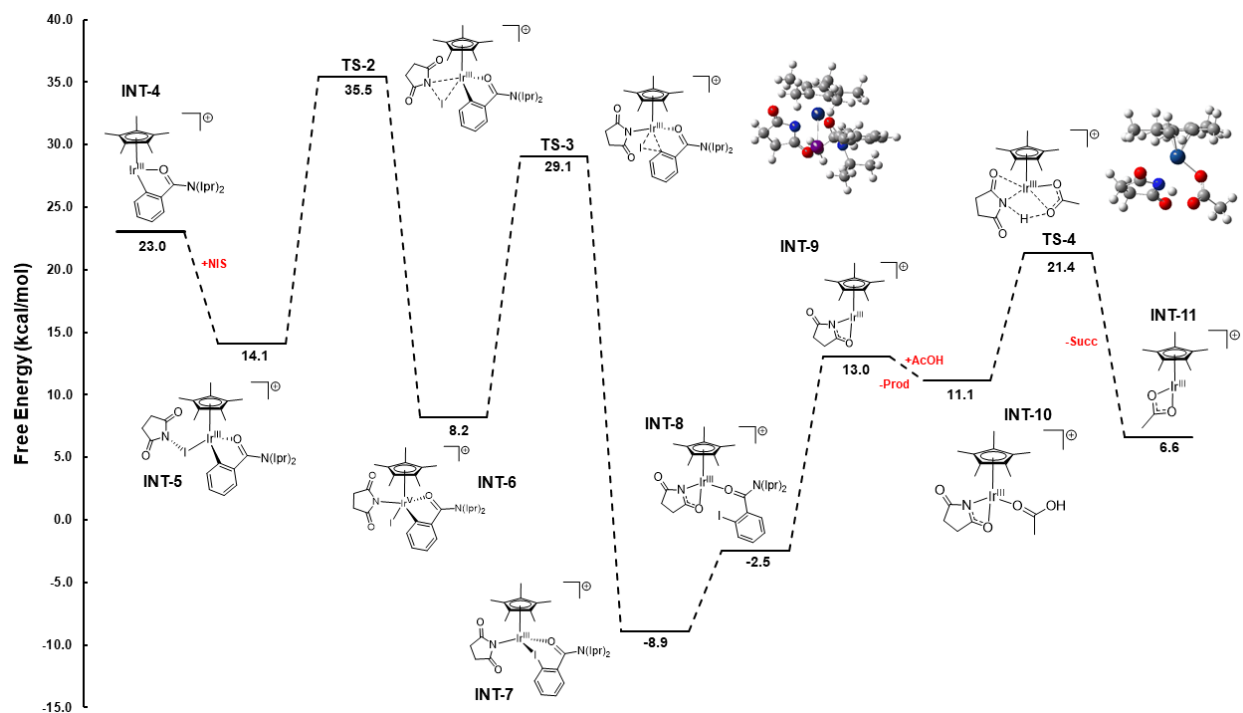


B) Oxidative Addition Pathway for the Iodination of *N,N*-diisopropylbenzamide



As shown in **Scheme 2.17**, addition of *N*-iodosuccinimide to **INT-6** results in **INT-7**. Oxidative addition of the coordinated NIS occurs through **TS-2** with an associated energy of 35.5 kcal mol⁻¹, to yield an Ir(V) iodide complex **INT-8** ($\Delta G^\circ = 8.2$ kcal mol⁻¹). This step is followed by reductive elimination through **TS-3** with an energy barrier of 29.1 kcal mol⁻¹, and results in **INT-9** ($\Delta G^\circ = -8.9$ kcal mol⁻¹). Product release from **INT-9** and protonation with acetic acid results in the regeneration of the catalyst through **TS-4** (21.4 kcal mol⁻¹).

Scheme 2.17. DFT (B3PW91-D3) calculated energetics for the Ir(III)-catalysed iodination with N-iodosuccinimide in 1,2-dichloroethane



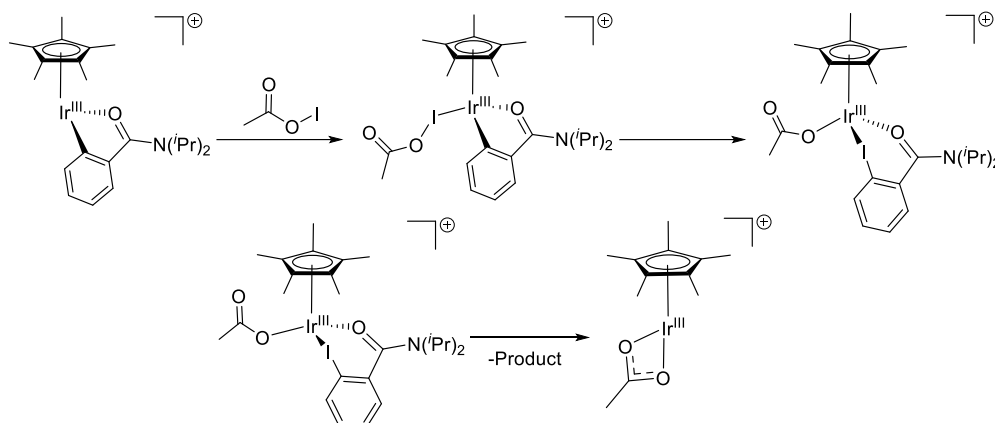
These results suggest that the functionalization step would be rate determining, as the oxidative addition of NIS occurs through the highest barrier at 35.5 kcal/mol. This energy barrier is also inaccessible under our reaction conditions, and therefore too high to be involved in the mechanism. Since we have shown the viability of forming the acetyl hypoiodites under our reaction conditions, we then turned to outline the same pathway using the acetyl hypoiodite as the halogen source participating in the cycle as outlined by **Scheme 2.18**.

Functionalization with *Acetyl Hypoiodite*

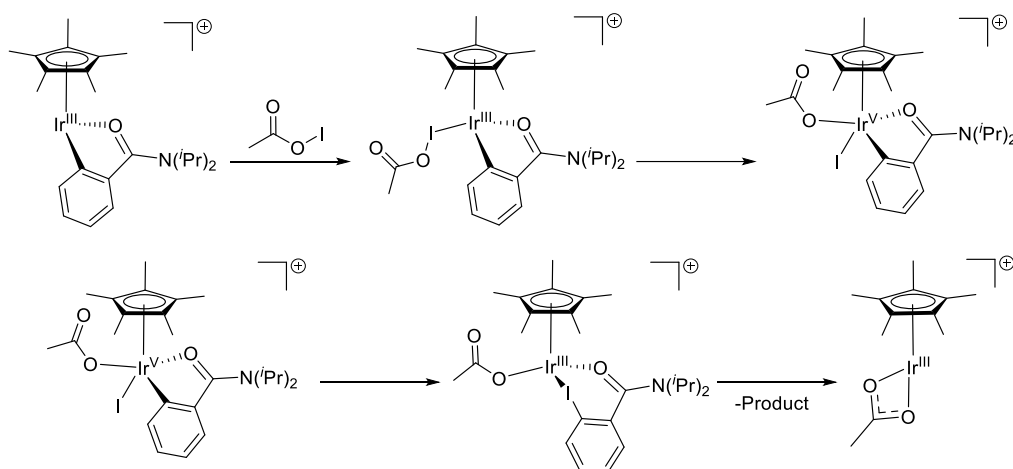
The viability of generating acetyl hypoiodite under our reaction conditions has been demonstrated both experimentally and computationally, therefore a pathway using acetyl hypoiodite as the halogen source was investigated. As with NIS, both a direct functionalization and an oxidative addition pathway were considered and compared computationally as depicted in **Scheme 2.18**.

Scheme 2.18. Proposed mechanism for the coordination of acetyl hypoiodite and the functionalization of benzamide

A) Direct Functionalization Pathway for the Iodination of *N,N*-diisopropylbenzamide



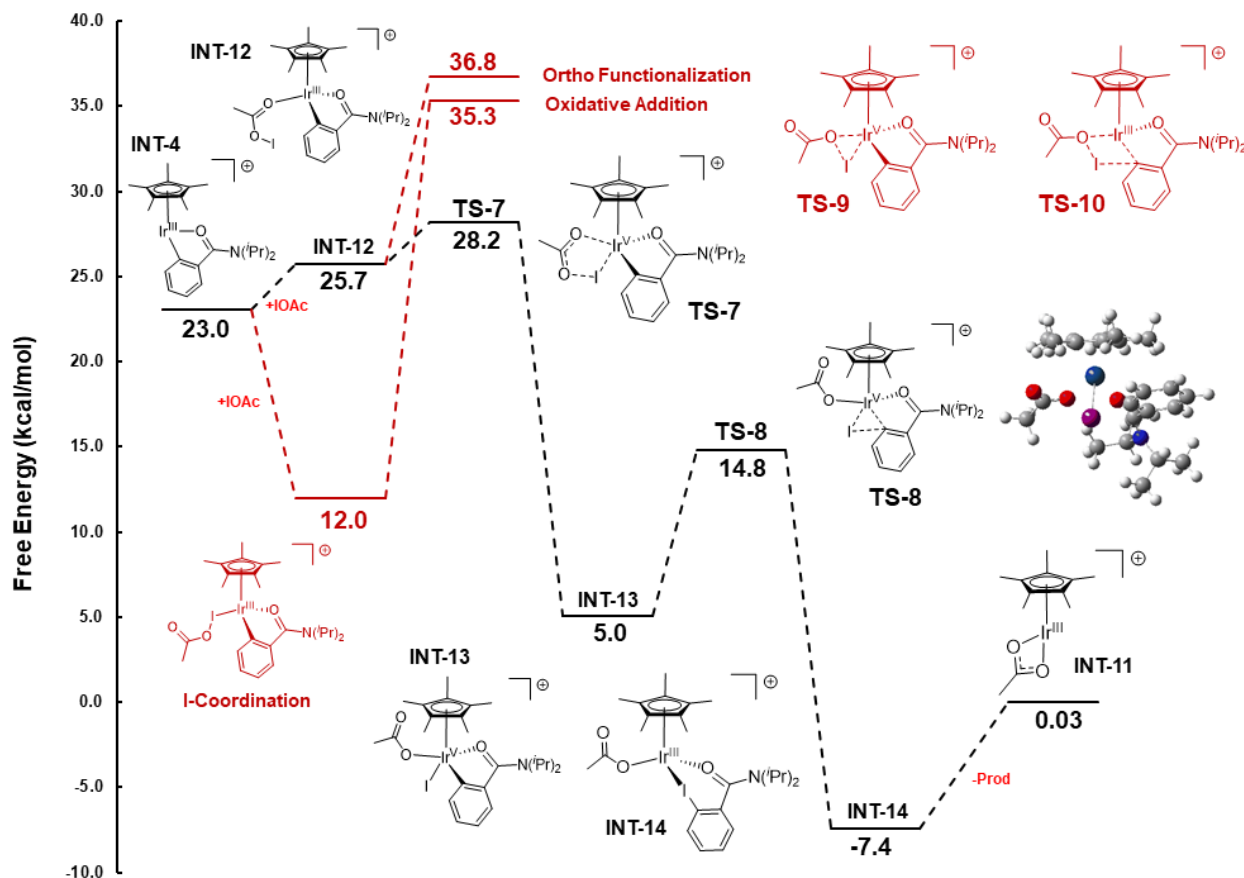
B) Oxidative Addition Pathway for the Iodination of *N,N*-diisopropylbenzamide



Even though iodine coordination is favored over oxygen coordination, iodine coordination is lower in energy by 13.7 kcal mol⁻¹, the barrier for oxidative addition is lower for the oxygen bound acetyl hypoiodite with a TS energy (**TS-7**) of 28.2 kcal mol⁻¹ compared to **TS-9** ($\Delta G^\ddagger = 35.3$ kcal mol⁻¹). Oxidative addition will yield **INT-13** ($\Delta G^\circ = 5.0$ kcal mol⁻¹). From there reductive elimination can occur through **TS-8** (14.8 kcal mol⁻¹) to yield **INT-14** ($\Delta G^\circ = -7.4$ kcal mol⁻¹). To complete the catalytic cycle, the halogenated product is released to regenerate **INT-13**. On the other hand, the direct functionalization

pathway remains unfavorable for the halogenation with acetyl hypoiodite due to the high energy associated with **TS-10** ($\Delta G^\ddagger = 36.8 \text{ kcal mol}^{-1}$) as shown in **Scheme 2.19**.

Scheme 2.19. DFT (B3PW91-D3) calculated energetics for the Ir(III)-catalyzed iodination with I(OAc) in 1,2-dichloroethane.

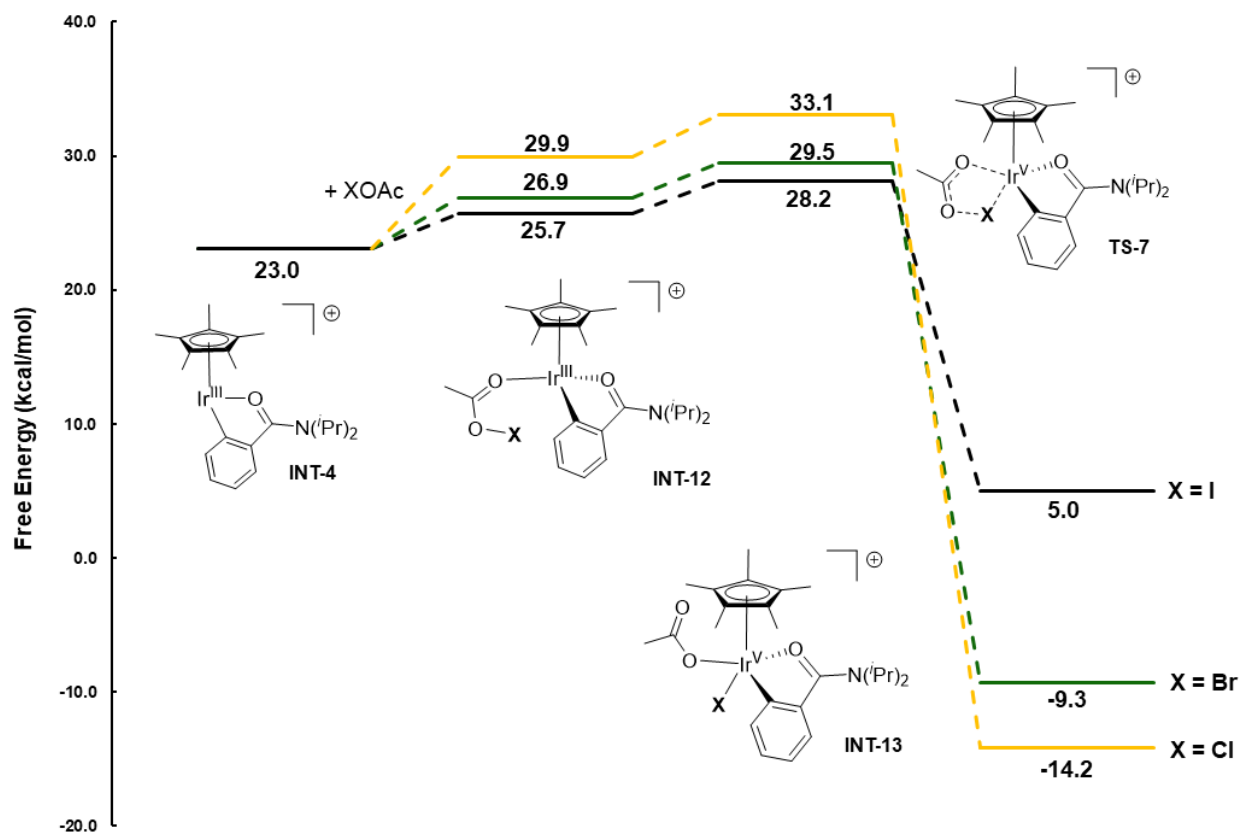


The computational data supports a mechanism where *N*-iodosuccinimide reacts with acetic acid to generate acetyl hypoiodite *in situ* which serves as the halogen source in the reaction. C–H bond activation occurs through a CMD type mechanism and the halogenation of the substrate appears to proceed through an Ir(V) intermediate which is formed as the oxidative addition product of the acetyl hypoiodite to the cyclometalated iridacycle (**INT-4**). To account for the differences in reactivity between NIS, NBS and NCS, we compared the energies for the oxidative addition step of each acetyl hypohalite (X(OAc) for X = I, Br, Cl).

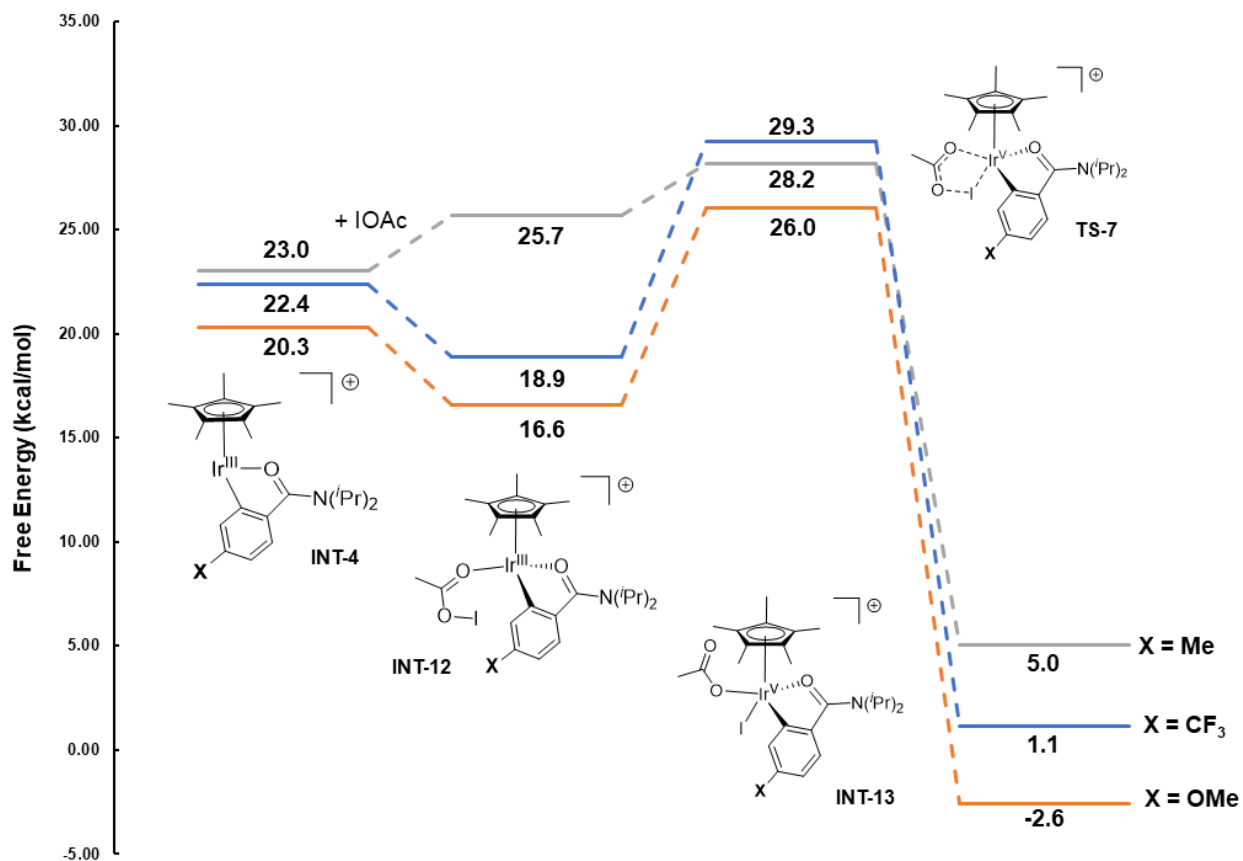
Halogen and Electronic Effect on RDS

From **Scheme 2.20**, there is a substantial difference between the oxidative addition of X(OAc) dependent on the halogen. The oxidative addition for IOAc proceeds through an accessible barrier of 26.9 kcal mol⁻¹, whereas the chlorination reaction was not observed experimentally and proceeds through a calculated barrier of 33.1 kcal mol⁻¹ (**TS-7**). The increased catalyst loading, and the reaction times required for the bromination reaction are also consistent with a calculated energy for **TS-7** of 28.2 kcal mol⁻¹. Additionally, a difference in the oxidative addition barriers of I(OAc) to **INT-12** was also observed when varying the substituent on the *para*-position of the benzamide (**Scheme 2.21**). Experimentally, all three benzamides yield the iodinated product in high yields, this is consistent with the computational data, where the fully protected benzamide has the smallest energy barrier for oxidative addition (2.5 kcal mol⁻¹), and both the *p*-CF₃ and *p*-MeO benzamides proceed through accessible barriers with energies of 28.2 kcal mol⁻¹ and 26.0 kcal mol⁻¹ respectively.

Scheme 2.20. DFT (B3PW91-D3) calculated energetics for the oxidative addition of X(OAc) (X = halide) in 1,2-dichloroethane



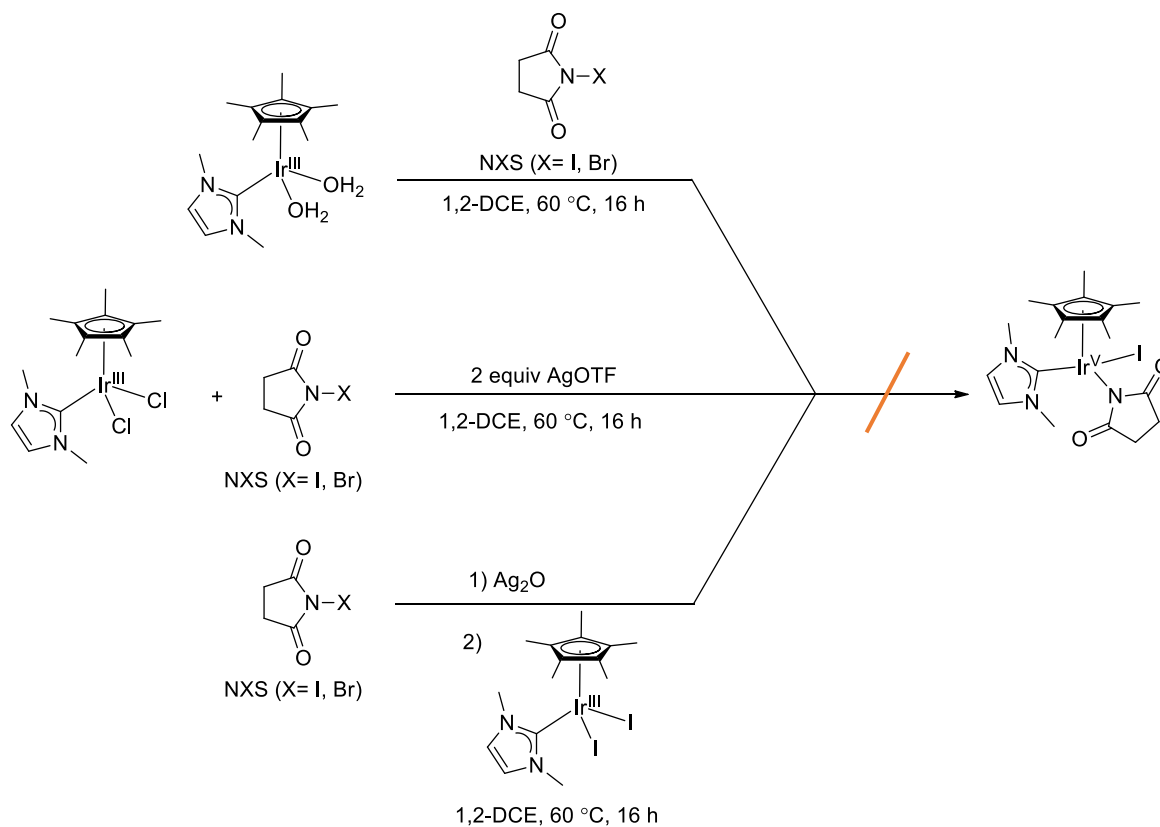
Scheme 2.21. DFT (B3PW91-D3) calculated energetics for the oxidative addition of I(OAc) to iridacycles bearing varying substituents in the *para*-position in 1,2-dichloroethane



Attempted Synthesis of Ir(V) –X

Having obtained such low energies for some of these Ir(V) halide intermediates (**Scheme 2.22**), our next goal was to independently synthesize and isolate some of these intermediates to attempt to demonstrate their catalytic competency. Depicted in **Scheme 2.22** are representative examples of the attempts at synthesizing the Ir(V) iodide, from a Cp*Ir(III)NHC complex. The NHC ligand would be a useful spectroscopic handle to monitor this reaction by $^1\text{H-NMR}$, and it serves as a robust ligand to stabilize the desired product. Unfortunately attempts up to this point to isolate an Ir(V) halide have been unsuccessful. Only halosuccinimides and iridium dimers have been crystallized from the crude reaction mixtures.

Scheme 2.22. Attempts at isolating an Ir(V) iodide complex



Conclusion

In this chapter, the Cp*Ir(III) catalyzed halogenation of benzamides using *N*-iodosuccinimide has been optimized and probed mechanistically. A variety of para-substituted benzamides were well tolerated in this reaction. Additionally, the reaction was adapted to enable the analogous bromination reaction. It was determined that the catalytic reaction has a first order dependence in iridium, a positive dependence in benzamide and an approximately zero order dependence in *N*-iodosuccinimide. In addition, based on H/D KIE experiments, C–H bond activation is involved during or prior to the rate determining step of the mechanism. Based on these data two reaction mechanisms were proposed, which differ solely in the nature of the halogen source. These were then investigated computationally. It was demonstrated that the formation of acetyl hypoiodite is favorable under our reaction conditions. Furthermore, for the C–H bond activation step, an acetate-assisted CMD mechanism was found to be more likely than an oxidative addition mechanism due to the high ground state energy of the intermediates for the oxidative addition pathway. Computational results suggest that functionalization from acetyl hypoiodite formed in situ is favored over direct *N*-iodosuccinimide functionalization due to the difference in barriers for the oxidative addition of these (acetyl hypohalite and *N*-halosuccinimide) substrates. Finally, experimental evidence supporting the proposed acetyl hypoiodite pathway with a series of stoichiometric studies has been provided. Thus, the implications of this study are that directed functionalization of the benzamide substrates utilized here is facilitated by the ease of oxidative addition of the halogenating substrate. This result is important for the further development of methods for the halogenation of aromatic substrates.

Experimental

General Considerations

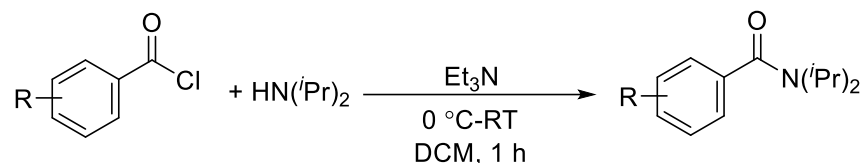
$\text{IrCl}_3 \cdot 3\text{H}_2\text{O}$ was purchased from Pressure Chemical Company. The following Ir complexes: $[\text{Cp}^*\text{IrCl}_2]_2$,⁷² $\text{Cp}^*\text{Ir}(\text{Me}_2\text{SO})(\text{OAc})_2$,¹⁵ $\text{Cp}^*\text{Ir}(\text{Me}_2\text{SO})(\text{OAc})_2$,¹⁵ $\text{Cp}^*\text{Ir}(\text{NHC})(\text{Cl}_2)_2$,⁶⁴ and $[\text{Cp}^*\text{Ir}(\text{H}_2\text{O})_3]\text{OTf}_2$ were prepared as previously reported. All other reagents were purchased from commercial sources and used as received unless stated otherwise.⁶⁴ All reactions were performed under air and using non-dry solvents unless otherwise noted. ^1H and ^{13}C NMR spectra were obtained at room temperature on a Varian Mercury 400 MHz spectrometer or a Varian Mercury 300 MHz spectrometer. Chemical shifts are listed in parts per million (ppm) and referenced to their residual protons or carbons of the deuterated solvents. Gas chromatography (GC) was performed on a Varian 3800 Gas Chromatograph with a Varian VF-53ms column. Elemental analyses were performed by Atlantic Micro Labs, Inc.

Computational Studies

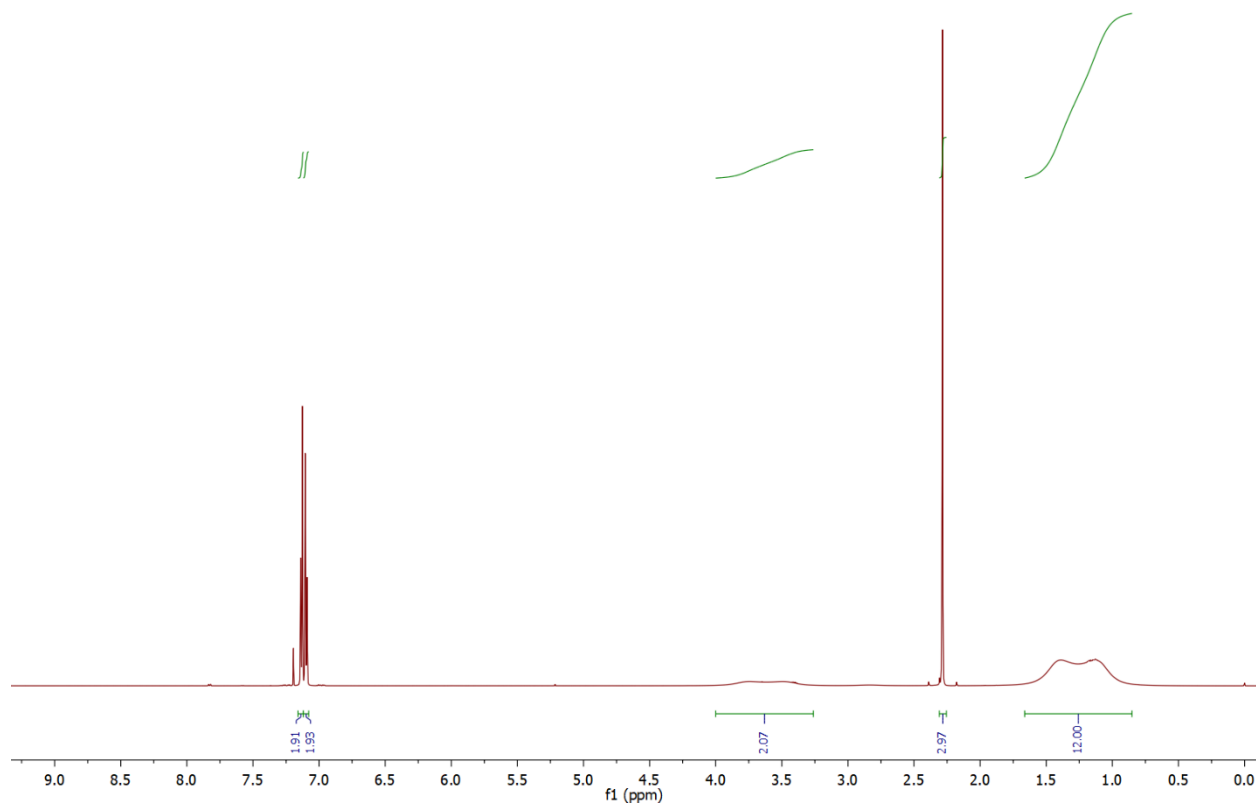
This study was carried out using density functional theory (DFT) with Gaussian09,⁷³ the B3PW91 functional with Grimmes dispersion correction (D3) as implemented through Gaussian was used.⁷⁴ All geometry optimizations were carried out using tight convergence criteria (“opt=tight”) on an ultrafine grid (“int=ultrafine”). The Stuttgart-Dresden (SDD) relativistic effective core potential (RECP) basis set was used for iridium with an additional f polarization function.^{75, 76} The def2-TZVP effective core potential (ECP)^{77, 78} and basis set was used for the halogens. The 6-31G** basis set was used for all other atoms.⁷⁹ Solvation energies were computed with geometries optimized in the gas phase using the SMD method,⁸⁰ with dichloroethane as the solvent, as implemented in Gaussian 09. In this method an IEFPCM calculation is performed with radii and electrostatic terms from Truhlar and co-workers’ SMD solvation model.⁸¹ Energetics were calculated using the 6-311++G** basis set for all atoms and the SDD basis set with an added f polarization function on iridium. The def2-TZVP ECP and basis set was used for the halogens. All energies are reported in kcal mol^{-1} .

Benzamide Derivative Synthesis

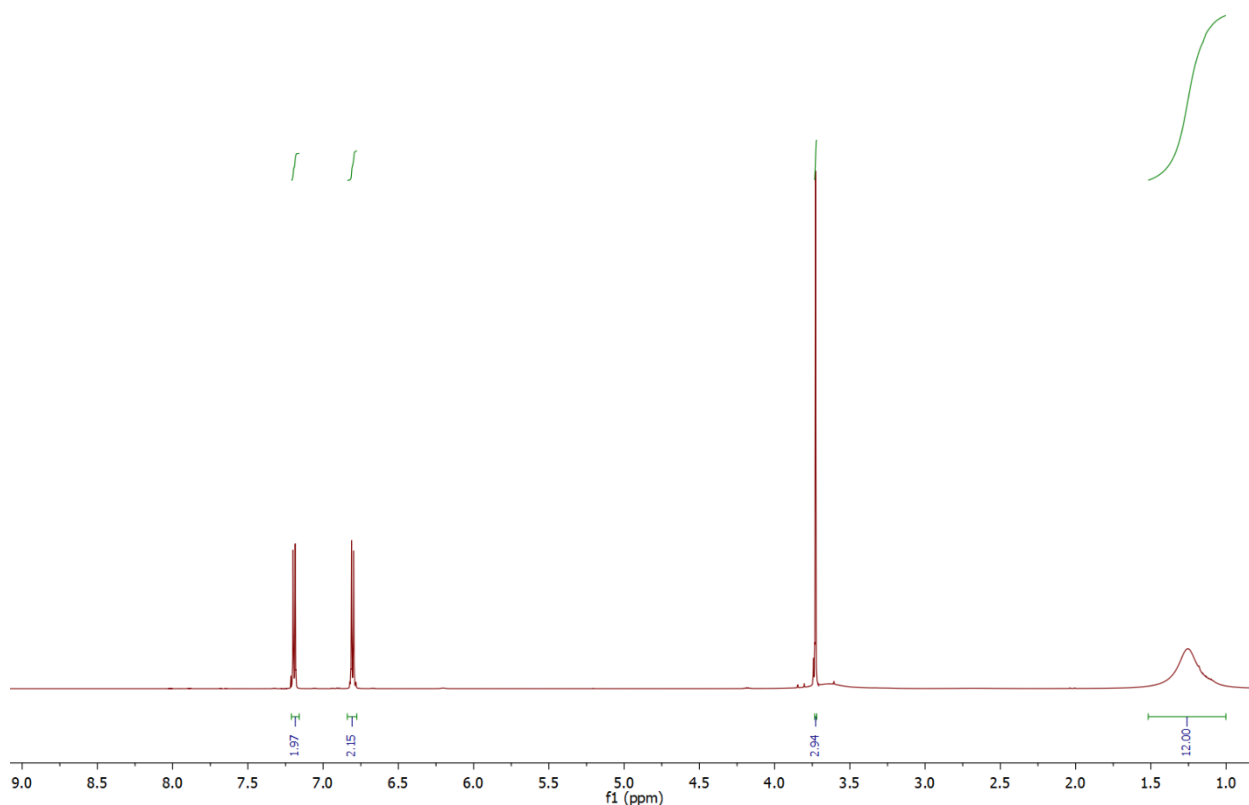
General Procedure for the synthesis of benzamides from acyl chlorides



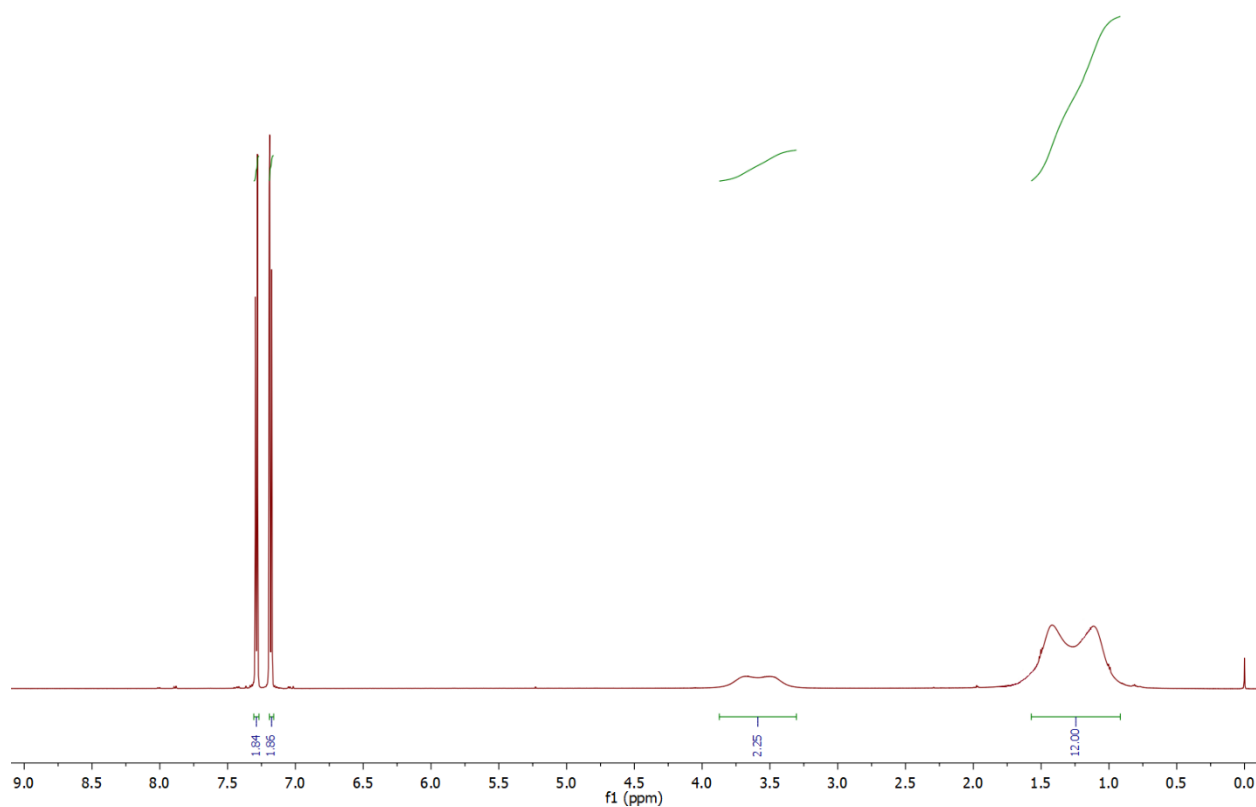
To a round bottom flask equipped with a magnetic stir bar, the corresponding amine (1.10 equiv), and triethylamine (1.20 equiv) in dichloromethane. The corresponding benzoyl chloride (1.05 equiv) was added dropwise at $0\text{ }^\circ\text{C}$. The reaction mixture was stirred and allowed to warm up to room temperature. The reaction mixture was diluted with dichloromethane, washed with a 1N HCl solution and brine. The organic layer was dried over sodium sulfate, filtered, and concentrated under reduced pressure. The crude solid was recrystallized from diethyl ether at $-20\text{ }^\circ\text{C}$, isolated by filtration, and washed with cold diethyl ether.



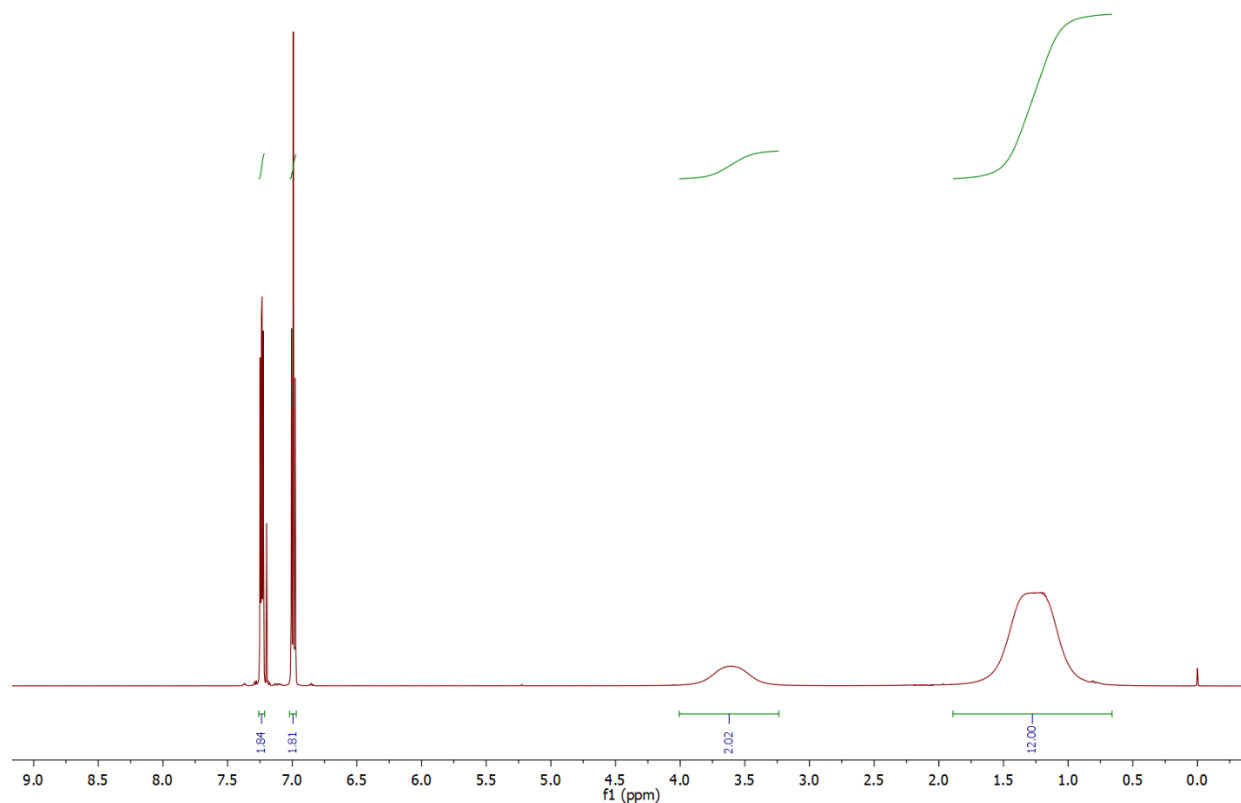
4-methyl-*N,N*-diisopropylbenzamide (1b). From 4-methylbenzoyl chloride and diisopropylamine using the general procedure on a 10 mmol scale. The crude solid was recrystallized from diethyl ether at -20 °C, isolated by filtration, and washed with cold diethyl ether. 93% isolated yield (2.04 g white solid). $^1\text{H-NMR}$ (400 MHz, CDCl_3) δ (ppm): 7.22-7.14 (m, 4H, aromatic protons), 3.75 (bs, 2H, 2 x $\text{CH}(i\text{Pr})$), 2.35 (s, 3H, *p*- CH_3), 1.40 (bs, 12H, 4 x $\text{CH}_3(i\text{Pr})$).



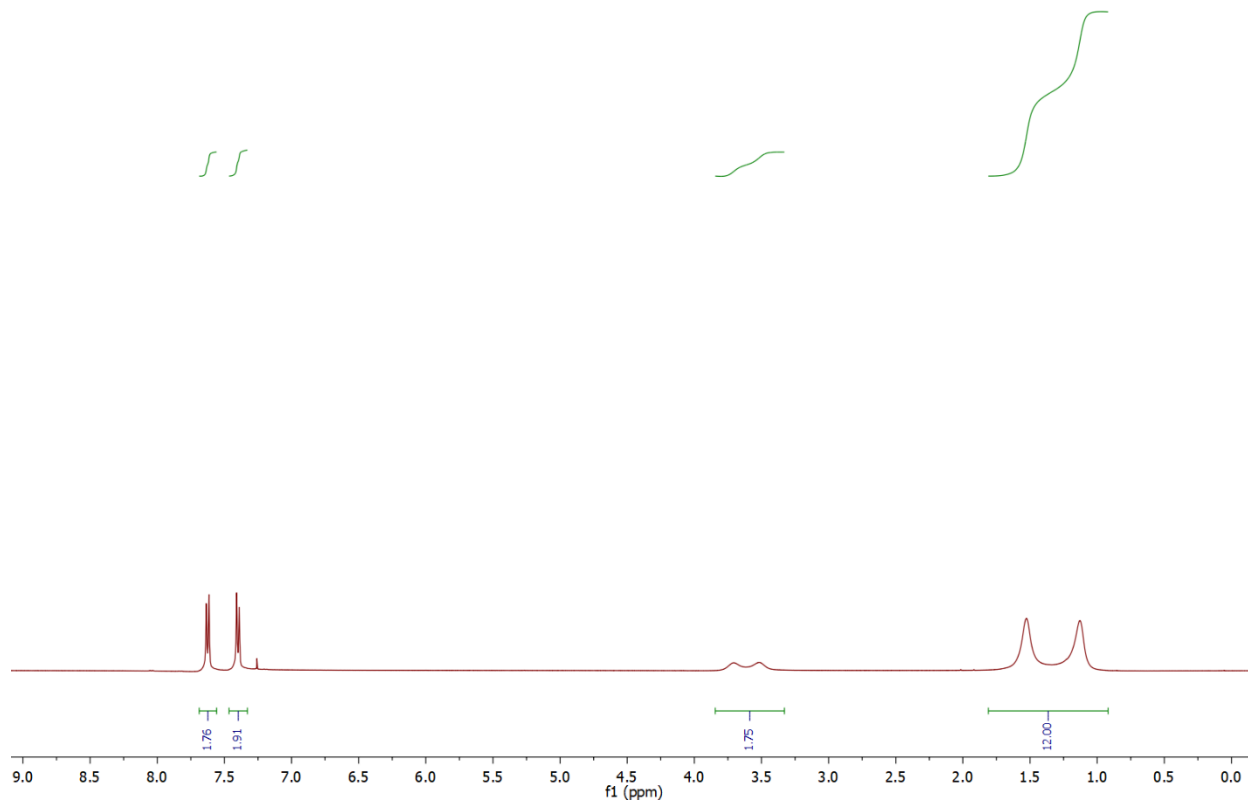
4-methoxy-*N,N*-diisopropylbenzamide (1c). From 4-methoxybenzoyl chloride and diisopropylamine using the general procedure on a 10 mmol scale. The crude mixture was diluted with dichloromethane and filtered through a pad of silica gel. The mixture was then concentrated under reduced pressure. The product was purified by SiO₂ gel column chromatography (pentane/EtOAc = 8/2). 60% isolated yield (1.41 g colorless viscous oil). ¹H-NMR (400 MHz, CDCl₃) δ (ppm): 7.23-7.20 (m, 2H, aromatic protons), 6.84-6.80 (m, 2H, aromatic protons), 3.73 (s, 3H, CH₃), 3.69 (bs, 2H, 2 x CH(ⁱPr).), 1.30 (bs, 12H, 4 x CH₃(ⁱPr)).



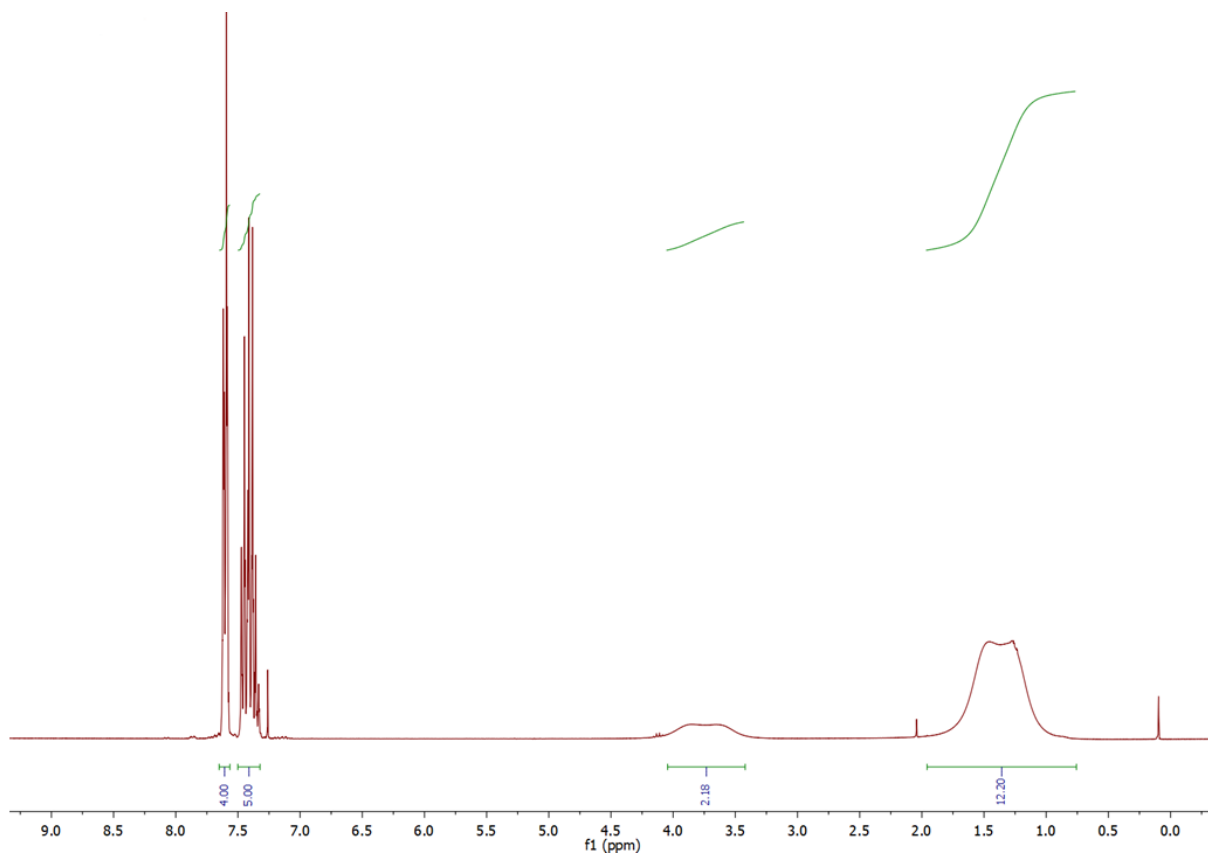
4-chloro-*N,N*-diisopropylbenzamide (1d). From 4-chlorobenzoyl chloride and diisopropylamine using the general procedure on a 10 mmol scale. The crude solid was recrystallized from diethyl ether at -20 °C, isolated by filtration, and washed with cold diethyl ether. 80% isolated yield (1.92 g white solid). ¹H-NMR (300 MHz, CDCl₃) δ (ppm): 7.37-7.33 (m, 2H, aromatic protons), 7.26-7.23 (m, 2H, aromatic protons), 3.71 (bs, 1H, CH(*i*Pr)), 3.59 (bs, 1H, CH(*i*Pr)), 1.40 (bs, 12H, 4 x CH₃(*i*Pr)).



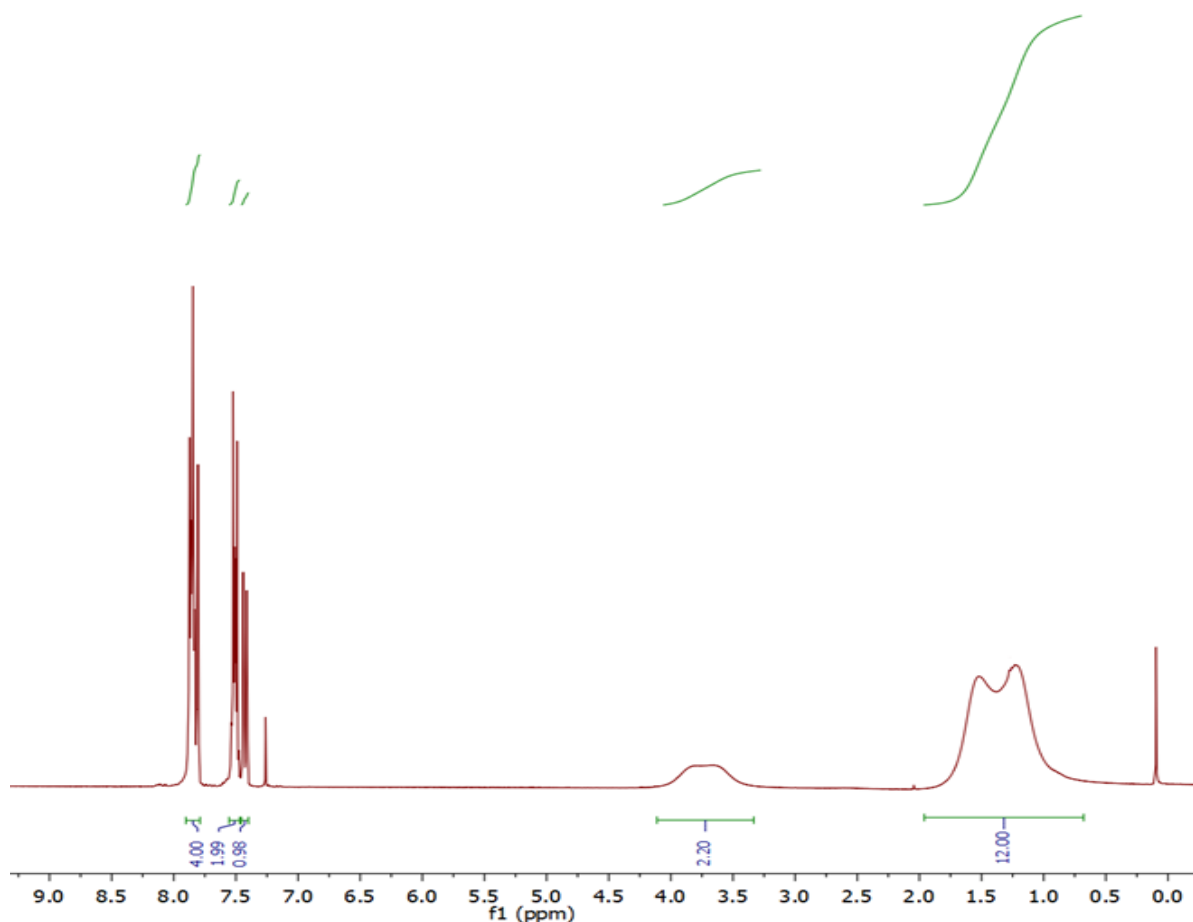
4-fluoro-*N,N*-diisopropylbenzamide (1e). From 4-fluorobenzoyl chloride and diisopropylamine using the general procedure on a 10 mmol scale. The crude solid was recrystallized from diethyl ether at -20 °C, isolated by filtration, and washed with cold diethyl ether. 90% isolated yield (2.01 g white solid). ¹H-NMR (300 MHz, CDCl₃) δ (ppm): 7.34-7.27 (m, 2H, aromatic protons), 7.09-7.02 (m, 2H, aromatic protons), (bs, 2H, 2 x CH(ⁱPr)), 1.34 (bs, 12H, 4 x CH₃(ⁱPr)).



4-trifluoromethyl-*N,N*-diisopropylbenzamide (1f). From 4-(trifluoromethyl)benzoyl chloride and diisopropylamine using the general procedure on a 10 mmol scale. The crude solid was recrystallized from diethyl ether at -20 °C, isolated by filtration, and washed with cold diethyl ether. 93% isolated yield (2.54 g white solid). ¹H-NMR (300 MHz, CDCl₃) δ (ppm): 7.63 (d, 2H, aromatic protons), 7.40 (d, 2H, aromatic protons), 3.69 (bs, 1H, CH(*i*Pr)), 3.54 (bs, 1H, CH(*i*Pr)), 1.52 (bs, 6H, 2 x CH₃(*i*Pr)), 1.15 (bs, 6H, 2 x CH₃(*i*Pr)).



***N,N*-diisopropyl-[1,1'-biphenyl]-4-carboxamide (1g).** From Biphenyl-4-carbonyl chloride and diisopropylamine using the general procedure on a 10 mmol scale. The crude solid was recrystallized from diethyl ether at -20 °C, isolated by filtration, and washed with cold diethyl ether. 85% isolated yield (2.40 g white solid). ¹H-NMR (400 MHz, CDCl₃): δ (ppm) = 7.58- 7.56 (m, 4H, aromatic protons), 7.42-7.41 (m, 2H, aromatic protons), 7.40-7.37 (m, 2H, aromatic protons), 7.36-7.32 (m, 1H, aromatic protons), 3.73 (bm, 2H, 2 x CH(*i*Pr)), 1.35 (bs, 12H *i*Pr).

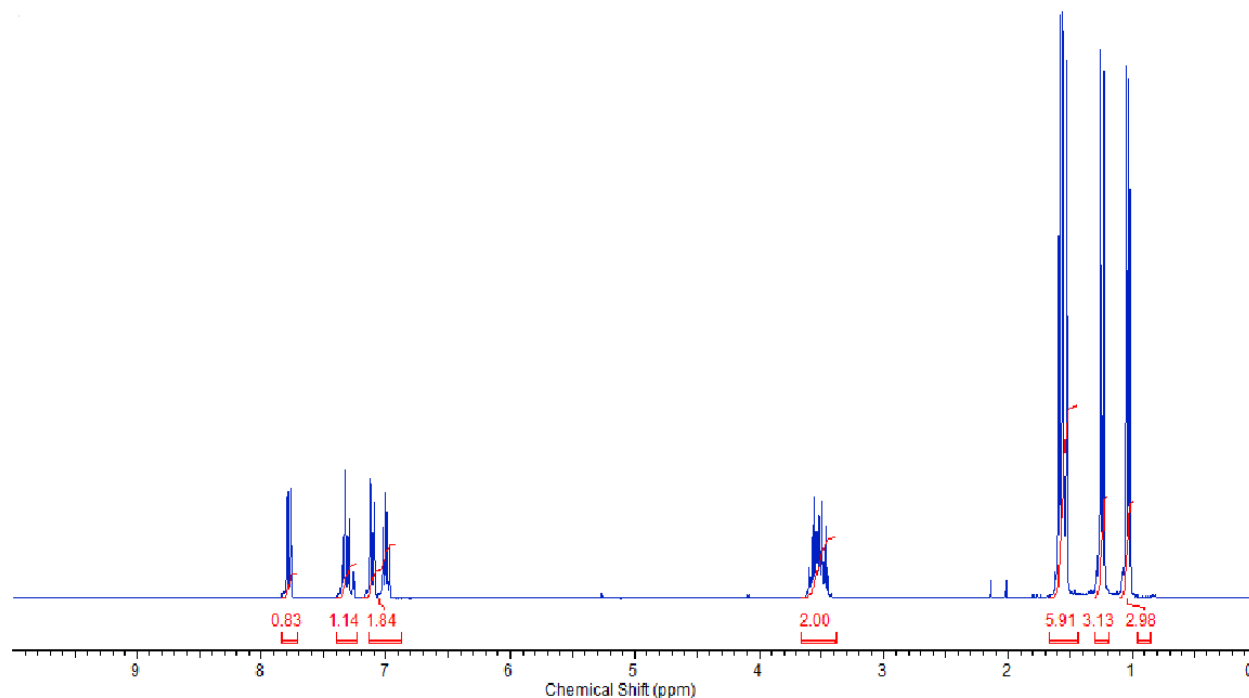


***N,N*-diisopropyl-2-naphthamide (1h).** From 2-naphthoyl chloride and diisopropylamine using the general procedure on a 10 mmol scale. The crude solid was recrystallized from diethyl ether at -20 °C, isolated by filtration, and washed with cold diethyl ether. 90% isolated yield (2.30 g white solid). ¹H-NMR (400 MHz, CDCl₃) δ (ppm): 7.87-7.81 (m, 4H, aromatic protons), 7.52-7.48 (m, 2H, aromatic protons), 7.43 (m, 1H, aromatic proton), 3.84 (bs, 1H, CH(*i*Pr)), 3.63 (bs, 1H, CH(*i*Pr)), 1.55 (bs, 6H, 2 x CH₃(*i*Pr)), 1.19 (bs, 6H, 2 x CH₃(*i*Pr)).

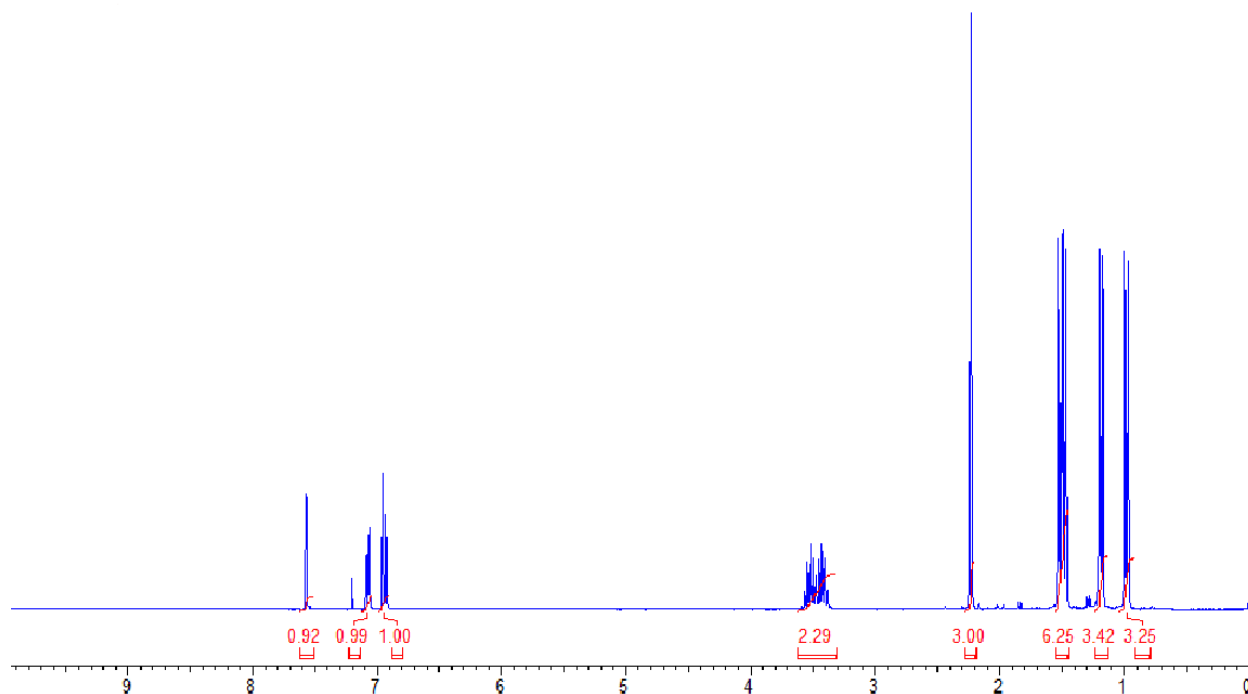
General Procedure for the Iridium Catalyzed Iodination of benzamides



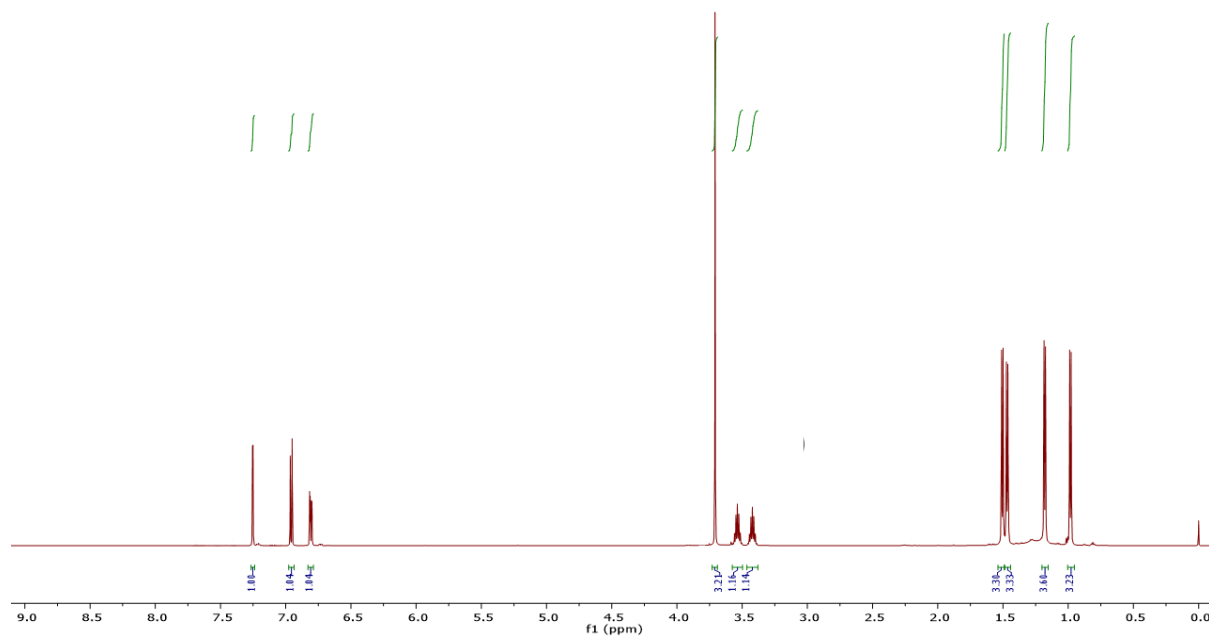
A foil covered screw cap test tube with a magnetic stirrer was charged with benzamide (1 mmol, 1.0 equiv), *N*-iodosuccinimide (1.5 mmol, 1.5 equiv), [Cp*IrCl₂]₂ (0.005 mmol, 0.5 mol%), silver triflate (0.02mmol, 2 mol%), acetic acid (2 mmol, 2 equiv) and 1 mL of 1,2-dichloroethane. The reaction mixture was stirred at 60 °C for 1 h in an oil bath. Upon completion, the solution was diluted with dichloromethane and filtered through celite. The solvent was removed under reduced pressure and the crude reaction mixture was purified by column chromatography on silica gel (SiO₂).



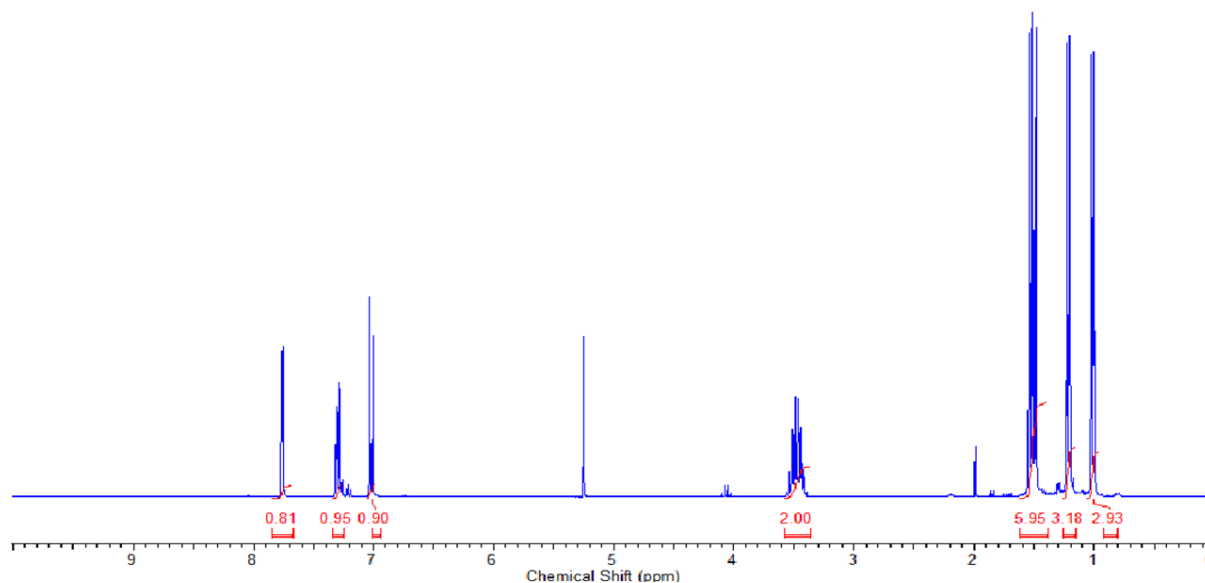
2-iodo-*N,N*-diisopropylbenzamide (2a). Utilizing the general procedure using 203.5 mg of *N,N*-diisopropylbenzamide (1 mmol, 1.0 equiv), 337.5 mg of *N*-iodosuccinimide (1.5 mmol, 1.5 equiv), 4.0 mg of [Cp*IrCl₂]₂ (0.005 mmol, 0.5 mol%), 5.14 mg of silver acetate (0.02 mmol, 2 mol%). The crude reaction mixture was concentrated under reduced pressure, dissolved in minimal dichloromethane and purified by SiO₂ gel column chromatography (15% EtOAc/DCM). 96% isolated yield (318.0 mg white solid). ¹H-NMR (300 MHz, CDCl₃) δ (ppm): 7.80 (m, 1H, aromatic proton), 7.34 (m, 1H, aromatic proton), 7.13 (m, 1H, aromatic proton), 7.02 (m, 1H, aromatic proton). 3.64-3.44 (m, 2H, CH(*i*Pr)), 1.59 (m, 6H, 2 x CH₃(*i*Pr)), 1.26 (d, J = 6.7 Hz, 3H, CH₃(*i*Pr)), 1.05 (d, J = 6.7 Hz, 3H, 2 x CH₃(*i*Pr)).



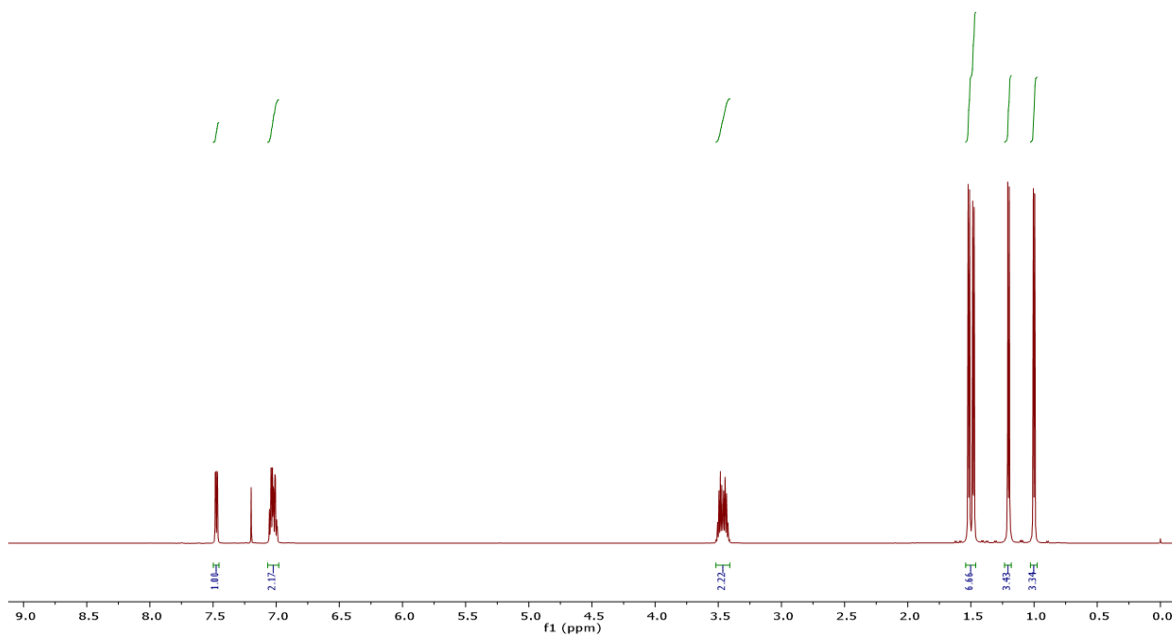
2-iodo-*N,N*-diisopropyl-4-methylbenzamide (2b). Utilizing the general procedure using 219.3 mg of 4-methyl-*N,N*-diisopropylbenzamide (1 mmol, 1.0 equiv), 337.5 mg of *N*-iodosuccinimide (1.5 mmol, 1.5 equiv), 4.0 mg of [Cp*IrCl₂]₂ (0.005 mmol, 0.5 mol%), 5.14 mg of silver acetate (0.02 mmol, 2 mol%). The crude reaction mixture was concentrated under reduced pressure, dissolved in minimal dichloromethane and purified by SiO₂ gel column chromatography (15% EtOAc/DCM). 95% isolated yield (328.0 mg white solid). ¹H-NMR (300 MHz, CDCl₃) δ (ppm): 7.62 (s, 1H, aromatic proton), 7.13 (d, 1H, aromatic proton), 3.65-3.43 (m, 2H, 2 x CH(*i*Pr)), 2.29 (s, 3H, *p*-Me). 1.56 (m, 6H, 2 x CH₃(*i*Pr)), 1.24 (d, J = 6.7 Hz, 3H, CH₃(*i*Pr)), 1.04 (d, J = 6.7 Hz, 3H, CH₃(*i*Pr)).



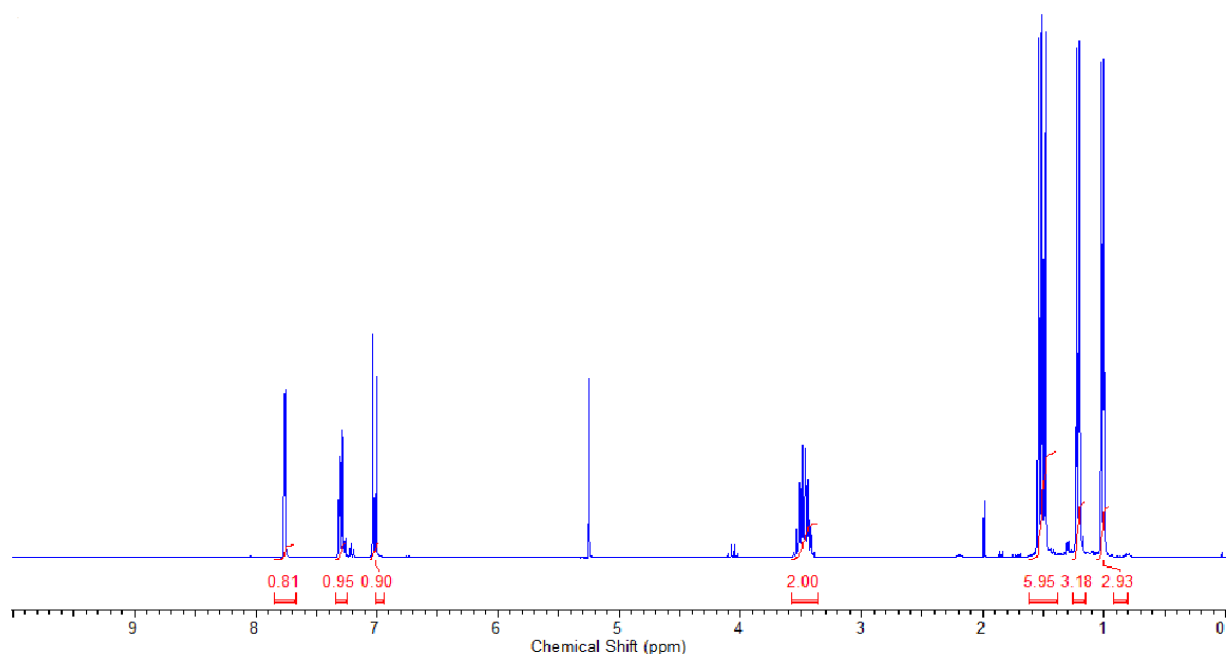
2-iodo-*N,N*-diisopropyl-4-methoxybenzamide (2c). Utilizing the general procedure using 235.3 mg of 4-methoxy-*N,N*-diisopropylbenzamide (1 mmol, 1.0 equiv), 337.5 mg of *N*-iodosuccinimide (1.5 mmol, 1.5 equiv), 4.0 mg of $[\text{Cp}^*\text{IrCl}_2]_2$ (0.005 mmol, 0.5 mol%), 5.14 mg of silver acetate (0.02 mmol, 2 mol%). The crude reaction mixture was concentrated under reduced pressure, dissolved in minimal dichloromethane and purified by SiO_2 gel column chromatography (15% EtOAc/DCM). 35% isolated yield (126.4 mg white solid). $^1\text{H-NMR}$ (400 MHz, CDCl_3), δ 8.07 (bs, 1H, aromatic proton), 7.62 (d, $J = 7.5$ Hz, 1H, aromatic proton) 7.24 (d, $J = 8.0$ Hz, 1H, aromatic proton), 3.57-3.48 (m, 2H, 2 x $\text{CH}(\text{iPr})$), 1.60 (s, 3H, OMe), 1.57 (m, 6H, 2 x $\text{CH}_3(\text{iPr})$), 1.29 (d, $J = 6.6$ Hz, 3H, $\text{CH}_3(\text{iPr})$), 1.09 (d, $J = 6.6$ Hz, 3H, $\text{CH}_3(\text{iPr})$).



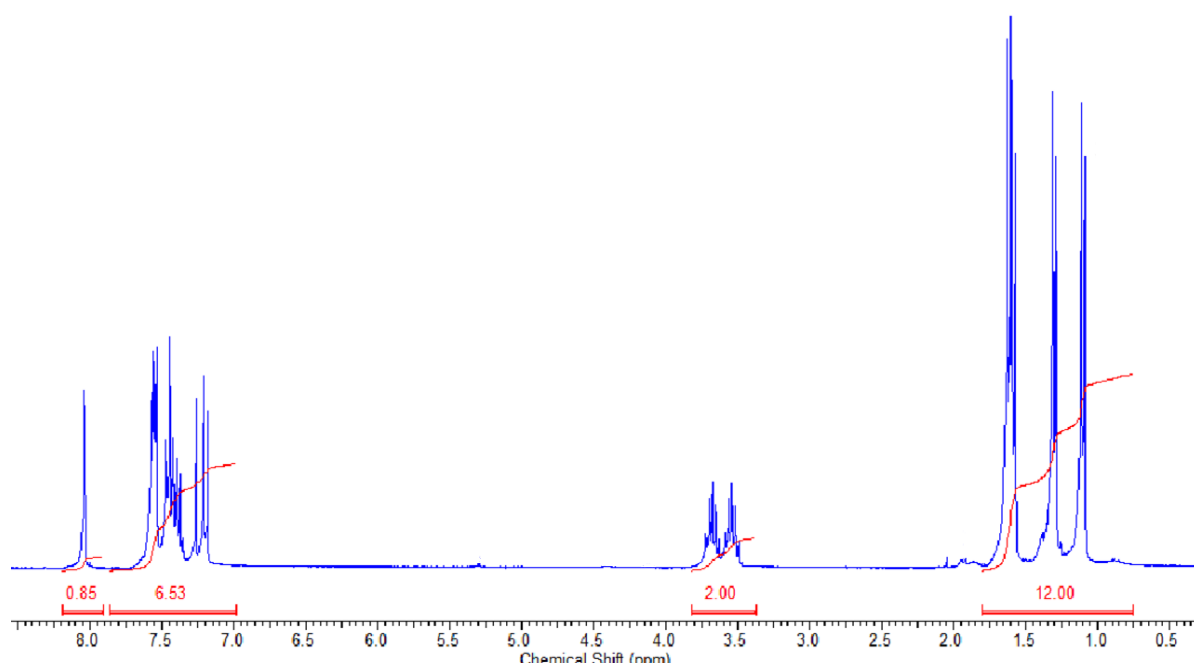
4-chloro-2-iodo-*N,N*-diisopropylbenzamide (2d). Utilizing the general procedure using 239.7 mg of 4-chloro-*N,N*-diisopropylbenzamide (1 mmol, 1.0 equiv), 337.5 mg of *N*-iodosuccinimide (1.5 mmol, 1.5 equiv), 4.0 mg of [Cp*IrCl₂]₂ (0.005 mmol, 0.5 mol%), 5.14 mg of silver acetate (0.02 mmol, 2 mol%). The crude reaction mixture was concentrated under reduced pressure, dissolved in minimal dichloromethane and purified by SiO₂ gel column chromatography (10% EtOAc/DCM). 93% isolated yield (340.0 mg white solid). ¹H-NMR (400 MHz, CDCl₃) δ 7.82 (d, J = 2.0 Hz, 1H, aromatic proton), 7.35 (dd, J = 8.4, 2.0 Hz, 1H, aromatic proton), 7.06 (d, J = 8.4 Hz, 1H, aromatic proton), 3.53 (m, 2H, 2 x CH(ⁱPr)), 1.57 (m, 6H, 2 x CH₃(ⁱPr)), 1.27 (d, J = 6.7 Hz, 3H, CH₃(ⁱPr)), 1.07 (d, J = 6.6 Hz, 3H CH₃(ⁱPr)).



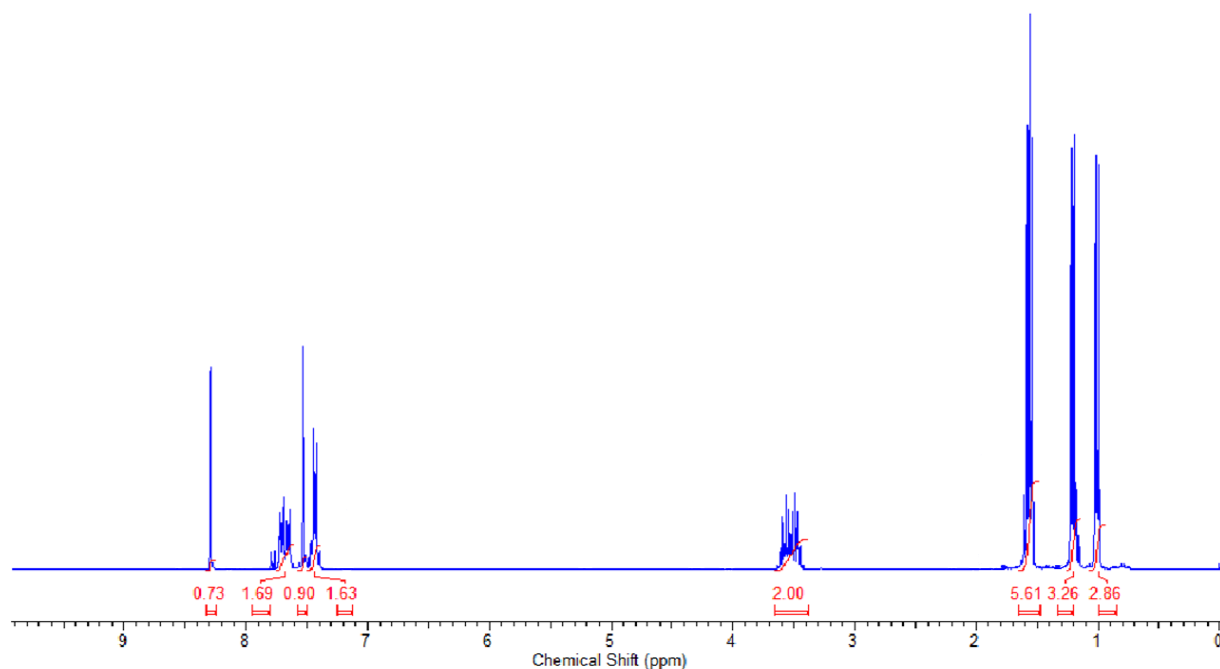
4-fluoro-2-iodo-*N,N*-diisopropylbenzamide (2e). Utilizing the general procedure using 223.3 mg of 4-fluoro-*N,N*-diisopropylbenzamide (1 mmol, 1.0 equiv), 337.5 mg of *N*-iodosuccinimide (1.5 mmol, 1.5 equiv), 4.0 mg of $[\text{Cp}^*\text{IrCl}_2]_2$ (0.005 mmol, 0.5 mol%), 5.14 mg of silver acetate (0.02 mmol, 2 mol%). The crude reaction mixture was concentrated under reduced pressure, dissolved in minimal dichloromethane and purified by SiO_2 gel column chromatography (10% EtOAc/DCM). 67% isolated yield (234.0 mg white solid). $^1\text{H-NMR}$ (300 MHz, CDCl_3) δ 7.55 (dd, $J = 8.0, 3.0$ Hz, 1H, aromatic proton), 7.09 (m, 2H, aromatic protons), 3.52 (m, 2H, $\text{CH}(\text{iPr})$), 1.57 (m, 6H, $\text{CH}_3(\text{iPr})$), 1.27 (d, $J = 6.7$ Hz, 3H, $\text{CH}_3(\text{iPr})$), 1.05 (d, $J = 6.6$ Hz 3H, $\text{CH}_3(\text{iPr})$).



2-iodo-*N,N*-diisopropyl-4-(trifluoromethyl)benzamide (2f). Utilizing the general procedure using 273.3 mg of 4-(trifluoromethyl)-*N,N*-diisopropylbenzamide (1 mmol, 1.0 equiv), 337.5 mg of *N*-iodosuccinimide (1.5 mmol, 1.5 equiv), 4.0 mg of [Cp*IrCl₂]₂ (0.005 mmol, 0.5 mol%), 5.14 mg of silver acetate (0.02 mmol, 2 mol%). The crude reaction mixture was concentrated under reduced pressure, dissolved in minimal dichloromethane and purified by SiO₂ gel column chromatography (15% EtOAc/DCM). 86% isolated yield (343.3 mg white solid). ¹H-NMR (400 MHz, CDCl₃) δ 8.07 (bs, 1H, aromatic proton) 7.62 (d, *J* = 7.5 Hz, 1H, aromatic proton), 7.24 (d, *J* = 8.0 Hz, 1H, aromatic proton), 3.57-3.48 (m, 2H, 2 x CH(*i*Pr)), 1.60 (m, 6H 2 x CH₃(*i*Pr)), 1.29 (d, *J* = 6.6 Hz, 3H CH₃(*i*Pr)), 1.09 (d, *J* = 6.7 Hz, 3H, CH₃(*i*Pr)).



3-iodo-*N,N*-diisopropyl-[1,1'-biphenyl]-4-carboxamide (2g). Utilizing the general procedure using 281.4 mg of *N,N*-diisopropyl-[1,1'-biphenyl]-4-carboxamide (1 mmol, 1.0 equiv), 337.5 mg of *N*-iodosuccinimide (1.5 mmol, 1.5 equiv), 4.0 mg of [Cp*IrCl₂]₂ (0.005 mmol, 0.5 mol%), 5.14 mg of silver acetate (0.02 mmol, 2 mol%). The crude reaction mixture was concentrated under reduced pressure, dissolved in minimal dichloromethane and purified by SiO₂ gel column chromatography (10% EtOAc/DCM). 80% isolated yield (325.8 mg white solid). ¹H-NMR (300 MHz, CDCl₃): δ = 8.04 (d, 1H), 7.59–7.53 (m, 2H), 7.49–7.37 (m, 3H), 7.20–7.18 (m, 1H), 7.22 (d, J = 7.8 Hz, 1H), 3.68 (m, 1H, CH(*i*Pr)), 3.53 (m, 1H CH(*i*Pr)), 1.60 (m, 6H, 2 x CH₃(*i*Pr)), 1.30 (d, J = 6.6 Hz 3H CH₃(*i*Pr)), 1.10 (d, J = 6.7 Hz 3H, CH₃(*i*Pr)).

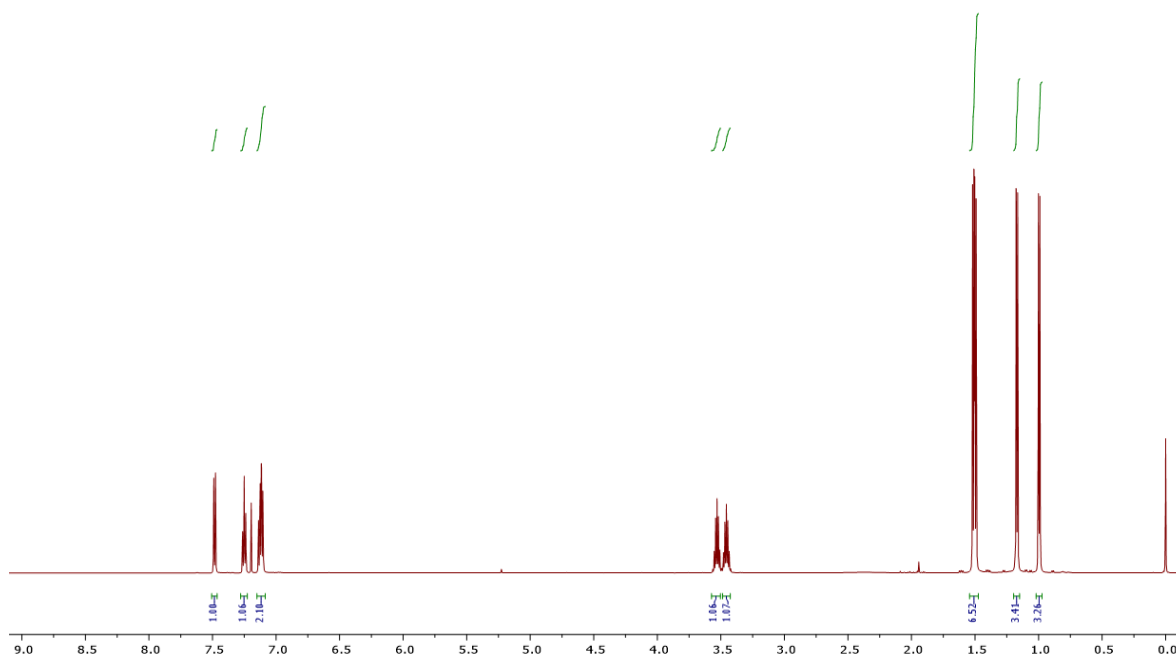


3-iodo-*N,N*-diisopropyl-2-naphthamide (2h). Utilizing the general procedure using 255.4 mg of *N,N*-diisopropyl-2-naphthamide (1 mmol, 1.0 equiv), 337.5 mg of *N*-iodosuccinimide (1.5 mmol, 1.5 equiv), 4.0 mg of $[\text{Cp}^*\text{IrCl}_2]_2$ (0.005 mmol, 0.5 mol%), 5.14 mg of silver acetate (0.02 mmol, 2 mol%). The crude reaction mixture was concentrated under reduced pressure, dissolved in minimal dichloromethane and purified by SiO_2 gel column chromatography (15% EtOAc/DCM). 90% isolated yield (343.1 mg white solid). $^1\text{H-NMR}$ (300 MHz, CDCl_3) δ 8.38 (s, 1H), 7.76 (m, 2H), 7.62 (s, 1H), 7.52 (m, 2H), 3.60 (m, 2H 2 x CH(*i*Pr)), 1.64 (m, 6H 2 x CH_3 (*i*Pr)), 1.29 (d, $J = 6.7$ Hz, 3H, CH_3 (*i*Pr)), 1.09 (d, $J = 6.6$ Hz, 3H, CH_3 (*i*Pr)).

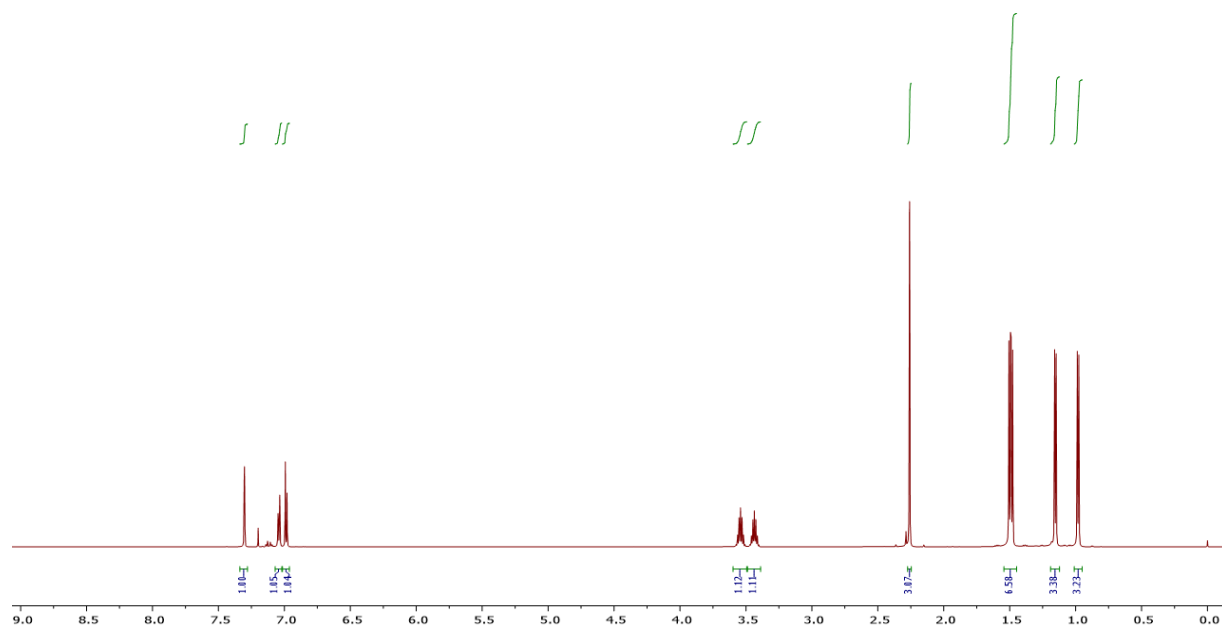
General Procedure for the Iridium Catalyzed Bromination of Benzamides



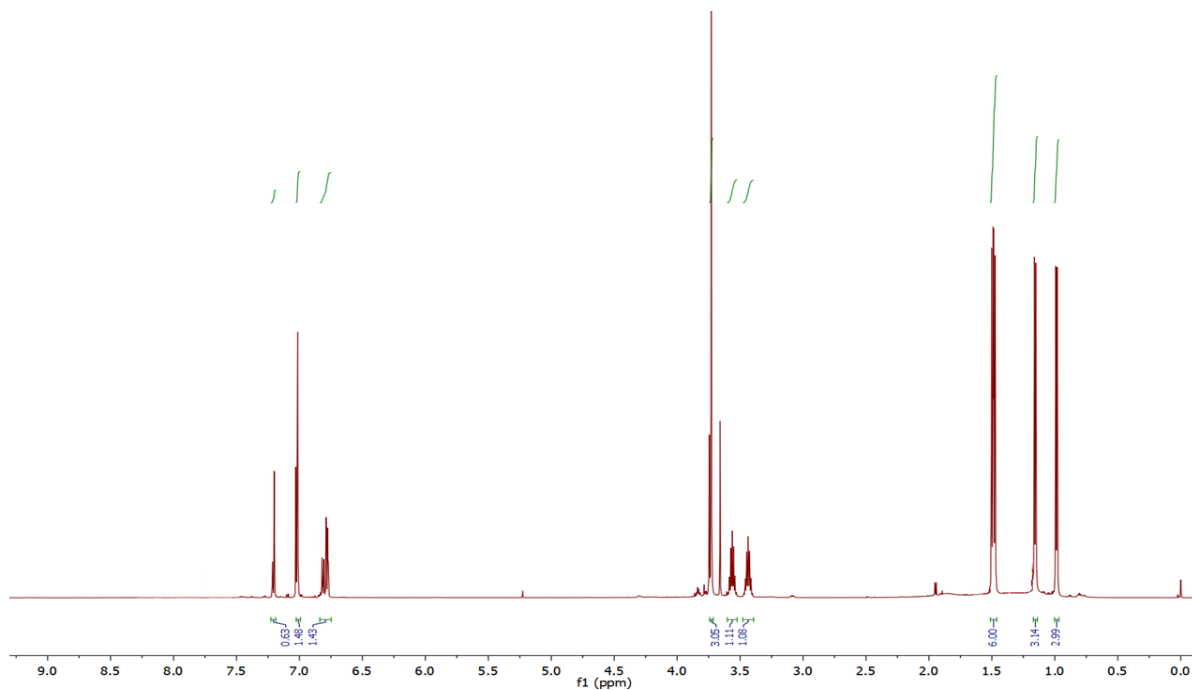
A foil covered screw cap test tube with a magnetic stirrer was charged with benzamide (1 mmol, 1.0 equiv), *N*-bromosuccinimide (1.5 mmol, 1.5 equiv), $[\text{Cp}^*\text{IrCl}_2]_2$ (0.06 mmol, 6 mol%), silver triflate (0.24 mmol, 24 mol%), acetic acid (2 mmol, 2 equiv) and 1 mL of 1,2-dichloroethane. The reaction mixture was stirred at 60 °C for 4 h in an oil bath. Upon completion, the solution was diluted with dichloromethane and filtered through celite. The solvent was removed under reduced pressure and the crude reaction mixture was purified by column chromatography on silica gel (SiO_2).



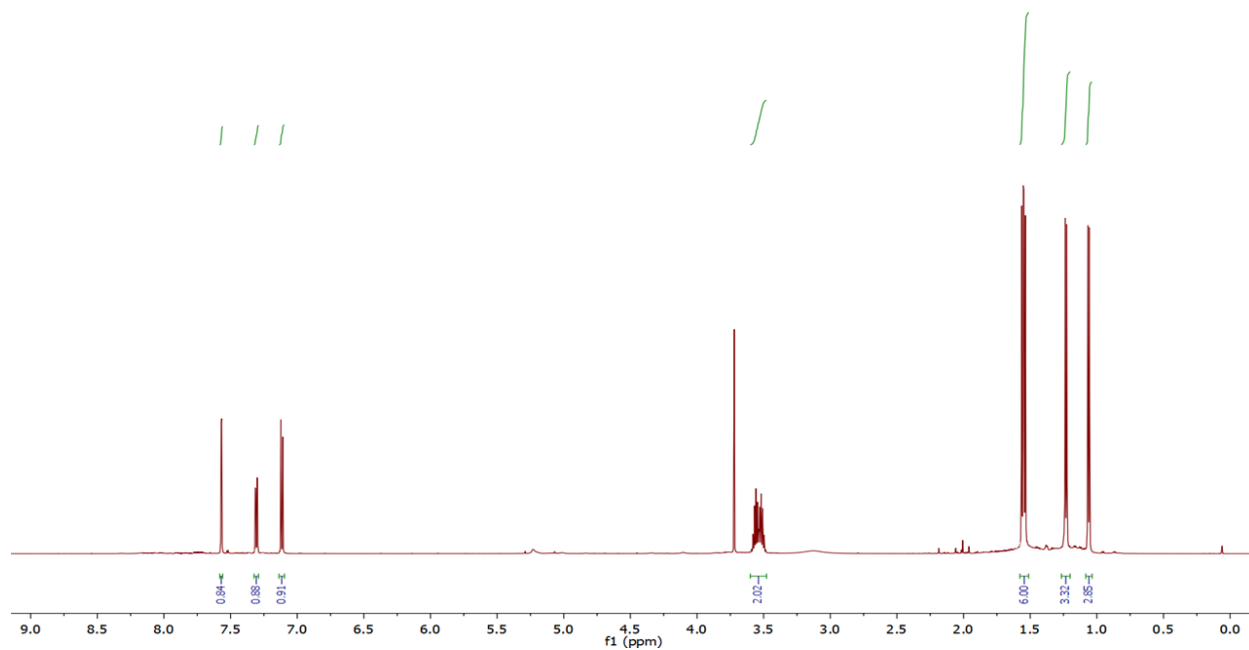
2-bromo-*N,N*-diisopropylbenzamide (3a). Utilizing the general procedure using 203.5 mg of *N,N*-diisopropylbenzamide (1 mmol, 1.0 equiv), 267 mg of *N*-bromodisuccinimide (1.5 mmol, 1.5 equiv), 48 mg of $[\text{Cp}^*\text{IrCl}_2]_2$ (0.06 mmol, 6 mol%), 5.14 mg of silver acetate (0.24 mmol, 24 mol%). The crude reaction mixture was concentrated under reduced pressure, dissolved in minimal dichloromethane and purified by SiO_2 gel column chromatography (10% EtOAc/DCM). 96% isolated yield (272.8 mg white solid). $^1\text{H-NMR}$ (300 MHz, CDCl_3) δ (ppm): 7.80 (d, $J = 8.0$ Hz, 1H, aromatic proton), 7.34 (m, 1H, aromatic proton), 7.13 (m, 1H, aromatic proton), 7.02 (m, 1H, aromatic proton). 3.64-3.44 (m, 2H, 2 x $\text{CH}(\text{iPr})$), 1.59-1.56 (m, 6H, 2 x $\text{CH}_3(\text{iPr})$), 1.26 (d, $J = 6.7$ Hz, 3H, $\text{CH}_3(\text{iPr})$), 1.05 (d, $J = 6.7$ Hz, 3H, $\text{CH}_3(\text{iPr})$).



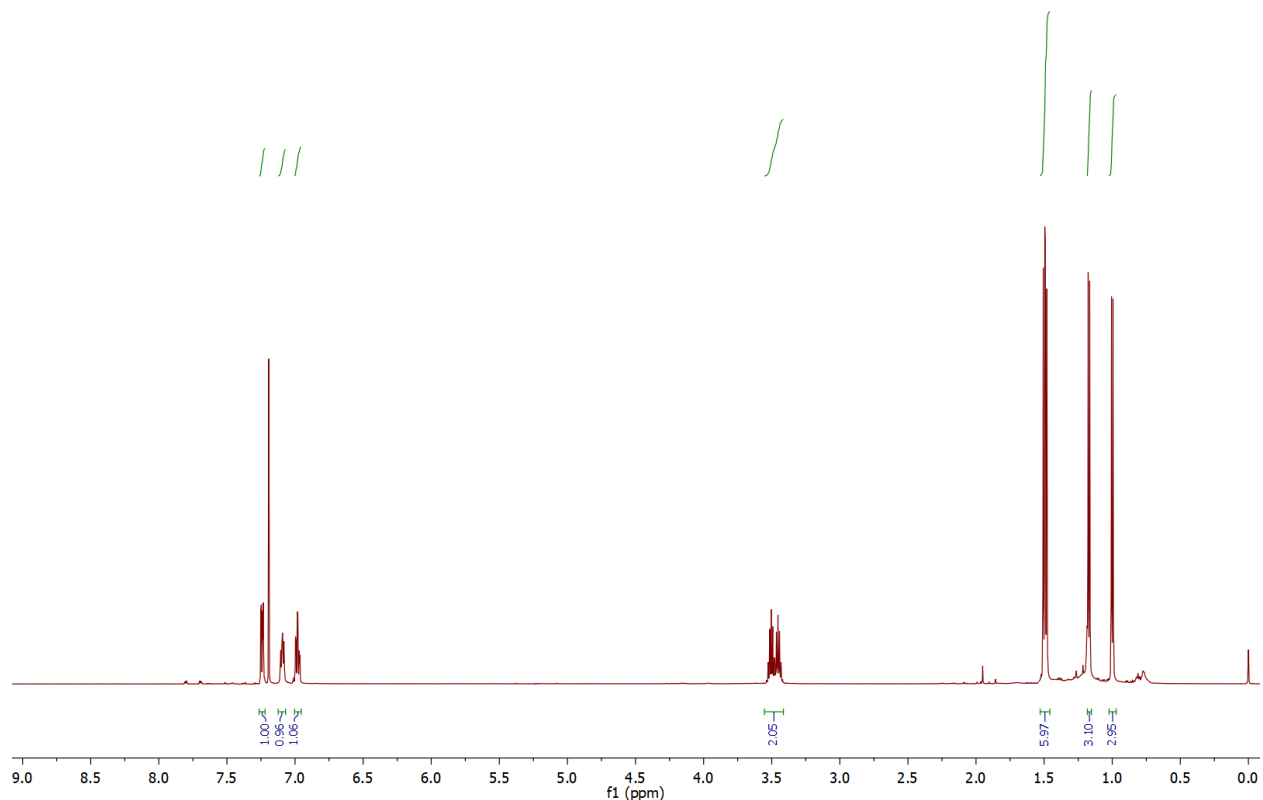
2-bromo-*N,N*-diisopropyl-4-methylbenzamide (3b). Utilizing the general procedure using 219.3 mg of 4-methyl-*N,N*-diisopropylbenzamide (1 mmol, 1.0 equiv), 267 mg of *N*-bromodosuccinimide (1.5 mmol, 1.5 equiv), 48 mg of $[\text{Cp}^*\text{IrCl}_2]_2$ (0.06 mmol, 6 mol%), 5.14 mg of silver acetate (0.24 mmol, 24 mol%). The crude reaction mixture was concentrated under reduced pressure, dissolved in minimal dichloromethane and purified by SiO_2 gel column chromatography (15% EtOAc/DCM). 95% isolated yield (283.3 mg white solid). $^1\text{H-NMR}$ (300 MHz, CDCl_3) δ (ppm): 7.37 (s, 1H, aromatic proton), 7.11 (d, $J = 7.7$ Hz, 1H, aromatic proton), 7.05 (d, $J = 7.7$ Hz, 1H, aromatic proton), 3.68-3.43 (m, 2H, 2 x $\text{CH}(\text{iPr})$), 2.32 (s, 3H, *p*- CH_3), 1.56 (m, 6H, 2 x $\text{CH}_3(\text{iPr})$), 1.22 (d, $J = 6.7$ Hz, 3H, $\text{CH}_3(\text{iPr})$), 1.04 (d, $J = 6.7$ Hz, 3H, $\text{CH}_3(\text{iPr})$).



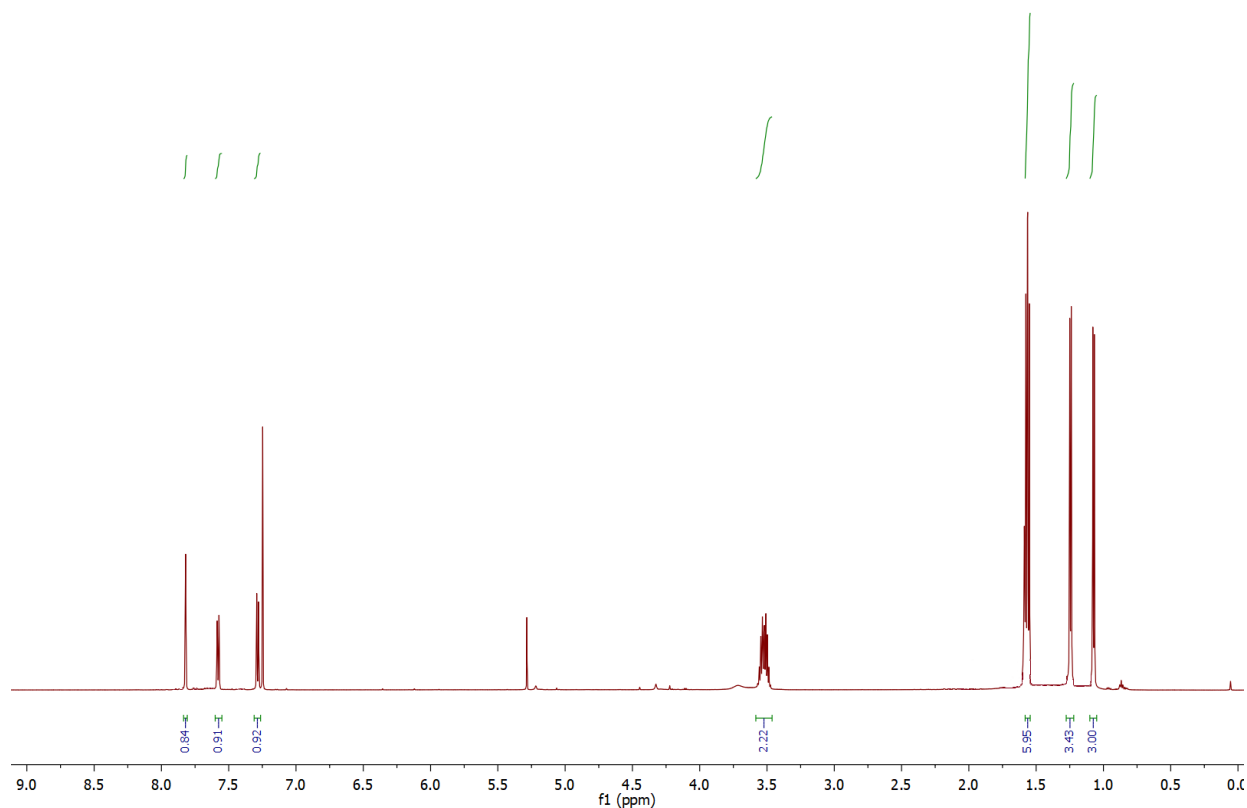
2-bromo-*N,N*-diisopropyl-4-methoxybenzamide (3c). Utilizing the general procedure using 235.3 mg of 4-methoxy-*N,N*-diisopropylbenzamide (1 mmol, 1.0 equiv), 267 mg of *N*-bromodossuccinimide (1.5 mmol, 1.5 equiv), 48 mg of [Cp*IrCl₂]₂ (0.06 mmol, 6 mol%), 5.14 mg of silver acetate (0.24 mmol, 2 mol%). The crude reaction mixture was concentrated under reduced pressure, dissolved in minimal dichloromethane and purified by SiO₂ gel column chromatography (15% EtOAc/DCM). 35% isolated yield (110.0 mg white solid). ¹H-NMR (300 MHz, CDCl₃) δ (ppm): 7.07 (d, *J* = 8.4 Hz, 1H, aromatic proton), 7.06 (d, *J* = 2.4 Hz, 1H, aromatic proton), 6.83 (d, *J* = 8.4 Hz, 1H, aromatic proton), 3.77 (s, 3H, OCH₃), 3.68-3.42 (m, 2H, 2 x CH(*i*Pr)), 1.54 (m, 6H, 2 x CH₃(*i*Pr)), 1.20 (d, *J* = 6.6 Hz, 3H, CH₃(*i*Pr)), 1.03 (d, *J* = 6.6 Hz, 3H, CH₃(*i*Pr)).



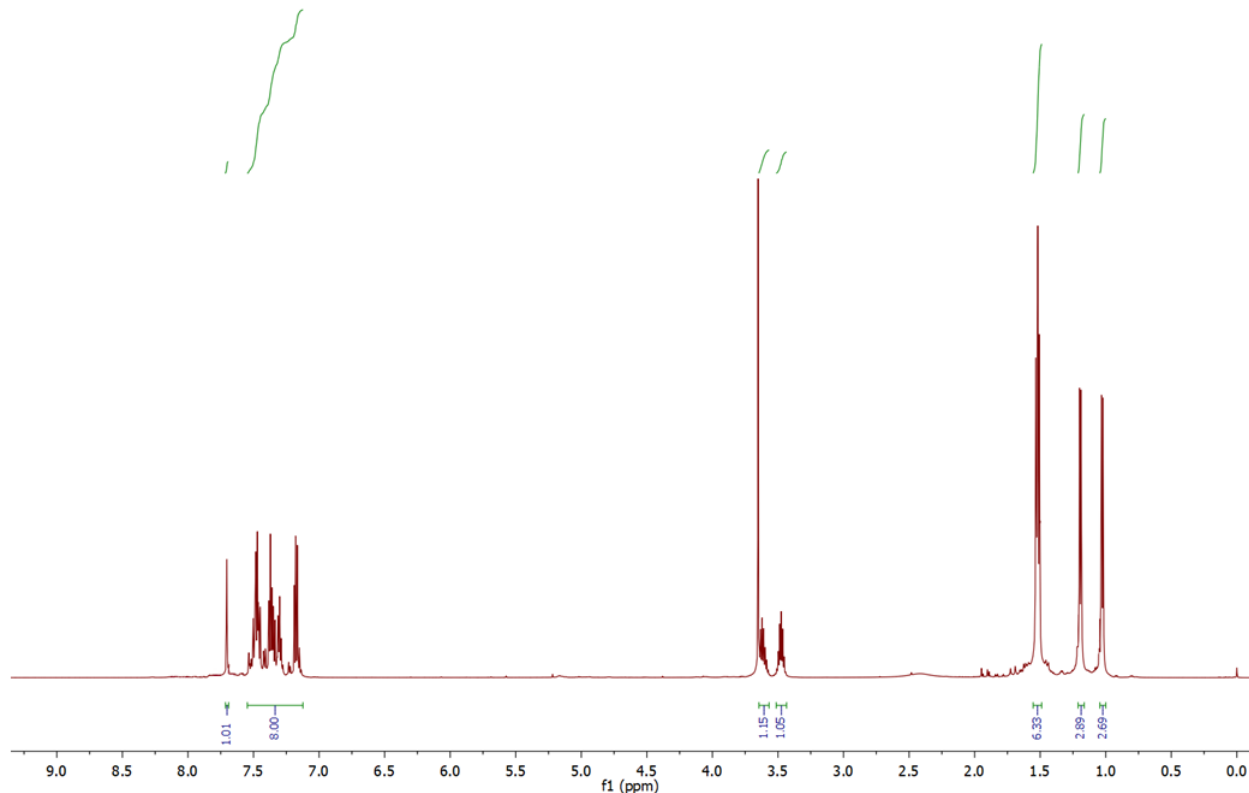
4-chloro-2-bromo-*N,N*-diisopropylbenzamide (3d). Utilizing the general procedure using 239.7 mg of 4-chloro-*N,N*-diisopropylbenzamide (1 mmol, 1.0 equiv), 267 mg of *N*-bromodosuccinimide (1.5 mmol, 1.5 equiv), 48 mg of $[\text{Cp}^*\text{IrCl}_2]_2$ (0.06 mmol, 6 mol%), 5.14 mg of silver acetate (0.24 mmol, 24 mol%). The crude reaction mixture was concentrated under reduced pressure, dissolved in minimal dichloromethane and purified by SiO_2 gel column chromatography (10% EtOAc/DCM). 93% isolated yield (296.3 mg white solid). $^1\text{H-NMR}$ (300 MHz, CDCl_3) δ (ppm): 7.57 (s, 1H, aromatic proton), 7.31 (dd, $J = 8.2$ and 1.9 Hz, 1H, aromatic proton), 7.11 (d, $J = 8.2$ Hz, 1H, aromatic proton), 3.66-3.43 (m, 2H, 2 x $\text{CH}(\text{iPr})$), 1.56 (m, 6H, 2 x $\text{CH}_3(\text{iPr})$), 1.23 (d, $J = 6.7$ Hz, 3H, $\text{CH}_3(\text{iPr})$), 1.06 (d, $J = 6.7$ Hz, 3H, $\text{CH}_3(\text{iPr})$).



4-fluoro-2-bromo-*N,N*-diisopropylbenzamide (3e). Utilizing the general procedure using 223.3 mg of 4-fluoro-*N,N*-diisopropylbenzamide (1 mmol, 1.0 equiv), 267 mg of *N*-bromodosuccinimide (1.5 mmol, 1.5 equiv), 48 mg of [Cp*IrCl₂]₂ (0.05 mmol, 5 mol%), 5.14 mg of silver acetate (0.24 mmol, 24 mol%). The crude reaction mixture was concentrated under reduced pressure, dissolved in minimal dichloromethane and purified by SiO₂ gel column chromatography (10% EtOAc/DCM). 67% isolated yield (202.5 mg white solid). ¹H-NMR (400 MHz, CDCl₃): δ 7.30 (s, 1H, aromatic proton), 7.15 (d, 1H aromatic proton), 7.04 (d, 1H, aromatic proton), 3.56 (m, 2H, 2 x CH(^{*i*}Pr)), 1.55 (m, 6H, 2 x CH₃(^{*i*}Pr)), 1.22 (d, J = 6.7 Hz, 3H, CH₃(^{*i*}Pr)), 1.05 (d, J = 6.7 Hz, 3H, CH₃(^{*i*}Pr)).



2-bromo-*N,N*-diisopropyl-4-(trifluoromethyl)benzamide (3f). Utilizing the general procedure using 273.3 mg of 4-(trifluoromethyl)-*N,N*-diisopropylbenzamide (1 mmol, 1.0 equiv), 267 mg of *N*-bromosuccinimide (1.5 mmol, 1.5 equiv), 48 mg of [Cp*IrCl₂]₂ (0.06 mmol, 6 mol%), 5.14 mg of silver acetate (0.24 mmol, 24 mol%). The crude reaction mixture was concentrated under reduced pressure, dissolved in minimal dichloromethane and purified by SiO₂ gel column chromatography (15% EtOAc/DCM). 86% isolated yield (302.9 mg white solid). ¹H-NMR (400 MHz, CDCl₃) δ (ppm): 7.82 (s, 1H, aromatic proton), 7.59 (d, J = 7.8 Hz, 1H, aromatic proton), 7.30 (d, J = 7.9 Hz, 1H, aromatic proton), 3.61-3.46 (m, 2H, 2 x CH(*i*Pr)), 1.57 (m, 6H, 2 x CH₃(*i*Pr)), 1.25 (d, J = 6.7 Hz, 3H, CH₃(*i*Pr)), 1.08 (d, J = 6.7 Hz, 3H, CH₃(*i*Pr)).



3-bromo-*N,N*-diisopropyl-[1,1'-biphenyl]-4-carboxamide (3g). Utilizing the general procedure using 281.4 mg of *N,N*-diisopropyl-[1,1'-biphenyl]-4-carboxamide (1 mmol, 1.0 equiv), 267 mg of *N*-bromodosuccinimide (1.5 mmol, 1.5 equiv), 48 mg of [Cp*IrCl₂]₂ (0.06 mmol, 6 mol%), 5.14 mg of silver acetate (0.24 mmol, 24 mol%). The crude reaction mixture was concentrated under reduced pressure, dissolved in minimal dichloromethane and purified by SiO₂ gel column chromatography (10% EtOAc/DCM). 80% isolated yield (288.2 mg white solid). ¹H-NMR (300 MHz, CDCl₃): δ = 7.76 (d, J = 1.6 Hz, 1H), 7.57–7.49 (m, 3H), 7.47–7.39 (m, 2H), 7.39–7.32 (m, 1H), 7.22 (d, J = 7.8 Hz, 1H), 3.68 (m, 1H, CH(*i*Pr)), 3.53 (m, 1H, CH(*i*Pr)), 1.59 (m, 6H, 2 x CH₃(*i*Pr)), 1.25 (d, J = 6.7 Hz, 3H, CH₃(*i*Pr)), 1.08 (d, J = 6.7 Hz, 3H, CH₃(*i*Pr)).

Synthesis of Cp*Ir(DMSO)(C₁₃H₁₉NO) (6(DMSO)). In a 5 mL storage tube equipped with a stir bar, was added Cp*Ir(DMSO)Cl₂ (119 mg, 0.25 mmol), *N,N*-diisopropylbenzamide (51.3 mg, 0.25 mmol), acetic acid (2 equiv, 28.6 μ L), and AgOTf (2 equiv, 128.5 mg) to 1,2-dichloroethane (2 mL) and stirred at 60 °C for 1 h. The crude reaction mixture was then filtered and concentrated under reduced pressure to remove excess solvent. The resulting residue was dissolved in minimal dichloromethane. To the concentrated dichloromethane solution excess pentane was added to afford a yellow precipitate. The precipitate was filtered to afford a yellow powder in 90% yield. ¹H-NMR (300 MHz, CDCl₃) δ (ppm): 7.68 (d, J = 6.0 Hz, 1H, aromatic proton), 7.56 (d, J = 6.0 Hz, 1H, aromatic proton), 7.38 (t, J = 6.0, 2H, aromatic proton), 7.20 (m, 1H, aromatic proton), 4.91 (bs, 1H, CH(*i*Pr)), 3.76 (bs, 1H, CH(*i*Pr)), 2.93 (s, 3H, CH₃(DMSO)), 2.56 (s, 3H, CH₃(DMSO)), 1.78 (bs, 15H, Cp*), 1.65-1.30 (m, 12H, 4 x CH₃(*i*Pr)). ¹³C-NMR (100.6 MHz, CD₂Cl₂) δ (ppm): 8.95, 43.13, 44.20, 52.92, 53.19, 53.46, 53.73, 54.00, 95.37, 124.67, 129.36, 133.71, 137.49. Elemental Analysis: Theory: (C, 40.49; H, 5.78; N, 1.57). Found: (C, 40.98; H, 5.15; N, 1.87).

References

1. Rakshit, S.; Patureau, F. W.; Glorius, F. *J. Am. Chem. Soc.* **2010**, *132*, 9585.
2. Zhang, J.; Qian, H.; Liu, Z.; Xiong, C.; Zhang, Y. *Eur. J. Org. Chem.* **2014**, 8110.
3. Morimoto, K.; Hirano, K.; Satoh, T.; Miura, M. *Chem. Lett.* **2011**, *40*, 600.
4. Hyster, T. K.; Rovis, T. *J. Am. Chem. Soc.* **2010**, *132*, 10565.
5. Mochida, S.; Umeda, N.; Hirano, K.; Satoh, T.; Miura, M. *Chem. Lett.* **2010**, *39*, 744.
6. Guimond, N.; Gouliaras, C.; Fagnou, K. *J. Am. Chem. Soc.* **2010**, *132*, 6908.
7. Luo, C. Z.; Jayakumar, J.; Gandeepan, P.; Wu, Y. C.; Cheng, C. H. *Org. Lett.* **2015**, *17*, 924
8. Morimoto, K.; Hirano, K.; Satoh, T.; Miura, M. *Org. Lett.* **2010**, *12*, 2068.
9. Morimoto, K.; Hirano, K.; Satoh, T.; Miura, M. *J. Org. Chem.* **2011**, *76*, 9548.
10. Jia, J.; Shi, J.; Zhou, J.; Liu, X.; Song, Y.; Xu, H. E.; Yi, W. *Chem. Commun.* **2015**, *51*, 2925.
11. Mochida, S.; Hirano, K.; Satoh, T.; Miura, M. *J. Org. Chem.* **2009**, *74*, 6295.
12. Unoh, Y.; Hashimoto, Y.; Takeda, D.; Hirano, K.; Satoh, T.; Miura, M. *Org. Lett.* **2013**, *15*, 3258.
13. Qi, Z.; Wang, M.; Li, X. *Org. Lett.* **2013**, *15*, 5440.
14. Umeda, N.; Hirano, K.; Satoh, T.; Shibata, N.; Sato, H.; Miura, M. *J. Org. Chem.* **2011**, *76*, 13.
15. Frasco, D. A.; Lilly, C. P.; Boyle, P. D.; Ison, E. A. *ACS Catal.* **2013**, *3*, 2421.
16. Satoh, T.; Miura, M. *Chem. Eur. J.* **2010**, *16*, 11212.
17. Song, G.; Wang, F.; Li, X. *Chem. Soc. Rev.* **2012**, *41*, 3651.
18. Kuhl, N.; Schröder, N.; Glorius, F. *Adv. Synth. Catal.* **2014**, *356*, 1443.
19. Shin, K.; Kim, H.; Chang, S. *Acc. Chem. Res.* **2015**, *48*, 1040.
20. Yu, D. G.; Suri, M.; Glorius, F. *J. Am. Chem. Soc.* **2013**, *135*, 8802.
21. Zhang, C.; Zhou, Y.; Deng, Z.; Chen, X.; Peng, Y. *Eur. J. Org. Chem.* **2015**, *8*, 1735.
22. Park, S. H.; Kwak, J.; Shin, K.; Ryu, J.; Park, Y.; Chang, S. *J. Am. Chem. Soc.* **2014**, *136*, 2492.
23. Wang, N.; Li, R.; Li, L.; Xu, S.; Song, H.; Wang, B. *J. Org. Chem.* **2014**, *79*, 5379.

24. Yang, Y.; Hou, W.; Qin, L.; Du, J.; Feng, H.; Zhou, B.; Li, Y. *Chem. Eur. J.* **2014**, *20*, 416.
25. Gwon, D.; Lee, D.; Kim, J.; Park S.; Chang, S. *Chem. Eur. J.* **2014**, *20*, 12421.
26. Gwon, D.; Park, S.; Chang, S. *Tetrahedron* **2015**, *71*, 4504.
27. Mochida, S.; Hirano, K.; Satoh, T.; Miura, M. *Org. Lett.* **2010**, *12*, 5776.
28. Mochida, S, Hirano, K, Satoh, T, Miura, M. *J. Org. Chem.* **2011**, *76*, 3024.
29. Patel, P.; Chang, S. *Org. Lett.* **2014**, *16*, 3328.
30. Kim, H.; Shin, K.; Chang, S.; *J. Am. Chem. Soc.* **2014**, *136*, 5904.
31. Suzuki, C.; Hirano, K.; Satoh, T.; Miura, M. *Org. Lett.* **2015**, *17*, 1597.
32. Hull, J. F.; Balcells, D.; Blakemore, J.D.; Incarvito, C.D.; Eisenstein, O.; Brudvig, G.W.; Crabtree, R.H. *J. Am. Chem. Soc.* **2009**, *131*, 8730.
33. Hintermair, U.; Sheehan, S.W.; Parent, A.R.; Ess, D.H.; Richens, D.T.; Vaccaro, P.H.; Brudvig, G.W.; Crabtree, R.H. *J. Am. Chem. Soc.* **2013**, *135*, 10837.
34. Zhou, M.; Schley, N.D.; Crabtree, R.H. *J. Am. Chem. Soc.* **2010**, *132*, 12550.
35. Zhou, M.; Balcells, D.; Parent, A.R.; Crabtree, R.H.; Eisenstein, O. *ACS Catal.* **2012**, *2*, 208.
36. Zhou, M.; Hintermair, U.; Hashiguchi, B.G.; Parent, A.R.; Hashmi, S.M.; Elimelech, M.; Periana, R.A.; Brudvig, G.W.; Crabtree, R.H.; *Organometallics* **2013**, *32*, 957.
37. Hohloch, S.; Kaiser, S.; Duecker, F.L.; Bolje, A.; Maity, R.; Kos̃mrlj, J.; Sarkar, B. *Dalton Trans.* **2015**, *44*, 686.
38. Schröder, N.; Wencel-Delord, J.; Glorius, F. *J. Am. Chem. Soc.* **2012**, *134*, 8298.
39. Kuhl, N.; Schröder, N.; Glorius, F. *Org. Lett.* **2015**, *15*, 3860.
40. Schröder, N.; Lied, F.; Glorius, F. *J. Am. Chem. Soc.* **2015**, *137*, 1448.
41. Hwang, H.; Kim, J.; Jeong, J.; Chang, S. *J. Am. Chem. Soc.* **2014**, *136*, 10770.
42. Zhang, P, Hong, L.; Li, G.; Wang.; R. *Adv. Synth. Catal.* **2015**, *357*, 345.
43. Qian, G.; Hong, X.; Liu, B.; Mao, H.; Xu, B. *Org. Lett.* **2014**, *16*, 5294.
44. Erbing, E.; Sanz-Marco, A.; Vazquez-Romero, A.; Malmberg, J.; Johanson, M. J.; Gomez-Bengoa, E.; Martin-Matute, B. *ACS Catal.* **2018**, *8*, 920.
45. Klein, D. R. *Organic Chemistry*, 2nd ed.; John Wiley & Sons, 2013.
46. Silverman, G. S.; Rakita, P. E. (Eds), *Handbook of Grignard Reagents*, Dekker, New York, **1996**.

47. *Handbook of Organopalladium Chemistry for Organic Synthesis*, ed. E. Negishi, Wiley Interscience, New York, **2002**, vol. 1.
48. Gribble, G. *Acc. Chem. Res.*, **1998**, *31*, 141.
49. Jeschke, P. *Pest Manage. Sci.* **2010**, *66*, 10.
50. Wilcken, R.; Zimmermann, M. O.; Lange, A.; Joerger, C. *J. Med. Chem.*, **2013**, *56*, 1363.
51. Hodgson, H. H. *Chem. Rev.* **1947**, *40*, 251.
52. Beak, P.; Brown, R.A. *J. Org. Chem.*, **1982**, *47*, 34.
53. Whitfield, S. R.; Sanford, M. S. *J. Am. Chem. Soc.* **2007**, *129*, 15142.
54. Whitfield, S. R.; Sanford, M. S. *Organometallics* **2008**, *27*, 1683.
55. Mei, T. S.; Wang, D. H.; Yu, J. Q. *Org. Lett.* **2010**, *12*, 3140.
56. Li, J. J.; Mei, T. S.; Yu, J. Q. *Angew. Chem., Int. Ed.* **2008**, *47*, 6452.
57. Bedford, R. B.; Engelhart, J. U.; Haddow, M. F.; Mitchell, C. J.; Webster, R. L. *Dalton Trans.* **2010**, *39*, 10464.
58. Bedford, R. B.; Haddow, M. F.; Mitchell, C. J.; Webster, R. L. *Angew. Chem., Int. Ed.* **2011**, *50*, 5524.
59. Dubost, E.; Fossey, C.; Cailly, T.; Rault, S.; Fabis, F. *J. Org. Chem.* **2011**, *76*, 6414.
60. Song, B.; Zheng, X.; Mo, J.; Xu, B. *Adv. Synth. Catal.* **2010**, *352*, 329.
61. Lied, F.; Lerchen, A.; Knecht, T.; Mück, L. C.; Glorius, F. *ACS Catal.* **2016**, *6*, 7839.
62. Zhang, T.; Qi, X.; Liu, S.; Bai, R.; Liu, C.; Lan, Y. *Chem. Eur. J.* **2017**, *23*, 2690.
63. Castanet, A. S.; Colobert, F.; Broutin, P. E. *Tetrahedron Lett.* **2002**, *43*, 5047.
64. Lehman, M. C.; Gary, J. B.; Boyle, P. D.; Sanford, M. S.; Ison, E. A. *ACS Catal.* **2013**, *3*, 2304.
65. Kepper, F. C.; Feiters, M. C.; Olofsson, B.; Kaiho, T.; Yanagida, S.; Zimmermann, M. B.; Carpenter, L. J.; Luther III, G. W.; Lu, Z.; Jonsson, M.; Kloo, L. *Angew. Chem. Int. Ed.* **2011**, *50*, 11598;
66. Kepper, F. C.; Feiters, M. C.; Olofsson, B.; Kaiho, T.; Yanagida, S.; Zimmermann, M. B.; Carpenter, L. J.; Luther III, G. W.; Lu, Z.; Jonsson, M.; Kloo, L. *Angew. Chem.* **2011**, *123*, 11802.

67. Muñiz, K.; García, B.; Martínez, C.; Piccinelli, A. *Chem. Eur. J.* **2017**, *23*, 1539.
68. Barluenga, J.; González, J. M.; Campos, P. J.; Asensio, G. *Angew. Chem. Int. Ed. Engl.* **1985**, *24*, 319.
69. Barluenga, J. *Pure Appl. Chem.* **1999**, *71*, 431.
70. Ashikari, Y.; Shimizu, A.; Nokami, T.; Yoshida, J. I. *J. Am. Chem. Soc.* **2013**, *135*, 16070.
71. Shimizu, A.; Hayashi, R.; Ashikari, Y.; Nokami, T.; Yoshida, J. I.; Beilstein. *J. Org. Chem.* **2015**, *11*, 242.
72. White, C.; Yates, A.; Maitlis, P. M.; Heinekey, D. M. *Inorganic Synthesis*; John Wiley & Sons, Inc., 2007; pp 228.
73. Frasco, D. A.; Mukherjee, S.; Sommer, R. D.; Perry, C. D.; Lambic, N. S.; Abboud, K. A.; Jakubikova, E.; Ison, E. A. *Organometallics* **2016**, *35*, 2435.
74. Frisch, M. J.; Trucks, G. W.; Schlegel, H. B.; Scuseria, G. E.; Robb, M. A. Inc., Wallingford, CT 2009.
75. Parr, R. G.; Yang, W. New York 1989.
76. Hehre, W. J.; Ditchfield, R.; Pople, J. A. *J. Chem. Phys.* **1972**, *56*, 2257.
77. Dolg, M.; Stoll, H.; Preuss, H.; Pitzer, R. M. *J. Phys. Chem.* **1993**, *97*, 5852.
78. Hay, P. J.; Wadt, W. R. *J. Chem. Phys.* **1985**, *82*, 270.
79. Rassolov, V. A.; Pople, J. A.; Ratner, M. A.; Windus, T. L., 6-31G* basis set for atoms K through Zn. *The Journal of Chemical Physics* 1998, *109* (4), 1223-1229.
80. Hay, P. J.; Wadt, W. R. *J. Chem. Phys.* **1985**, *82*, 299.
81. Marenich, A. V.; Cramer, C. J.; Truhlar, D. G. *J. Phys. Chem. B* **2009**, *113*, 6378.
82. Tomasi, J.; Mennucci, B.; Cammi, R. *Chem. Rev.* **2005**, *105*, 2999.
83. Engelman, K. L.; Feng, Y.; Ison, E. A. *Organometallics* **2011**, *30*, 4572.
84. For comparable KIE values: (a) Ref. 38; (b) L. Wang and L. Ackerman, *Chem. Commun.*, **2014**, *50*, 1083.
85. K. Muñiz, B. García, C. Martínez and A. Piccinelli, *Chem. Eur. J.*, **2017**, *23*, 1539.
86. (a) Gorelsky, S. I.; Lapointe, D.; Fagnou, K.; *J. Am. Chem. Soc.*, **2008**, *130*, 10848.; (b) Walsh, A. P.; Jones, W. D.; *Organometallics*, **2015**, *34*, 3400; (c) Gorelsky, S. I.; Lapointe, D.; Fagnou, K.; *J. Org. Chem.*, **2012**, *77*, 658; (d) Jiang,

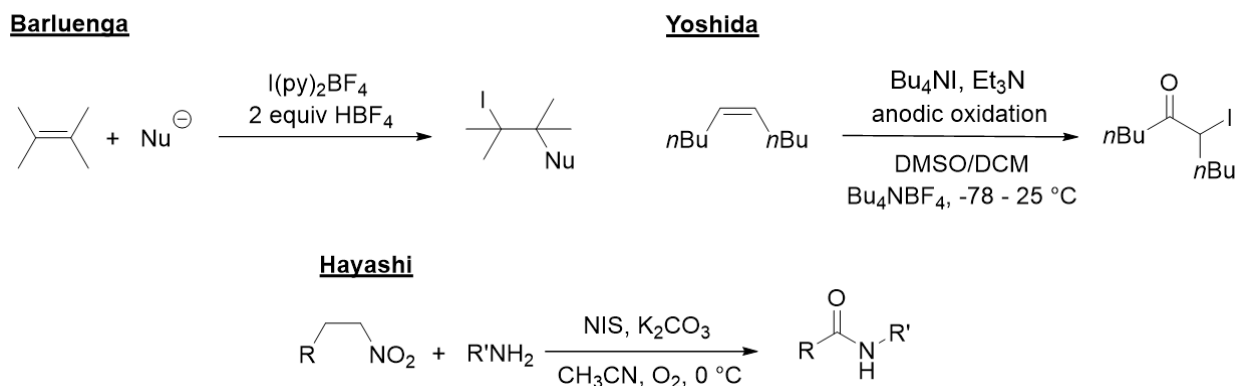
J.; Ramozzi, R.; Morokuma, K.; *Chem. Eur. J.*, **2015**, 21, 11158.; (e) Ackermann, L.; *Chem. Rev.*, **2011**, 111, 1315.

CHAPTER 3 – Improvement of the Generation of Hypervalent Halonium Species for the Halogenation of Benzamides

Introduction

As mentioned in Chapter 2, hypervalent iodine reagents have gained interest in the synthetic community as versatile reagents for several organic reactions. So far, there have been several applications for hypervalent halogens, mostly hypervalent iodine. Although iodine (III) and iodine (V) species have been extensively studied,¹⁻³⁰ much less is known about halogen(I) intermediates. A few hypervalent halogen (I) systems based on nitrogen,³¹⁻⁴² oxygen,⁴³⁻⁴⁷ and sulfur⁴⁸⁻⁵³ Lewis basic sites have been developed, but very little is known structurally and experimentally in terms their reactivity (**Scheme 3.1**).

Scheme 3.1. Reactivity of hypervalent iodine (I)



The halogen-bonding interaction between the halogen (I) precursor and the Lewis base (as solvent, catalyst or additive) leads to the formation of these stable key intermediates, which facilitate these reactions. It has been shown that the halogen-bonding interaction between the Lewis base and the halogen (I) atom increases the electrophilicity of the halogen center.⁵⁴⁻⁵⁶ This observation lends itself to further investigation, as the Lewis acidic and basic components of these electrophilic halogen (I) adducts can be tuned to enhance or enable reactivity, as demonstrated in chapter 2. This chapter deals with the study of the isolated acetyl hypohalite species characterized in Chapter 2, and how it can be modulated to improve reactivity towards the halogenation of benzamides.

Results and Discussion

Chlorinations and Brominations

From the $^1\text{H-NMR}$ spectrum (**Figure 2.16**) of a solution containing *N*-halosuccinimide with tetrabutylammonium acetate (TBAOAc), the rapid formation of a new species was observed at room temperature. Furthermore, it was demonstrated computationally that the formation of the acetyl hypohalites is accessible, and the difference in reactivity was likely due to the oxidative addition step involving the hypohalite species. This allowed us to model the rate determining step of the reaction with varying carboxylates to see if the oxidative addition of acetyl hypochlorite became more accessible. From **Scheme 3.2** we can see the oxidative addition for the species containing trifluoromethyl ($-\text{CF}_3$) is more accessible with an oxidative addition barrier at $18.7 \text{ kcal mol}^{-1}$ than the oxidative addition of the species containing a methyl ($-\text{CH}_3$), by $3.3 \text{ kcal mol}^{-1}$, or *tert*-butyl ($-\text{C}(\text{CH}_3)_3$) group, by $0.6 \text{ kcal mol}^{-1}$, with barriers for oxidative addition at $22.0 \text{ kcal mol}^{-1}$ and $19.3 \text{ kcal mol}^{-1}$ respectively. This is likely due to the strength of the O-Cl bond.

With this observation the chlorination reaction was attempted with trifluoroacetic acid as an additive instead of acetic acid. The reaction did not take place with NCS after attempting a variety of conditions, varying temperature, times, catalyst loadings, additives, etc. Interestingly, when the chlorine source was changed from NCS to trichloroisocyanuric acid (TCC), 54% conversion of *N,N*-diisopropylbenzamide was observed (**Figure 3.1**). TCC is a stronger chlorine source than NCS, with a reported “active chlorine content” of 91.5% (percentage of active chlorine in the molecule in the oxidation of hydroiodic acid).⁵⁷

Scheme 3.2. DFT (B3PW91-D3) calculated energetics for the oxidative addition of Cl(carboxylate) to **INT-4** in 1,2-dichloroethane solvent

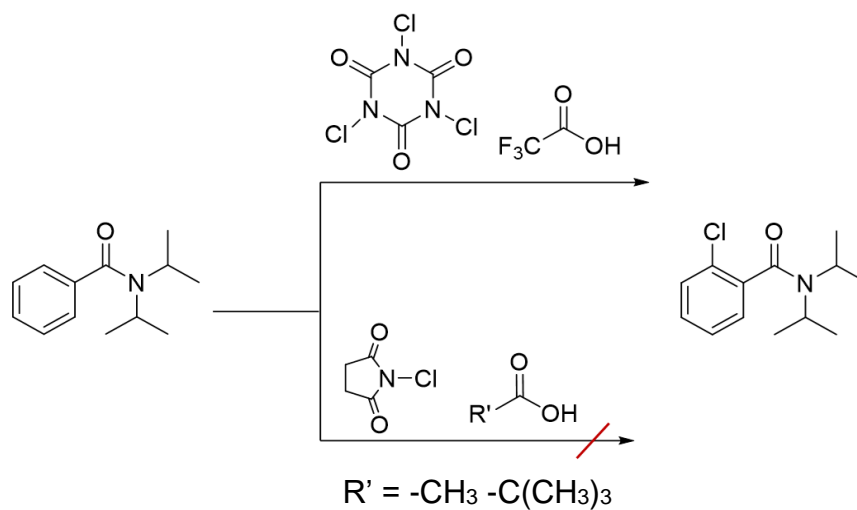
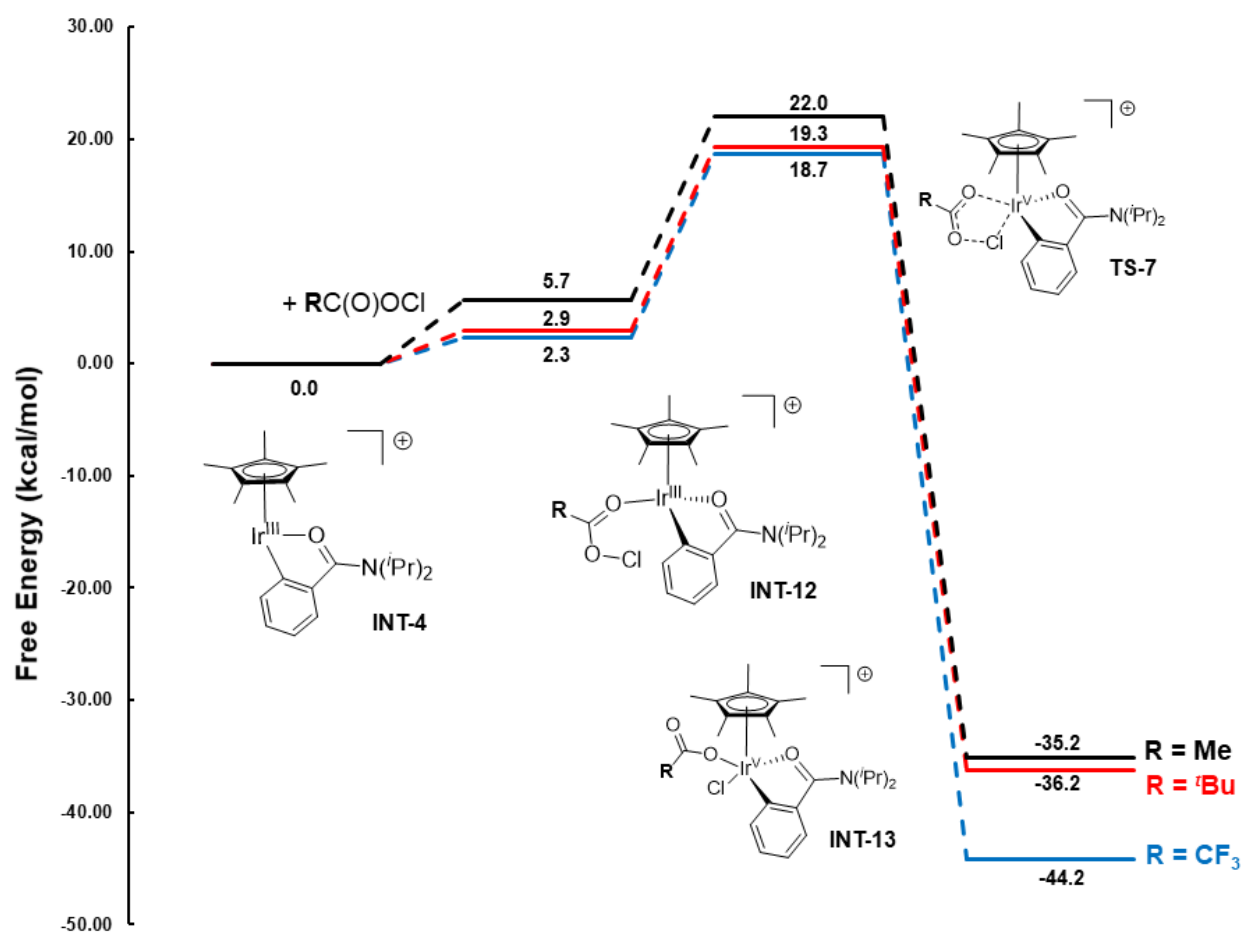
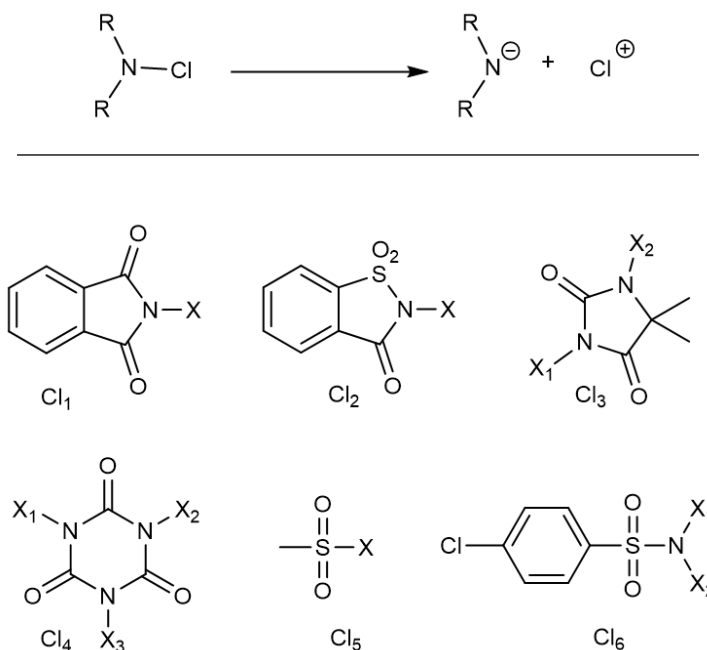


Figure 3.1. Species compatible for the chlorination of *N,N*-diisopropylbenzamide

In other words, TCC has a weaker N-Cl bond than NCS, as shown computationally in **Scheme 3.3**. Based on these results, we hypothesize that the appropriate halogen source, weak enough N-X bond (X = halogen), and Lewis basic additive will generate the respective hypohalite species *in situ*, which then undergoes oxidative addition. We then calculated a series of bond dissociation energies (BDE) for a variety of halogen sources in order to screen for appropriate candidates to optimize the halogenation reaction. For the chlorine sources with multiple chlorine equivalents, the bases were denoted as follows: the first dissociation, dissociation of X1, is referred to as “base”, the second dissociation, dissociation of X2, is referred to as “base2”, and the third dissociations as ‘base3”. From the chlorinating agents screened, NCS, Cl₁, Cl₃ and Cl₄ were used experimentally. Product formation was observed exclusively with Cl₄, as expected from the computational results. It seems that a BDE ≥ 285 kcal mol⁻¹ is too high for an appropriate chlorinating agent under our reaction conditions, as TCC has a BDE of 268 kcal mol⁻¹ for its first N-Cl dissociation.

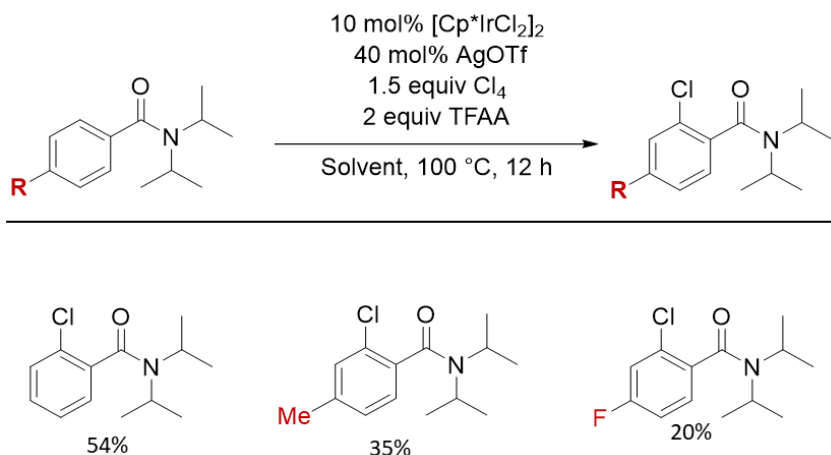
Cl Source	BDE (Kcal/mol)
NCS	293.71
Cl ₁	291.79
Cl ₂	274.77
Cl _{3_base}	285.36
Cl _{3_base2}	293.57
Cl _{3_base3}	628.77
Cl _{4_base}	267.72
Cl _{4_base2}	580.85
Cl _{4_base3}	940.03
Cl _{5_Cl}	308.93
Cl _{6_base}	280.16
Cl _{6_base2}	637.34

Scheme 3.3. BDE table for a series of electrophilic chlorinating agents



To show the improvement on the chlorination reaction, three substrates were used. An unsubstituted benzamide, *N,N*-diisopropylbenzamide, an electron-rich benzamide, 4-methoxy-*N,N*-diisopropylbenzamide, and an electron-deficient benzamide, 4-trifluoromethyl-*N,N*-diisopropylbenzamide. As depicted in **Scheme 3.4**, all three substituents in the *para*-position were tolerated and yielded the corresponding chlorinated benzamide in moderate yields. Harsher conditions are required to enable the chlorination, higher catalyst loading, higher temperatures, and longer reaction times. This is consistent with the computational results from Chapter two.

Scheme 3.4. Scope of chlorinated *para*-substituted *N,N*-diisopropylbenzamides



Based on the success of this approach, the BDE of a variety of brominating agents was examined to improve upon the previous system, based on acetic acid, which did not have the same effectiveness as the conditions for the iodination reaction. As shown in **Scheme 3.4**, The brominating agent Br₃ had the lowest BDE at 236 kcal mol⁻¹ for its first N-Br dissociation. When this bromine source in our reaction was used in the presence of TFAA, unsubstituted benzamide, *p*-CH₃ benzamide, *N,N*-diisopropylbenzamides were brominated with the same effectiveness. Moreover, we can see that the naphthyl and biaryl benzamides were isolated in high yields when compared to the conditions with acetic acid. The bromination reaction with the *p*-F benzamide, *p*-Cl benzamide and *p*-CF₃ benzamide were also higher yielding. This serves as further evidence for BDEs as a feature to consider when choosing a halogen source for generating these electrophilic hypohalite species.

Scheme 3.5. BDE table for a series of electrophilic brominating agents

Br Source	BDE (Kcal/mol)
NBS	254.63
Br ₁	252.83
Br ₂	263.23
Br _{3_base}	235.50
Br _{3_base2}	514.46
Br ₄	236.46
Br _{5_base}	247.46
Br _{5_base2}	255.52
Br ₆	361.61

$$\text{R}_2\text{N}-\text{Br} \longrightarrow \text{R}_2\text{N}^{\ominus} + \text{Br}^{\oplus}$$

Br₁

Br₂

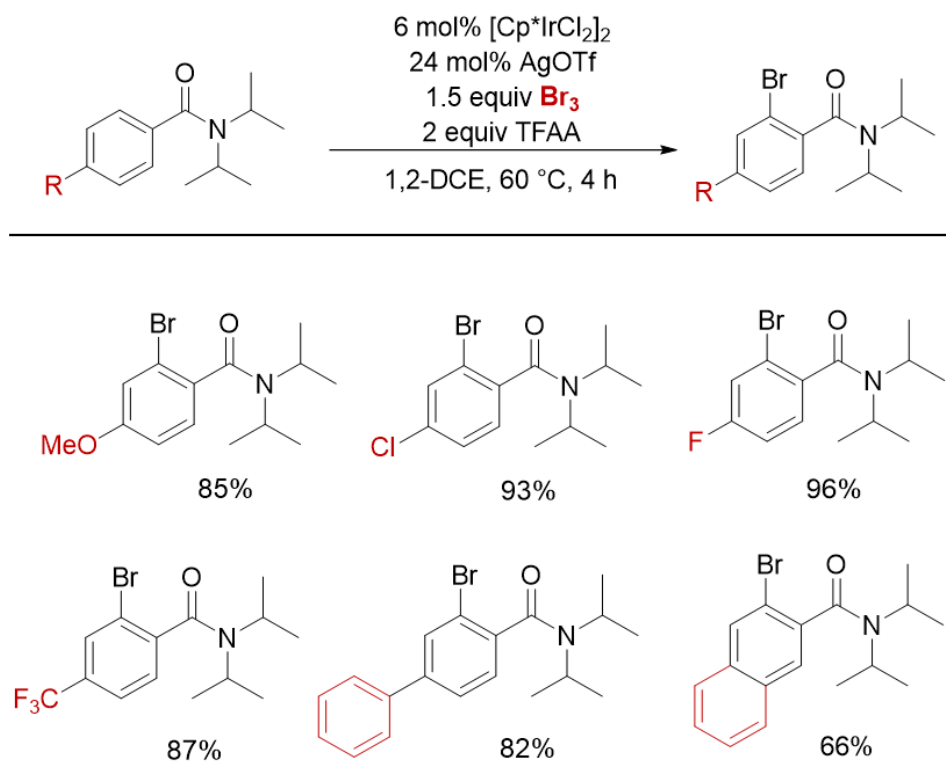
Br₃

Br₄

Br₅

Br₆

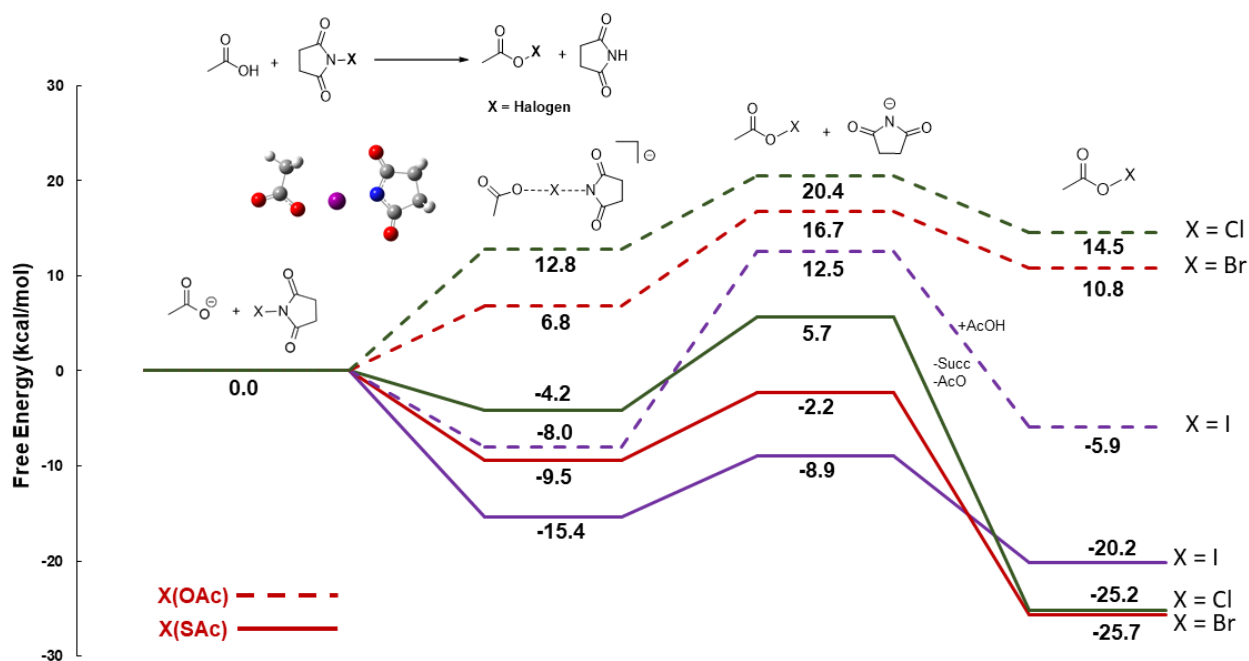
Scheme 3.6. Scope of brominated *para*-substituted *N,N*-diisopropylbenzamides under adjusted reaction conditions



Lewis base effect on chlorinations

Just as the halogen sources were studied for their effect on the RDS of the reaction, it stands to reason that the Lewis base component of the halogen (I) adducts should be further studied for the impact they may have on the chlorination of benzamides. In **Scheme 3.6**, the halogen (I) adduct formation is modeled with acetate and thioacetate as the Lewis base. From this we can see the halogen (I) adducts from acetate are higher in energy than those from thioacetate. This is consistent with previous reports of more basic, or electronegative Lewis bases generating more reactive or electrophilic hypohalite species.⁵⁸ This shows that these halogen (I) adducts are accessible with various Lewis bases.

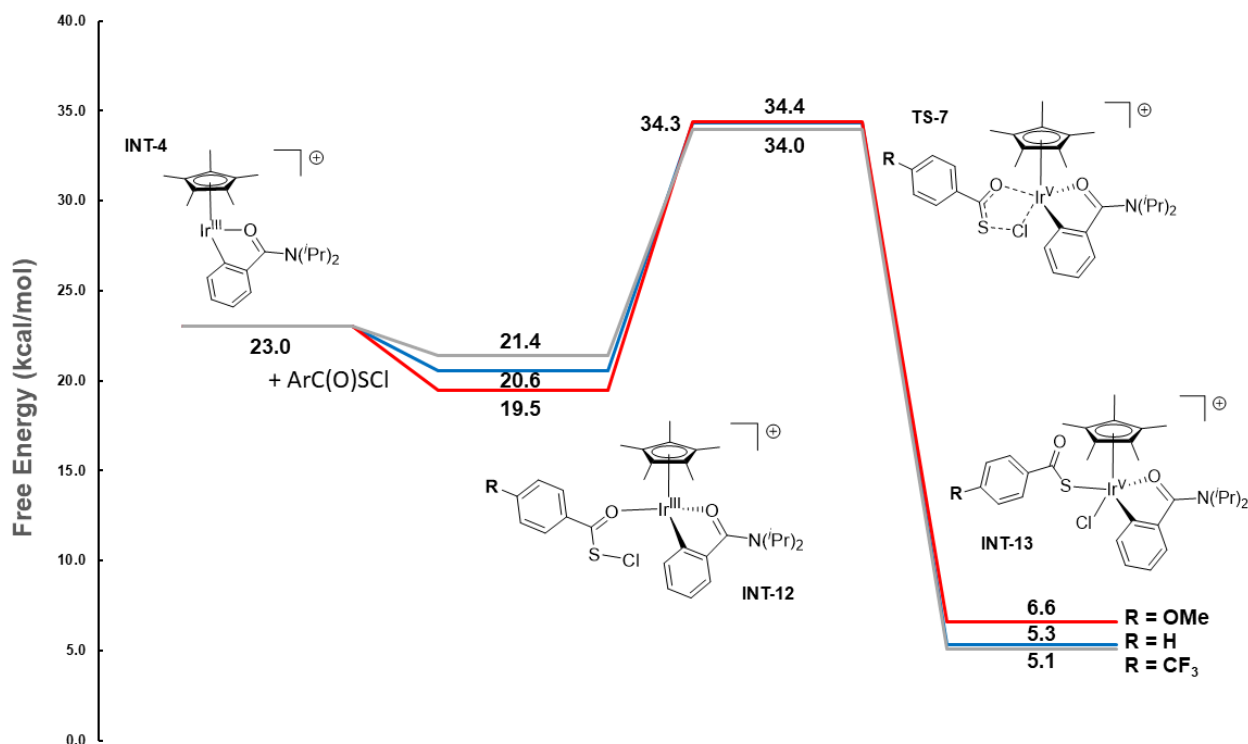
Scheme 3.7. Comparison between the association of halosuccinimide with acetate and thioacetate



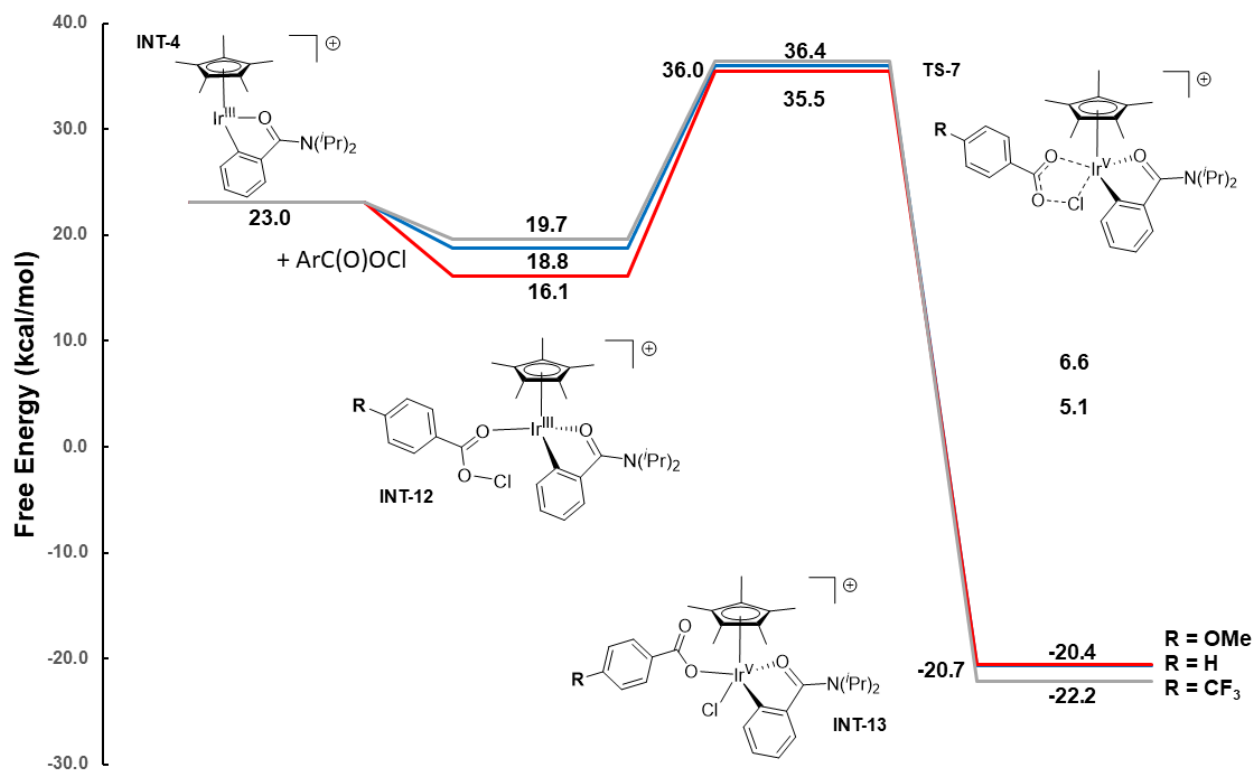
From this we proceeded to model the RDS of the chlorination reaction with various benzoates and benzoate analogues, where the electronics in the para-position was changed. Benzoates and benzoate derivatives are convenient Lewis bases to model computationally, as these are easily accessible synthetically, as many isolated benzoate halogen (I) adducts can be found in the literature. From **Scheme 3.7** we can see the

oxidative addition for a series of benzoate hypochlorites, in **Scheme 3.8** the oxidative addition for a series of thiobenzoate hypochlorites, and in **Scheme 3.9** the oxidative addition of a series of N-methylbenzamide species. A few observations can be made when all three benzoate analogues are compared. **INT-12** is stabilized by an electron-rich Lewis base, when compared to an electron-deficient Lewis base. In addition, when the oxidative addition RDS was compared, these benzoate and benzoate analogue hypochlorite species are higher in energy than the oxidative addition for the carboxylate hypochlorite species (**Scheme 3.2**). Moreover, the benzoate and thiobenzoate hypochlorite species have comparable barriers for oxidative addition, within 1 kcal mol⁻¹, while the benzamide hypochlorite species have a higher energy associated to the oxidative addition step (48.8 kcal mol⁻¹ – 49.3 kcal mol⁻¹).

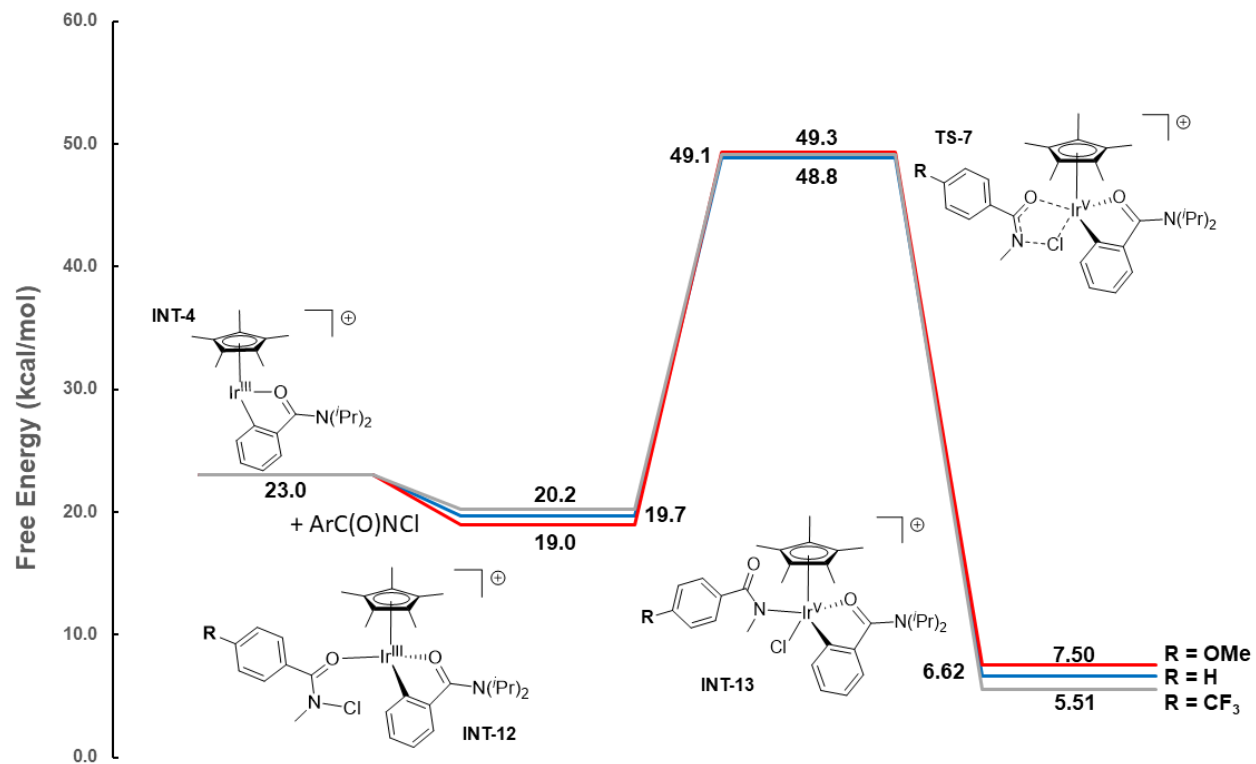
Scheme 3.8. DFT (B3PW91-D3) calculated energetics for the oxidative addition of Cl(thiobenzoate) to **INT-4** in 1,2-dichloroethane solvent



Scheme 3.9. DFT (B3PW91-D3) calculated energetics for the oxidative addition of Cl(benzoate) to **INT-4** in 1,2-dichloroethane solvent



Scheme 3.10. DFT (B3PW91-D3) calculated energetics for the oxidative addition of Cl(N-Methylbenzamide) to **INT-4** in 1,2-dichloroethane solvent

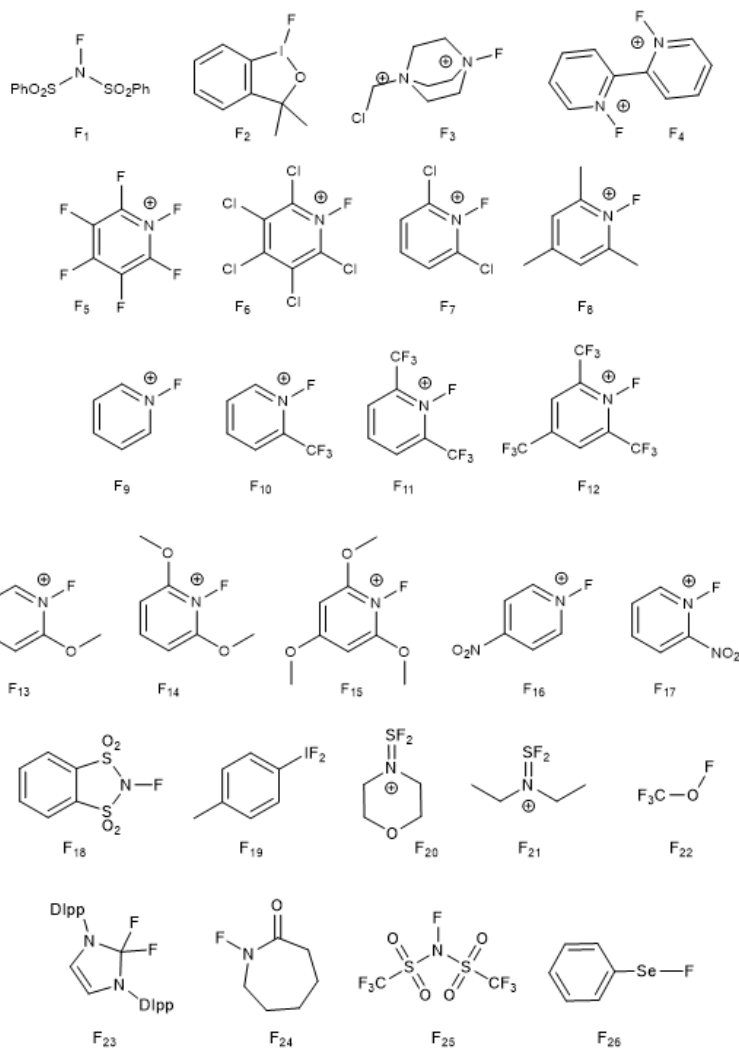
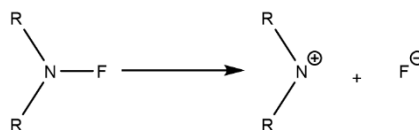


Fluorinations

Following the success of this approach, a variety of electrophilic fluorinating sources were screened in order to identify any possible candidates to extend this chemistry for the fluorination of benzamides. As shown in **Scheme 3.6**, the BDEs for several electrophilic fluorinating agents have been calculated. In comparison to the BDEs of NIS, NBS and TCC, and Br₄, the BDE for these fluorinating agents are orders of magnitude higher. This explains why no reactivity has been observed with F₁, F₃, and F₈. A few observations can be drawn from the BDEs screened. Firstly, considering the fluorine sources containing an N-F bond, cationic species have a lower BDE than neutral species. In addition, for electron-deficient species, fluorine sources bearing a -CF₃ or -NO₂ group, have a lower N-F BDE when compared to more electron-rich sources, like those bearing -CH₃ or -OMe groups. This is clear when pyridinium sources (F₄-F₁₇), and F₁ and F₂₅ are compared. Secondly, fluorine sources not based on nitrogen (I-F, S-F, O-F, and Se-F), have higher fluorine BDEs than those sources containing an N-F bond.

F Source	BDE (Kcal/mol)
F1	416.75
F2	487.09
F3	373.83
F4_base	367.45
F4_base2	765.19
F5	350.80
F6	365.60
F7	375.80
F8	406.89
F9	397.73
F10	383.50
F11	369.74
F12	362.77
F13	392.85
F14	387.82
F15	390.63
F16	385.61
F17	372.45
F18	410.54
F19	459.86
F20	412.80
F21	416.32
F22	523.12
F23	394.24
F24	480.40
F25	384.33
F26	473.83

Scheme 3.11. BDE table for a series of electrophilic fluorinating agents



Conclusion

In this chapter, the Lewis basic and Lewis acidic components of the acetyl hypohalite species involved in the halogenation of benzamides were studied in more detail. A computational study was done to screen electrophilic halogen sources by their BDEs, as this was identified as a key factor in acetyl hypohalite formation. The appropriate combination of halogen source and carboxylate improved the yield of the bromination of benzamides and enabled the chlorination as well. This is highlighted by the high isolated yields of the scope for the bromination reaction and the moderate to low yields of the benzamides studied. Attempts to improve the chlorination of benzamides included the analysis of the RDS of the reaction, oxidative addition of the hypochlorite species, with a variety of Lewis bases. It was shown that benzoate and benzoate derived Lewis bases did not have a positive effect on the RDS. The oxidative addition of these species was higher in energy ($48.8 \text{ kcal mol}^{-1}$ – $49.3 \text{ kcal mol}^{-1}$) than the energies associated with the oxidative addition for the acetyl hypochlorite species ($18.7 \text{ kcal mol}^{-1}$ – $22.0 \text{ kcal mol}^{-1}$). In addition, the BDE for a variety of electrophilic fluorine sources were calculated. The BDEs for these electrophilic fluorine sources ranged between $350.8 \text{ kcal mol}^{-1}$ – $523.1 \text{ kcal mol}^{-1}$ and are too high to enable the formation of an analogous hypofluorite species, when compared to the BDEs of the halogen sources that have worked under our reaction conditions. Experimental attempts at the fluorination of benzamides with electrophilic sources F₁, F₃, and F₈ have not been fruitful, and the computational data would support the lack of hypofluorite formation. This work will allow for further understanding and exploration of the reactivity of these hypohalite species generated under our reaction conditions.

Experimental

General Considerations

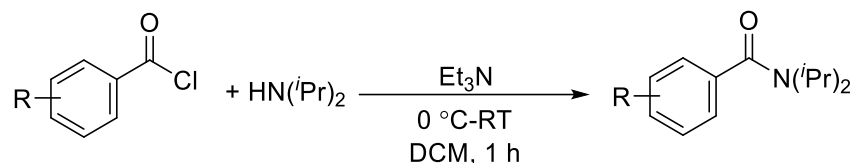
$\text{IrCl}_3 \cdot 3\text{H}_2\text{O}$ was purchased from Pressure Chemical Company. $[\text{Cp}^*\text{IrCl}_2]_2$, was prepared as previously reported. All other reagents were purchased from commercial sources and used as received unless stated otherwise. All reactions were performed under air and using non-dry solvents unless otherwise noted. ^1H and spectra were obtained at room temperature on a Varian Mercury 400 MHz spectrometer. Chemical shifts are listed in parts per million (ppm) and referenced to their residual protons or carbons of the deuterated solvents.

Computational Studies

This study was carried out using density functional theory (DFT) with the Gaussian09,⁵⁹ implementation of the B3PW91 functional, with Grimmes dispersion correction (D3) as implemented through Gaussian.⁶⁰ All geometry optimizations were carried out using tight convergence criteria (“opt=tight”) on an ultrafine grid (“int=ultrafine”). The Stuttgart-Dresden (SDD) relativistic effective core potential (RECP) basis set was used for iridium with an additional f polarization function.^{61, 62} The def2-TZVP effective core potential (ECP)^{63, 64} and basis set was used for the halogens. The 6-31G** basis set was used for all other atoms.⁶⁵ Solvation energies were computed with geometries optimized in the gas phase using the SMD method,⁶⁶ with dichloroethane as the solvent, as implemented in Gaussian 09. In this method an IEFPCM calculation is performed with radii and electrostatic terms from Truhlar and co-workers’ SMD solvation model.⁶⁷ Energetics were calculated using the 6-311++G** basis set for all atoms and the SDD basis set with an added f polarization function on iridium. The def2-TZVP ECP and basis set was used for the halogens. All energies are reported in kcal mol^{-1} .

Benzamide Derivative Synthesis

General Procedure for the synthesis of benzamides from acyl chlorides



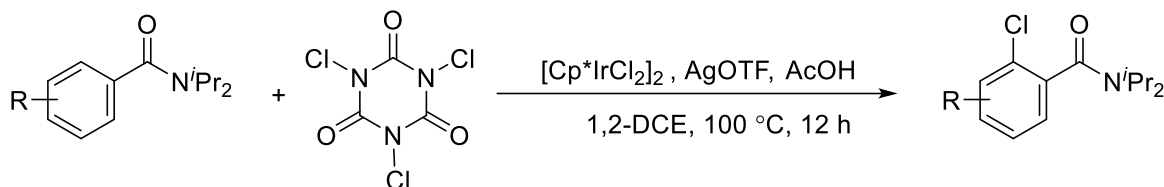
To a round bottom flask equipped with a magnetic stir bar, the corresponding amine (1.10 equiv), and triethylamine (1.20 equiv) in dichloromethane. The corresponding benzoyl chloride (1.05 equiv) was added dropwise at $0\text{ }^\circ\text{C}$. The reaction mixture was stirred and allowed to warm up to room temperature. The reaction mixture was diluted with dichloromethane, washed with a 1N HCl solution and brine. The organic layer was dried over sodium sulfate, filtered, and concentrated under reduced pressure. The crude solid was recrystallized from diethyl ether at $-20\text{ }^\circ\text{C}$, isolated by filtration, and washed with cold diethyl ether. $^1\text{H-NMR}$ data for the benzamides used in this study can be found in chapter 2.

General Procedure for the Iridium Catalyzed Bromination of Benzamides



A foil covered screw cap test tube with a magnetic stirrer was charged with benzamide (1 mmol, 1.0 equiv), *N*-bromosuccinimide (1.5 mmol, 1.5 equiv), $[\text{Cp}^*\text{IrCl}_2]_2$ (0.06 mmol, 6 mol%), silver triflate (0.24mmol, 24 mol%), acetic acid (2 mmol, 2 equiv) and 1 mL of 1,2-dichloroethane. The reaction mixture was stirred at $60\text{ }^\circ\text{C}$ for 4 h in an oil bath. Upon completion, the solution was diluted with dichloromethane and filtered through celite. The solvent was removed under reduced pressure and the crude reaction mixture was purified by column chromatography on silica gel (SiO_2). $^1\text{H-NMR}$ data for the brominated benzamides used in this study can be found in chapter 2.

General Procedure for the Iridium Catalyzed Chlorination of Benzamides



A foil covered screw cap test tube with a magnetic stirrer was charged with benzamide (0.1 mmol, 1.0 equiv), Trichloroisocyanuric acid (TCC) (0.15 mmol, 1.5 equiv), [Cp*IrCl₂]₂ (0.010 mmol, 10 mol%), silver triflate (0.40 mmol, 40 mol%), trifluoroacetic acid (0.2 mmol, 2 equiv) and 1 mL of 1,2-dichloroethane. The reaction mixture was stirred at 100 °C for 12 h in an oil bath. Upon completion, the solution was diluted with dichloromethane and filtered through celite. The solvent was removed under reduced pressure.

2-chloro-*N,N*-diisopropylbenzamide. Utilizing the general procedure using 20.4 mg of *N,N*-diisopropylbenzamide (0.1 mmol, 1.0 equiv), 34.9 mg of TCC (0.15 mmol, 1.5 equiv), 8.0 mg of [Cp*IrCl₂]₂ (0.01 mmol, 10 mol%), 10.5 mg of silver acetate (0.40 mmol, 40 mol%). ¹H-NMR (300 MHz, CDCl₃) δ (ppm): 7.39 – 7.34 (m, 1H, aromatic proton), 7.29 – 7.24 (m, 2H, aromatic proton), 7.22 – 7.16 (m, 1H, aromatic proton), 3.60 (m, 1H, CH(*i*Pr)), 3.52 (m, 1H, CH(*i*Pr)), 1.57 (d, J = 6.8 Hz, 3H), CH₃(*i*Pr), 1.56 (d, J = 6.8, 3H, CH₃(*i*Pr)), 1.21 (d, J = 6.7 Hz, 3H, CH₃(*i*Pr)), 1.06 (d, J = 6.7 Hz, 3H, CH₃(*i*Pr)).

2-chloro-*N,N*-diisopropyl-4-methylbenzamide. Utilizing the general procedure using 21.9 mg of 4-methyl-*N,N*-diisopropylbenzamide (0.1 mmol, 1.0 equiv), 34.9 mg of TCC (0.15 mmol, 1.5 equiv), 8 mg of [Cp*IrCl₂]₂ (0.01 mmol, 10 mol%), 10.5 mg of silver acetate (0.40 mmol, 40 mol%). ¹H-NMR (300 MHz, CDCl₃) δ (ppm): 7.18 (s, 1H, aromatic proton), 7.10 – 7.02 (m, 2H, aromatic proton), 3.61 (m, 1H, CH(*i*Pr)), 3.50 (m, 1H, CH(*i*Pr)), 2.32 (s, 3H, *p*-CH₃), 1.55 (dd, J = 6.8, 4.0 Hz, 6H, 2 x CH₃(*i*Pr)), 1.19 (d, J = 6.7 Hz, 3H, CH₃(*i*Pr)), 1.04 (d, J = 6.6 Hz, 3H, CH₃(*i*Pr)).

2-chloro-4-fluoro-*N,N*-diisopropylbenzamide. Utilizing the general procedure using 22.3 mg of 4-fluoro-*N,N*-diisopropylbenzamide (0.1 mmol, 1.0 equiv), 34.9 mg of TCC (0.15 mmol, 1.5 equiv), 8 mg of [Cp*IrCl₂]₂ (0.01 mmol, 10 mol%), 10.5 mg of silver acetate (0.40 mmol, 40 mol%). ¹H-NMR (400 MHz, CDCl₃): δ 7.21 – 7.08 (m, 2H, aromatic proton), 6.99 (m, 1H, aromatic proton), 3.53 (m, 2H, 2 x CH(*i*Pr)), 1.54 (dd, J = 6.8, 2.6 Hz, 6H, 2 x CH₃(*i*Pr)), 1.20 (d, J = 6.7 Hz, 3H, CH₃(*i*Pr)), 1.05 (d, J = 6.7 Hz, 3H, CH₃(*i*Pr)).

References

- 1) Carreras, V.; Sandtorv, A. H.; Stuart, D. R.; *J. Org. Chem.* **2017**, *82*, 1279.
- 2) Malmedy, F.; Wirth, T.; *Eur. J. Org. Chem.* **2017**, 786.
- 3) Zhao, J.; Li, S.; *J. Org. Chem.* **2017**, *82*, 2984.
- 4) Singh, K.; Kaur, A.; Mithu, V. S.; Sharma, S.; *J. Org. Chem.* **2017**,
- 5) Zhou, Y.; Zhang, X.; Zhang, Y.; Ruan, L.; Zhang, J.; Zhang-Negrerie, D.; Du, Y.; *Org. Lett.* **2017**, *19*, 150.
- 6) Maiti, S.; Mal, P.; *Org. Lett.* **2017**, *19*, 2454.
- 7) Morimoto, K.; Ohnishi, Y.; Koseki, D.; Nakamura, A.; Dohi, T.; Kita, Y.; *Org. Biomol. Chem.* **2016**, *14*, 8947.
- 8) Sandtorv, A. H.; Stuart, D. R.; *Angew. Chem.* **2016**, *128*, 16044.
- 9) Brown, M.; Kumar, R.; Rehbein, J.; Wirth, T.; *Chem. Eur. J.* **2016**, *22*, 4030.
- 10) Morimoto, K.; Sakamoto, K.; Ohshika, T.; Dohi, T.; Kita, Y.; *Angew. Chem.* **2016**, *128*, 3716.
- 11) Arnold, A. M.; Ulmer, A.; Gulder, T.; *Chem. Eur. J.* **2016**, *22*, 8728.
- 12) Mariappan, A.; Rajaguru, K.; Merukan Chola, N.; Muthusubramanian, S.; Bhuvanesh, N.; *J. Org. Chem.* **2016**, *81*, 6573.
- 13) Sakamoto, R.; Inada, T.; Selvakumar, S.; Moteki, S. A.; Maruoka, K.; *Chem. Commun.* **2016**, *52*, 3758.
- 14) Yoshimura, A.; Zhdankin, V. V.; *Chem. Rev.* **2016**, *116*, 3328.
- 15) Miyamoto, K.; Yokota, Y.; Suefuji, T.; Yamaguchi, K.; Ozawa, T.; Ochiai, M.; *Chem. Eur. J.* **2014**, *20*, 5447.
- 16) Kasahara, T.; Jang, Y. J.; Racicot, L.; Panagopoulos, D.; Liang, S. H.; Ciufolini, M. A.; *Angew. Chem.* **2014**, *126*, 9791.
- 17) Fra, L.; Millan, A.; Souto, J. A.; Muniz, K.; *Angew. Chem.* **2014**, *126*, 7477.
- 18) Uyanik, M.; Hayashi, H.; Ishihara, K.; *Science* **2014**, *345*, 291.
- 19) Souto, J. A.; Martínez, C.; Velilla, I.; Muñoz, K.; *Angew. Chem. Int. Ed.* **2013**, *52*, 1324; *Angew. Chem.* **2013**, *125*, 1363.
- 20) Wagh, Y. S.; Tiwari, N. J.; Bhanage, B. M.; *Tetrahedron Lett.* **2013**, *54*, 1290.
- 21) Ochiai, M.; Yamane, S.; Hoque, M.; Saito, M.; *Chem. Commun.* **2012**, *48*, 5280.
- 22) M.; Uyanik, H.; Okamoto, T.; Yasui, K.; Ishihara, *Science* **2010**, *328*, 1376.

- 23) Altermann, S. M.; Richardson, R. D.; Page, T. K.; Schmidt, R. K.; Holland, E.; Mohammed, U.; Paradine, S. M.; French, A. N.; Richter, C.; Bahar, A. M.; Witulski, B.; Wirth, T.; *Eur. J. Org. Chem.* **2008**, 5315.
- 24) Kieltsch, I.; Eisenberger, P.; Togni, A.; *Angew. Chem.* **2007**, 119, 768.
- 25) Wirth, T.; *Angew. Chem.* **2005**, 117, 3722.
- 26) Tohma, H.; Takizawa, S.; Maegawa, T.; Kita, Y.; *Angew. Chem.* **2000**, 112, 1362.
- 27) De Mico, A.; Margarita, R.; Parlanti, L.; Vescovi, A.; Piancatelli, G.; *J. Org. Chem.* **1997**, 62, 6974.
- 28) Stang, P. J.; Zhdankin, V. V.; *Chem. Rev.* **1996**, 96, 1123.
- 29) Frigerio, M.; Santagostino, M.; Sputore, S.; Palmisano, G.; *J. Org. Chem.* **1995**, 60, 7272.
- 30) Koser, G. F.; Relenyi, A. G.; Kalos, A. N.; Rebrovic, L.; Wettach, R. H.; *J. Org. Chem.* **1982**, 47, 2487.
- 31) Barluenga, J.; González, J. M.; Campos, P. J.; Asensio, G.; *Angew. Chem.* **1985**, 97, 341.
- 32) Barluenga, J.; Vázquez-Villa, H.; Ballesteros, A.; González, J. M.; *J. Am. Chem. Soc.* **2003**, 125, 9028.
- 33) Barluenga, J.; Vazquez-Villa, H.; Ballesteros, A.; Gonzalez, J. M.; *Adv. Synth. Catal.* **2005**, 347, 526.
- 34) Barluenga, J.; Trincado, M.; Rubio, E.; González, J. M.; *Angew. Chem. Int. Ed.* **2006**, 45, 3140; *Angew. Chem.* **2006**, 118, 3212.
- 35) Takaku, K.; Shinokubo, H.; Oshima, K.; *Tetrahedron Lett.* **1996**, 37, 6781.
- 36) Okitsu, T.; Nakazawa, D.; Taniguchi, R.; Wada, A.; *Org. Lett.* **2008**, 10, 4967.
- 37) Cui, X. L.; Brown, R. S.; *J. Org. Chem.* **2000**, 65, 5653.
- 38) Neverov, A. A.; Feng, H. X.; Hamilton, K.; Brown, R. S.; *J. Org. Chem.* **2003**, 68, 3802.
- 39) Homsí, F.; Associe, C.; *J. Org. Chem.* **1999**, 64, 81.
- 40) Grossman, R. B.; Trupp, R. J.; *Can. J. Chem.* **1998**, 76, 1233.
- 41) Wang, Y.; Hoong, C.; Rauniyar, V.; Toste, F. D.; *J. Am. Chem. Soc.* **2012**, 134, 12928.

- 42) Li, J.; Lear, M. J.; Kawamoto, Y.; Umemiya, S.; Wong, A. R.; Kwon, E.; Sato, I.; Hayashi, Y. *Angew. Chem.* **2015**, *127*, 13178.
- 43) Lines, R.; Parker, V. D.; *Acta Chem. Scand. B* **1980**, *34*, 47.
- 44) Shono, T.; Matsumura, Y.; Katoh, S.; Ikeda, K.; Kamada, T.; *Tetrahedron Lett.* **1989**, *30*, 1649.
- 45) Ashikari, Y.; Shimizu, A.; Nokami, T.; Yoshida, J. I.; *J. Am. Chem. Soc.* **2013**, *135*, 16070.
- 46) Muniz, K.; Garcia, B.; Martinez, C.; Piccinelli, A.; *Chem. Eur. J.* **2017**, *23*, 1539.
- 47) Martinez, C.; Muniz, K.; *Angew. Chem.* **2015**, *127*, 8405.
- 48) Denmark, S. E.; Burk, M. T.; *Proc. Natl. Acad. Sci. USA* **2010**, *107*, 20655.
- 49) Zhou, L.; Tan, C. K.; Jiang, X.; Chen, F.; Yeung, Y.Y.; *J. Am. Chem. Soc.* **2010**, *132*, 15474.
- 50) Zhou, L.; Chen, J.; Tan, C. K.; Yeung, Y. Y.; *J. Am. Chem. Soc.* **2011**, *133*, 9164.
- 51) Tan, C. K.; Zhou, L.; Yeung, Y. Y.; *Org. Lett.* **2011**, *13*, 2738.
- 52) Tripathi, C. B.; Mukherjee, S.; *Angew. Chem.* **2013**, *125*, 8608.
- 53) Tripathi, C. B.; Mukherjee, S.; *J. Org. Chem.* **2012**, *77*, 1592.
- 54) Denmark, S. E.; Beutner, G. L.; *Angew. Chem.* **2008**, *120*, 1584.
- 55) Jensen, W. B.; *The Lewis Acid-Base Concepts*, Wiley-Interscience, New York, **1980**.
- 56) Jensen, W. B.; *Chem. Rev.* **1978**, *78*, 1.
- 57) Tilstam, U.; Weinmann, H.; *Org. Process Res. Dev.* **2002**, *6*, 384.
- 58) Denmark, S. E.; Beutner, G. L.; *Angew. Chem. Int. Ed.*, **2008**, *47*, 1560.
- 59) Frasco, D. A.; Mukherjee, S.; Sommer, R. D.; Perry, C. D.; Lambic, N. S.; Abboud, K. A.; Jakubikova, E.; Ison, E. A. *Organometallics* **2016**, *35*, 2435.
- 60) Frisch, M. J.; Trucks, G. W.; Schlegel, H. B.; Scuseria, G. E.; Robb, M. A. Inc., Wallingford, CT 2009.
- 61) Parr, R. G.; Yang, W. New York 1989.
- 62) Hehre, W. J.; Ditchfield, R.; Pople, J. A. *J. Chem. Phys.* **1972**, *56*, 2257.
- 63) Dolg, M.; Stoll, H.; Preuss, H.; Pitzer, R. M. *J. Phys. Chem.* **1993**, *97*, 5852.
- 64) Hay, P. J.; Wadt, W. R. *J. Chem. Phys.* **1985**, *82*, 270.
- 65) Rassolov, V. A.; Pople, J. A.; Ratner, M. A.; Windus, T. L., 6-31G* basis set for atoms K through Zn. *The Journal of Chemical Physics* 1998, *109* (4), 1223-1229.

- 66) Hay, P. J.; Wadt, W. R. *J. Chem. Phys.* **1985**, *82*, 299.
- 67) Marenich, A. V; Cramer, C. J.; Truhlar, D. G. *J. Phys. Chem. B* **2009**, *113*, 6378.